Symmetry breaking of biofilaments

Tanguy Saïbi

École doctorale C2MP
Chimie Mécanique Matériaux Physique

THESE

pour obtenir le titre de

Docteur de l'université de Lorraine

Mention Biophysique

Soutenue publiquement le 7/12/2021, par :

Tanguy Idir Saïbi

Symmetry breaking of bio-filaments

Devant le jury composé de :

Catherine Quilliet Maitresse de conférence, Université Grenoble Alpes	**Rapporteure**
Jean-Francois Joanny Professeur, Collège de France	**Rapporteur**
René Messina Professeur, Université de Lorraine	**Examinateur**
Igor Kulic Chargé de recherche, CNRS - Institut Charles Saudron - Strasbourg	**Examinateur**
Hervé Mohrbach Professeur, Université de Lorraine	**Directeur de thèse**

Laboratoire de Physique et Chimie Théorique (LPCT) - UMR CNRS 7019
Université de Lorraine, 1 Boulevard Arago, 57070 Metz, France

"The person who moves a mountain begins by carrying away small stones. "

Confucius

Remerciements

Il est temps de remercier ici celles et ceux qui m'ont accompagné pendant ces cinq années et ont contribué à la réalisation de ce manuscrit. En effet, sans vous, encadrants, famille, amis, élèves, collègues, il ne m'aurait pas été possible d'aller au bout de MON Koh Lanta.

Je tiens donc, très sincèrement, à tous vous remercier.

Le jury

Honneur à celui qui a réussi à encadrer mon travail, me guider, me soutenir, m'enrichir, mon très cher directeur de thèse **Hervé Mohrbach**. Malgré les conditions particulièrement compliquées qui ont accompagné mes recherches et la rédaction de ce manuscrit, tu t'es toujours montré à l'écoute, patient et d'excellent conseil. Je te remercie infiniment pour tout ce que tu m'as appris scientifiquement, humainement et d'être la personne que tu es.

Merci à **Catherine Quilliet** de me faire l'honneur d'être rapporteure et membre de ce jury,
Merci à **Jean-François Joanny** de me faire l'honneur d'être rapporteur et membre de ce jury,
Merci à **Igor M. Kulic** d'avoir accepté d'être examinateur mais également d'avoir beaucoup collaboré aux différents travaux exposés à travers cette thèse,
Merci à **René Messina** de bien vouloir participer à ce jury et d'en être examinateur.

Les proches

Merci à tous mess amis qui ont régulièrement eu une pensée, un mot de soutien, et ce depuis le début de ce parcours. Il vous a fallu redoubler d'ingéniosité pour varier les formules d'encouragement et essayer de rester, un peu, intéressés par cette thèse. Cinq ans, c'est long, trèèèèès long...

Merci aux collègues, enseignants - préparateurs - personnels de direction - personnels administratifs - inspecteurs (il n'y pas d'ordre), qui m'ont soutenu directement (ah cette barre de gélatine) ou indirectement (emploi du temps enviés par tant de collègues, échanges, propos rassurants et motivants, notamment les autres docteurs du lycée, et il y en a quelques uns).

Merci à toutes les personnes avec qui j'ai échangé lors de voyages ou concours et qui m'ont donné envie de m'accrocher par leurs beaux exemples de parcours réussis.

Une pensée aussi pour mes élèves qui, de par leur bonne humeur, leur joie de vivre et leur grande envie de bien faire, donnent du sens à mon métier et l'envie de me dépasser pour aller plus loin. Vous avez également contribué en me fatiguant très peu au quotidien, bien joué. Certains seront même destinataires de ce manuscrit, puisqu'ils s'y sont intéressés (ne seriez vous pas fous?)

Une pensée, également, à ceux qui nous ont quittés pendant cette période pendant laquelle ils se sont battus, avec leurs proches. Une pensée pour Camille-Juliette B., pour Vincent U., pour Sandra P. et pour Mina S.

La famille, grande famille!

Un grand merci à tous les membres de ma famille. Merci d'avoir respecté, même si vous ne l'avez pas toujours comprise, cette aventure. Vous êtes trop nombreux pour que je vous cite ici, mais, peu importe la manière, vous m'avez toujours apporté du soutien. MERCI!

Merci Maman pour m'avoir permis d'acquérir très tôt une grande autonomie, de bien me connaitre. J'ai apprécié ton soutien indéfectible, du berceau à aujourd'hui.

Un énorme merci à l'un de mes modèles, celui qui a toujours dit :"Oui, tout va bien, et tout ira bien." de notre quartier à notre maison et cela sans jamais perdre son sourire, malgré les épreuves traversées. Tu ne le sais peut-être pas, mais tu as été un modèle pour beaucoup d'entre nous de par ton abnégation et la personne saine que tu es. On s'était perdu de vue mais il n'y a pas de hasard, ton retour a coïncidé avec le démarrage de cette thèse pour laquelle tu auras été d'un grand soutien (technique et moral). Donc un immense merci à toi, frère Acem!.

Khaled, même si tu ne t'en rends pas toujours compte, tu es l'exemple parfait de la résilience au quotidien. Ces milles vies (professionnelles) que tu as vécues, et cette force qu'il t'a fallu pour mener à bien tous tes projets sont aussi une grande source de motivation pour moi. Un grand merci à toi frère Khaled!

Merci à toi, Karim (ou Ayachi pour les non-intimes), de m'avoir apporté tant de sérénité et de confiance pendant toutes ces années. Un soutien sans faille, même à distance, toujours capable de dédramatiser les choses sans qu'elles ne perdent leur valeur. Un exemple aussi, vu ton parcours (humain comme professionnel), et ce que tu m'apportes. Tu n'as jamais eu peur de rien, de vivre des expériences aux quatre coins du monde, d'avoir une position et de l'assumer. Bref, merci d'être dans les parages mon frère!

Idir Saïbi, mon grand père, mon inspiration pour tout. Tu n'es malheureusement plus là pour que je puisse partager tout ce que je vis avec toi, mais je suis persuadé que, quelque part, tu es près de moi. Tu m'as tellement apporté, m'a appris tellement de choses, notamment de toujours m'accrocher, d'y croire et de rester "propre" comme on dit chez nous donc respectueux de toutes et tous que je peux affirmer que, sans toi, rien n'aurait été possible. Apporter autant de valeur et d'amour en montrant l'exemple autant par les actes que par les paroles. Respect Papi, tu es la preuve qu'on peut ne pas être diplômé mais largement hors-concours.

Sandra, je ne te le dis certainement pas suffisamment, mais rien n'aurait été possible sans toi. Même quand le quotidien devient compliqué, tu sais me soutenir et m'encourager. Tout cela avec amour, je crois; tu as sacrifié beaucoup de choses, tu t'es merveilleusement bien occupé de nos minettes, tout en remplissant mille et une missions et, dans tout ça, tu m'as laissé beaucoup de temps pour bosser et as même fait semblant, par moments, de t'intéresser à ce travail. Tu as déjà dit que tu me considérais comme ton pilier, la réciproque est tout aussi vraie. J'ai d'autant plus de chance de t'avoir comme soutien (et plus encore) qu'avec toi le risque d'instabilité, et donc d'auto-flambage, reste très faible (ce sera la blague scientifique de ce manuscrit, high level on est d'accord). Te quiero muchachita.

Lena, toujours curieuse de savoir/comprendre ce que je fais et soucieuse de savoir que je vais bien. Une telle curiosité (notamment scientifique) et un si grand nombre de questions que je ne peux pas te décevoir. La seule de sa génération à avoir compris que je ne pourrai pas signer d'ordonnances après tout ça. Juste envie d'être à ta hauteur ma fille, au moins aujourd'hui, car je sais que la grande padawan que tu es dépassera rapidement son père. Je t'aime ma grenouille.

Tessa, courageuse (et un peu râleuse, mais cela va de paire) au quotidien. Tu m'as donné de la force et le sourire tous les jours. Et l'envie de me surpasser, comme tu le fais au quotidien. Tu es incroyable, dans ce que tu vis ou fais, tu es une source d'inspiration, et pas que pour moi. Très curieuse, et fûtée (trop?), bref, laisse moi encore croire un peu de temps que je peux t'apprendre des choses. Alors oui, cette thèse ne porte pas sur la guerre, mais, promis, on reprendra ce sujet bientôt ma petite (grande) puce.

Mes filles, je suis fier d'être allé au bout de ce parcours de recherche, mais ce n'est infiniment rien comparé à ma fierté d'être votre père.

Abstract

The interpretation of micromanipulation experiments of biological macromolecules has only been possible thanks to the development of polymer science. Indeed, the theories developed in polymer physics are the tool of theorists to interpret the increasingly precise and complex experiments. Biological macromolecules are in general more complex than classical polymers with flexible chains, because their basic units, the "monomers", are very often macromolecules themselves. The most appropriate model for biopolymers is the worm-like chain model that imparts bending rigidity to biological filaments. Because of its simplicity and usefulness in interpreting micromanipulation experiments of single biological macromolecules, this model has become the basic model for any theoretical approach to the biophysics of biofilaments. The confotronics model of microtubules leads to the fundamental phenomenon of spontaneous symmetry breaking that explains how a microtubule, a hollow cylinder, can, under certain circumstances, form a micron-sized superhelix. This requires a general physical principle for the mechanism of spontaneous breaking of these biofilaments. We assume that biofilaments, being always immersed in a fluid medium, can experience surface stresses that create a mismatch between the elastic properties of the surface layer and the core. Such a mismatch leads a filament into a frustrated elastic state. The filament can reduce this frustration and minimize its elastic energy by adopting a bent conformation in a spontaneous symmetry breaking process induced by a new type of self-bending elastic instability. My work, presented in this thesis, has attempted to explore this new elastic instability in different biofilament models in both linear and nonlinear elasticity domains. The basic elements of linear elasticity and the physics of individual chains or bundles are presented in chapter 2. Chapter 3 is devoted to the general theory of buckling, the basic idea of this thesis being related to self-buckling. Chapter 4 presents the physical and biological properties of cytoskeleton biofilaments and some key experiments that support our theoretical work. In chapter 5, I have tried to review the general notions of ground state and symmetry breaking in order to place them in the context of biophysics. This chapter also introduces the basic ideas behind confotronics theory. This chapter can provide a new and broader perspective on biofilament physics. The last three chapters, 6 to 8, present my work on elastic instability and spontaneous symmetry breaking induced by surface stresses. This area of research was completely unknown to me when I started this project, so I decided to write a story that tells all the topics I learned on the way to the results presented here. As a teacher, I tried to write a very educational thesis with all the necessary concepts introduced at the beginning of each chapter. I hope that the thesis can be read by beginners in this field, as I was when I started.

Résumé

Passionné par les sciences, la physique en particulier, j'ai toujours montré une grande curiosité scientifique. Je me suis donc naturellement orienté vers des études scientifiques (MPSI/MP/licence/master) au bout desquelles j'ai obtenu les titres me permettant d'enseigner dans le secondaire (certification puis agrégation). J'ai voulu me lancer dans ce travail de recherche pour poursuivre ma progression en tant que scientifique, assouvir une certaine curiosité, mais également continuer à donner envie à mes proches de s'intéresser aux sciences voire de s'orienter vers une profession scientifique. Ainsi, au début de l'année 2016, j'ai eu l'opportunité de démarrer cette thèse auprès d'Hervé Mohrbach (Laboratoire de Physique et Chimie Théorique). N'ayant que peu d'expérience en bio-physique, bien que possédant une bonne maitrise des concepts physiques et mathématiques sous-jacents, il m'a été nécessaire de me documenter très largement afin de comprendre globalement ces problématiques associées aux virus et, plus généralement, aux filaments biologiques.
Souhaitant produire une thèse accessible au plus grand nombre, j'ai choisi de lui donner un format pédagogique, tant sur le fond que sur la forme. Ainsi, autant que faire se peut, j'ai introduit dans les différentes parties des éléments permettant de cerner à notre échelle et dans la vie quotidienne certains concepts physiques (loi de Hooke, flambage, instabilité, etc). Chaque partie théorique permet d'entrer progressivement dans le travail spécifique de cette thèse. Autant que possible, je pars de situations connues et maitrisées par tout étudiant de licence/master afin de permettre à chacun de comprendre l'enchainement des idées. Ces introductions doivent permettre de saisir "avec les mains" les modèles proposés dans cette thèse. De même, la thèse est construite comme une histoire en plusieurs épisodes pour rendre sa lecture plus confortable.
Nous nous intéresserons aux filaments biologiques du cytosquelette qui ont des comportements anormaux par rapport aux théories standards basées sur la physique des polymères. En particulier ces filaments ont souvent des formes hélicoïdales, mais aussi courbées et parfois circulaires en fonctions des conditions expérimentales. On suppose habituellement que ces formes sont générées par l'interaction de ces filaments avec des protéines du milieu cellulaire. Partant de la description d'un filament isolé, nous étendrons notre réflexion à un système couplé de deux filaments puis passerons à un système à trois filaments avant de prendre en considération des systèmes continus, dans le cas linéaire puis le cas non linéaire. Nous supposons que l'origine de ces formes serait davantage liée à des causes internes et prenons ainsi en compte la différence d'environnement rencontré par la surface dans/hors le filament.

Chapter : Loi de Hooke, Worm-like chaine et faisceau de filaments

Cette thèse porte sur les instabilités élastiques dans les structures fibreuses avec un accent sur les biofilaments, notamment ceux du cytosquelette des cellules. Cette idée vient de l'observation que les biofilaments bien qu'intrinsèquement rigides aux échelles considérées, peuvent spontanément former des formes très courbes, parfois circulaires et même hélicoïdales. Toutes ces formes font appel à la théorie de l'élasticité.

Dans ce chapitre introductif, nous commencerons par le tout début de la théorie de l'élasticité en définissant le régime linéaire de l'élasticité ou régime de Hooke (par opposition à la théorie de l'élasticité non linéaire abordée au chapitre 8) des ressorts et des fils. Bien que la théorie de Hooke soit applicable à l'étude des petites déformations des tiges élastiques macroscopiques, ce n'est en général pas le cas pour les biofilaments. Il s'agit de filaments microscopiques qui vivent dans un environnement à température finie (in vivo et vitro) et sont donc soumis à des fluctuations thermiques. Il a été prouvé que les déformations élastiques des biofilaments induites par la température sont bien décrites par le modèle de chaîne semi-flexible également appelé **worm-like chain model**. Ses propriétés de base sont rappelées dans ce chapitre. Les biomolécules étant souvent des faisceaux de filaments individuels, nous introduirons également le **railway track model**, un faisceau de deux chaînes semi-flexibles qui s'avère être au cœur de cette thèse.

Cette analyse montrera qu'en présence de cisaillement, le faisceau a deux comportements différents selon l'échelle d'observation. Alors qu'il se comporte comme une chaîne semi-flexible à courte distance, il affiche une très grande rigidité apparente à la flexion à une échelle plus grande et peut donc être considéré comme une tige élastique avec des fluctuations thermiques supprimées.

Flambage et auto-flambage

Dans le chapitre 2, nous avons vu que des chaînes microscopiques semi-flexibles vues comme de fines tiges élastiques immergées dans un bain thermique peuvent modéliser de véritables bio-macromolécules comme l'ADN. L'objectif de cette thèse est de convaincre le lecteur que ce modèle est une simplification excessive lorsqu'il s'agit d'étudier les filaments du cytosquelette. Une question fondamentale à laquelle nous tentons de répondre tout au long de cette thèse est : comment expliquer que des filaments isotropes rigides forment des conformations courbes très persistantes à l'échelle d'observation $\left(L \lesssim l_p\right)$, étant entendu que ces états courbes ne peuvent pas être activés thermiquement ?
Les chapitres 6 à 8 sont consacrés à cette question. Une réponse provient de la confotronique qui est résumée dans le chapitre 5. Une deuxième réponse repose sur une nouvelle idée qui découle du concept d'auto-flambage (self-buckling) qui résulte d'une instabilité élastique appelée auto-enroulement (autocoiling). Il est proposé que cette nouvelle instabilité puisse être induite par des contraintes sur la surface du filament. Les deux approches, la confotronique et l'auto-enroulement, reposent sur le concept physique essentiel de rupture spontanée de symétrie. Avant de lancer nos recherches dans cette direction, nous proposons une introduction très visuelle au flambage et à l'auto-flambage des objets macroscopiques du quotidien. Nous terminerons ce chapitre par un rappel du flambage du modèle du worm-like chain.

Bio-macromolecules du cytosquelette

La cellule est le principal composant des êtres vivants. Mais ce que les gens ne savent généralement pas, c'est que les cellules ne sont pas comme des gouttes d'eau : elles possèdent une structure capable de les maintenir. Elles possèdent un "squelette". Celui-ci, au contraire du squelette qui porte notre corps, est constitué de bio-filaments. Il est appelé cytosquelette et est un réseau élastique hautement dynamique composé principalement de trois types de filaments jouant un rôle structurel et mécanique. Les microtubules sont, avec les filaments intermédiaire et les micro-filaments, l'un filaments présents dans une cellule. Parmi les trois types de filaments biologiques présents, nous nous intéressons spécifiquement aux filaments intermédiaires ainsi qu'aux microtubules. Dans les deux cas, nous présenterons des expériences clés mettant en avant les propriétés élastiques, notamment leurs réponses à des contraintes mécaniques de différents types. L'étude se concentrera ensuite uniquement sur les microtubules.

État fondamental, confotronique et brisure de symétrie

L'état fondamental d'un système physique est l'état d'énergie minimale. Si cet état a moins de symétries que l'Hamiltonien du système, on dit qu'il y a une rupture (brisure) de symétrie. Comme exemples de brisure de symétrie, nous avons vu le flambage dans le plan d'une tige élastique et celui d'un filament. Si la déformation n'est pas contrainte dans un plan mais peut évoluer dans un espace tridimensionnel, alors le système est invariant en rotation et il existe un nombre infini d'états de flambage possibles obtenus par rotation autour de l'axe vertical. Nous reviendrons sur ce point important lorsque nous discuterons de l'énergie de mode zéro des microtubules et potentiellement de tous les biofilaments qui résulte de la rupture de l'invariance rotationnelle pendant un processus d'auto-flexion.
La vision simpliste des macromolécules biologiques comme celles du cytosquelette considérées comme de simples filaments élastiques n'est alors plus acceptable. Par conséquent, il a été suggéré que la complexité moléculaire du monomère pourrait permettre aux sous-unités de subir des réarrangements entre plusieurs états conformationnels et via une interaction coopérative conduisant à des comportements complexes de l'ensemble de l'assemblage. Le terme confotronique a été récemment proposé pour l'étude unifiée de ces états conformationnels de grandes assemblées de systèmes d'unités commutables souples en biologie. Comme nous allons le voir, la confotronique des biofilaments est intimement liée au concept de rupture de symétrie et à l'existence d'un état fondamental non trivial.

Dans la dernière partie de ce chapitre, nous nous pencherons sur le comportement du microtubule. Ses blocs de construction élémentaires, les dimères de tubuline, se polymérisent tête-bêche en protofilaments linéaires qui s'associent côte à côte pour former la structure en tube creux. Malgré la connaissance de sa structure et de nombreuses expériences sondant ses propriétés élastiques, la compréhension de la mécanique des microtubules pose encore des problèmes difficiles. Nous regarderons, à travers différents modèles, les états fondamentaux possibles pour ces microtubules.

Brisure de symétrie - faisceau de trois filaments

Après avoir étudié un système à deux filaments, en deux dimensions (voir 2), il a semblé logique et pertinent d'étendre le modèle à un ensemble de trois filaments. La présence d'une contrainte préalable dans le modèle et la frustration entre les états élastiques préférés externes et internes soulèvent la question de la rupture de symétrie par un mécanisme plus simple qui ne nécessite pas de commutabilité. La contrainte à l'extérieur d'un filament peut-elle entraîner un décalage avec la contrainte à l'intérieur de celui-ci, ce qui conduit à un conflit et à une instabilité de forme ? Une telle instabilité surface-noyau a été récemment proposée pour l'instabilité de courbure des filaments intermédiaires et a été appelée autocoiling. Nous allons ainsi explorer plus en détail la faisabilité de ce mécanisme de rupture de symétrie.
Le modèle mécaniste le plus simple consiste en une structure à trois couches avec deux couches extérieures qui préfèrent individuellement la même longueur contractée et une couche intermédiaire qui a une longueur préférentielle différente. Il s'agit d'une généralisation du railway track model à trois filaments qui décrit un faisceau où la contrainte extérieure est différente de celle de l'intérieur, exactement la situation que nous voulons étudier. Dans ce type de modèle, les filaments sont irréversiblement liés à leurs voisins les plus proches par des liaisons transversales discrètes qui sont en général flexibles en cisaillement le long de l'axe du faisceau mais inextensibles latéralement. A première vue, l'analyse de la section réseau anisotrope dans le chapitre 5 tend à montrer que ce type de modèles appartient à la catégorie des modèles d'élasticité linéaire et ne peut pas conduire à une rupture spontanée de symétrie.Nous posons donc la question plus générale : un faisceau de filaments élastiques sans aucune non-linéarité peut-il avoir un état fondamental non trivial ? Nous verrons que, malgré la discussion précédente, c'est effectivement possible.

Brisure de symétrie induite par une tension de surface : régime linéaire

Dans ce chapitre, nous adoptons une sorte de version continue des modèles à trois filaments présentés au chapitre 6. Ici, l'effet d'une contrainte de surface sur la forme des filaments, vus comme des tiges élastiques, est étudié avec le formalisme de la tension de surface des solides. La question principale est alors la suivante : la frustration induite par le décalage entre l'état élastique de surface qui est sous contrainte et le cœur sans contrainte de la tige peut-elle conduire à une instabilité élastique ? En d'autres termes, la tension de surface peut-elle modifier le module de flexion de

la tige de telle sorte que la rigidité apparente qui en résulte puisse disparaître pour une valeur critique de la tension de surface ? Cette question est d'une importance fondamentale, car elle pourrait expliquer la récurrence observée des conformations courbes persistantes des biofilaments, mais aussi avoir des conséquences pratiques, comme la possibilité pour les biofilaments d'actionner des fibres changeant de forme. Avant d'aborder ce sujet, nous rappellerons le concept de tension superficielle dans les liquides mais aussi dans les matériaux mous comme les gels avec des exemples visuels et des expériences maison.

Brisure de symétrie induite par une tension de surface : régime non-linéaire

Les chapitres précédant mettent en évidence la nécessité de la prise en compte de la déformation de la section transversale, ce que ne font pas la plupart des modèles de flambage des filaments. De même, la prise compte de la non-linéarité semble pertinente dans la description de l'état fondamental non trivial. C'est une caractéristique très commune en physique que les états dans le régime de brisure de symétrie sont des solutions d'équations différentielles non linéaires. L'autre modèle développé ici est en quelque sorte une version continue du faisceau discret mais est plus adapté aux déformations dans l'espace. Dans ce modèle, la tige est continue et la contrainte exercée par la surface sur le noyau est modélisée par un terme de tension de surface. Nous avons constaté que la tension superficielle pouvait contribuer négativement au module de flexion d'une tige, rendant la tige plus molle, au point que la flexion apparente disparaisse. Il a également été constaté que l'instabilité élastique d'un barreau lors du flambage ne peut pas conduire à un état fondamental hélicoïdal mais seulement à un arc plan. La limitation majeure du modèle continuum est qu'il ne peut décrire que l'instabilité élastique par auto-flexion mais pas la forme (nouvel état fondamental) de la tige dans la phase de rupture. En effet, si nous voulons décrire le régime après l'auto-flexion, nous devons déterminer la forme de la tige dans le régime d'élasticité non linéaire qui a été développé pour l'étude des déformations finies. Malheureusement, la résolution des équations élastiques non linéaires d'une tige pliée de section circulaire s'est avérée être un problème mathématique extrêmement difficile. Nous avons donc décidé de revisiter le problème classique de flexion d'élasticité non linéaire incompressible d'une poutre rectangulaire qui est l'exemple paradigmatique pour l'étude des déformations non linéaires des matériaux élastiques.

Conclusion

Ce manuscrit porte sur les concepts d'instabilité élastique et de rupture spontanée de symétrie et de leur pertinence dans l'univers des biofilaments. Les microtubules sont au centre de la recherche biophysique depuis plusieurs décennies. Un large éventail d'expériences biophysiques a fourni des preuves qu'ils présentent un comportement élastique et dynamique unique probablement hérité de leur structure complexe de nanotubes auto-assemblés. En présence d'une précontrainte interne, presque tous les systèmes considérés ont tendance à s'enrouler en une superhélice afin de minimiser leur précontrainte. La thèse constitue une réponse provisoire à la question fondamentale : comment une structure tubulaire rigide se déforme en une superhélice à grande échelle? Une première réponse est venue du concept récemment introduit de la confotronique. Il a été constaté qu'une sous-unité élastique non linéaire est nécessaire pour que la multistabilité apparaisse, une propriété qui peut induire une instabilité élastique et, à son tour, une brisure spontanée de symétrie.
Le mécanisme général proposé dans cette thèse est un mécanisme d'auto-buckling où les filaments exposés à des contraintes de surface deviennent élastiquement instables. Dans cet esprit, le chapitre 6 introduit un modèle simple qui est un faisceau à deux dimensions (planaire) de trois filaments extensibles réticulés, où le filament central a une longueur libre plus grande que les deux autres à la surface du faisceau. Il est connu qu'un faisceau de chaînes semi-flexibles n'est généralement pas instables et que l'état fondamental est la forme rectiligne (chapitres 2 et 5). Néanmoins, nous avons montré que la relaxation de la condition d'interdistance fixe entre les filaments est suffisante pour induire une instabilité élastique de l'état droit : il s'agit du modèle élastique purement linéaire le plus simple avec une rupture de symétrie spontanée. Le chapitre 7 présente un modèle qui peut être considéré comme une généralisation continue du faisceau de trois filaments, qui n'est pas limité aux déformations planes et est donc plus réaliste, où la contrainte de surface est modélisée par un terme de tension de surface. Pour une valeur critique de la tension de surface, la rigidité en flexion disparaît, ce qui conduit à l'instabilité élastique de la tige. Au niveau de l'élasticité linéaire, le véritable état de base incurvé n'est pas atteint et il faut considérer la théorie de l'élasticité non linéaire développée pour l'étude des grandes déformations (8). Cette thèse montre que le self-buckling des filaments exposés à des contraintes de surface est un mécanisme physique viable qui pourrait expliquer l'apparition des conformations courbes des biofilaments. Néanmoins, notre analyse indique qu'une contrainte de surface peut induire une brisure de symétrie vers un arc circulaire mais pas à une forme hélicoïdale.

Contents

List of Figures

Chapter 1

Introduction

The subject which is the most commonly associated with physics is chemistry and it is the subject physics-chemistry which is taught in secondary school. Much less known is the physics associated with biology, i.e. biophysics. However for centuries and until the $XVII^{th}$ century it was not rare that scientists were interested in all the fields, physics, chemistry and biology. Physics was the dominant fundamental science during all the XIX^{th} and the first half of the XX^{th} century with the extraordinary discoveries of the relativity and the quantum mechanics which upset our daily life by their applications. During the twentieth century, the progress of biology led to major discoveries whose consequences and applications in our daily lives are still growing. The crucial moment was of course the discovery of the double helix structure of the DNA molecule and since then biology has not stopped going from discovery to discovery. Biology has perhaps become the major science of the XXI^{st} century and this is undoubtedly what pushes physicists to be more and more interested in biology. Of course physics has always had a role in the development of observation techniques and the physical advances in the field of microscopy have brought to biology new techniques allowing to observe and to study finer and finer details in the world of the living. Recently, new microscopy techniques have made it possible to push back the resolution limit imposed by the diffraction of optical microscopes to reach resolutions of $30nm$ or even $20nm$. These methods allow the visualization of single molecules of very small sizes under physiological conditions.

In addition to the observation techniques, the physics-biology association is also at the origin of important developments in the last twenty years of experimental techniques such as the optical clamp laser and magnetic tweezers allow the observation and manipulation of single biological molecules. The progressive improvement of the methods of micromanipulation of single molecules of the living world, such as DNA, RNA, proteins or filaments of the cytoskeleton of the cells, have allowed more and more precise measurements of their physical, mechanical and elastic properties.

These properties, depending on physiological conditions and applied stresses, are associated with the biological roles of these molecules. Therefore, knowing the physical properties helps to understand the biological functions of these molecules and, more generally, the cell's mechanics.

The interpretation of micromanipulation experiments of biological macromolecules has been possible only thanks to the development of polymer science which has exploded since the 1960s and inspired the whole field of soft matter and led to fundamental applications in materials science. In the last twenty years, with the advancement of micromanipulation techniques, polymer physics has begun to take an interest in the world of living matter. Indeed, the theories developed in polymer physics are the tool of theorists to interpret the increasingly precise and complex experiments. Biological marcomolecules are in general more complex than classical polymers with flexible chains (without curvature rigidity), because their basic motifs, their "monomers" are very often themselves macromolecules.

The most suitable model for biopolymers is the worm-like chain model which somehow gives a bending (and sometimes twisting) rigidity to the biological filaments. Many observations, such as the response of biopolymers under stretching, torsion or compression forces require the worm-like chain model to be interpreted. Because of its simplicity and usefulness in the interpretation of micromanipulation experiments of single biological macromolecules, the worm-like chain model has become the basic model for any theoretical approach to biofilament biophysics.

However, after the initial successes, our knowledge of important biopolymers, such as the microtubule, actin or intermediate filaments, has been refined and several experimental results fall outside the interpretative framework of the worm-like chain model. In the face of these experimental "anomalies", it has become increasingly clear that the worm-like chain model should be extended by taking into account the internal structure of biopolymers. Any sophistication of the model supposed to reproduce the internal structure of biofilaments can lead to a more complex model that simply adds higher order corrections, but can also sometimes lead to more fundamental new principles. This seems to be the case for the cytoskeleton's filaments whose behaviors are not understandable with worm-like chain type models but require radically new assumptions. One approach has been to introduce internal degrees of freedom that mimic the internal dynamics (if any) of elementary biofilament components such as microtubules. In the latter case, the possibility that the microtubule's subunits, the tubulin dimers can fluctuate between two conformations (straight and curved) has allowed the construction of a complex theory that agrees with almost all experimental results. This type of model does not lead to corrections to the worm-like chain, but

to radical conceptual changes. In particular, the possibility that the behavior of large structures depends on elementary units that can fluctuate between several confirmations has led to the concept of confotronics.

The confotronic model of microtubule leads to the fundamental phenomenon of spontaneous symmetry breaking which explains how a microtubule, a hollow cylinder, can under certain circumstances, form a superhelix of micron's size pitch, in agreement with some key observations. In addition, there is growing amount of evidence that the other two macromolecules of the cytoskeleton, actin and intermediate filaments, do also have superhelical shape. This calls for a general physical principle driving the spontaneous breaking mechanism of these biofilaments. In this thesis, we assume that biofilaments being always immerged in a fluid medium can experiment surface stresses that create a mismatch between the elastic properties at both the surface layer and the core. Such a mismatch leads to a filament in a frustrated elastic state. The filament can reduce this frustration and minimize its elastic energy by adopting a curved conformation in a process of spontaneous symmetry breaking induced by a new kind of self-buckling elastic instability. My work presented in this thesis was trying to explore this new elastic instability in different models of biofilaments in both the linear and non-linear regimes of elasticity.

The basic elements of linear elasticity and the physics of individual worm-like chain or in bundles are presented in chapter 2. Chapter 3 is devoted to the general theory of buckling as the basic idea of this thesis is related to self-buckling. Chapter 4 presents the physical and biological properties of the biofilaments of the cytoskeleton and some key experiments that support our theoretical work. In chapter 5 I have tried to review the general notions of ground state, symmetry breaking in order to place them in the context of biophysics. This chapter also presents the basic ideas underlining the confotronic's theory. This chapter can give a new and wider perspective on the physics of biofilaments. The last three chapters, 6 to 8, present my work on the elastic instability and spontaneous symmetry breaking induced by surface stresses.

This field of research was totally unknown to me when I started this project, so I decided to write a story that tells all the topics I have learnt on the road to the results presented here. As a teacher, I have tried to write a very pedagogical thesis with all necessary concepts introduced in the beginning of every chapter. It is my hope than, in this manner, the thesis can also be readable for beginners in this field, like I was when I started.

Chapter 2

Hooke's law, worm-like chain and bundle

This thesis is about elastic instabilities in fibrous structures with an emphasis on biofilaments, especially those of the cytoskeleton of cells. This idea comes from the observation that biofilaments although intrinsically rigid (we will define this concept more precisely) at scales considered, can spontaneously form very curved, sometimes circular and even helicoidal shapes. All these shapes rely on elasticity theory.
In this introductory chapter, we will start from the very beginning of elasticity theory by defining the linear regime of elasticity or the Hooke's regime (in contrast to the non-linear elasticity theory, discussed in chapter (8) of springs and strings. Although Hooke's theory is applicable to the study of small deformations of macroscopic elastic rods, usually it is not the case for biofilaments. Those are microscopic filaments that live in a finite temperature environment (in vivo and in vitro) and are therefore submitted to thermal fluctuations. Temperature driving elastic deformations of biofilaments have been proven to be well described by the model of semi-flexible chain also called worm-like chain. Its basic properties are recalled in this chapter. Since biomolecules are often bundles of individual filaments we will also introduce the railway-track model, a bundle of two semi-flexible chains that turns out to be at the core of this thesis.

2.1 Hooke's law

During the 17^{th} century, Robert Hooke studied the laws of elasticity and tried to find a relationship between the size (or displacement) of the deformation and the magnitude of the force exerted on the material.
He stated that, for relatively small deformations of an object, **the size of the deformation is proportional to the force exerted on the object**. He also stated that the object returns to its original size once the force stops acting.
When he published his law, he use a Latin anagram (ceiiinosssttvu) that he didn't explain before being sure that the law could be proved through spring experiments.
We will first study this law, using springs and strings.

Home made experiments with springs

Here we use a spring and several masses in order to measure both the elongation of the spring and the force exerted. To get the force, we have two options : either using a dynamometer or calculating the weight corresponding to the mass ($P = mg$).

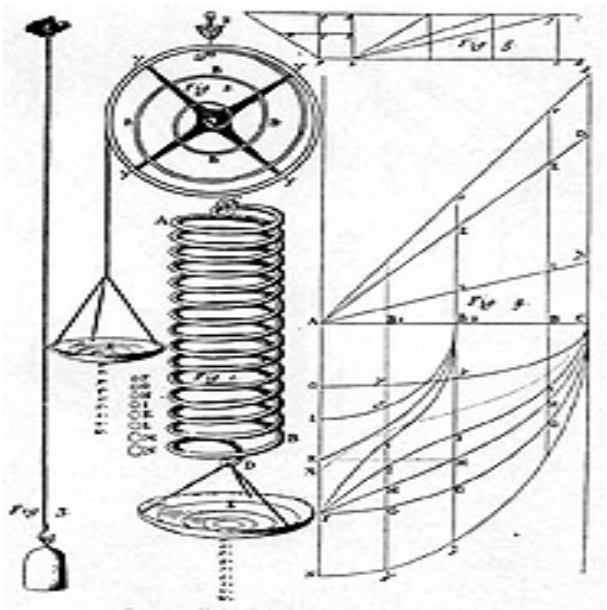

(A) Hooke's experiment

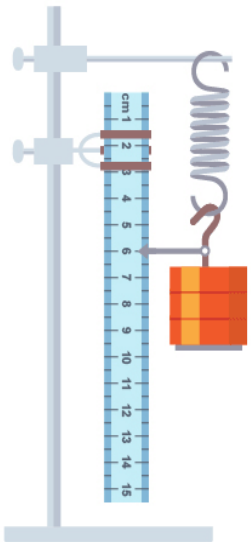

(B) My experiment

FIGURE 2.1: Two set-ups for the experiment

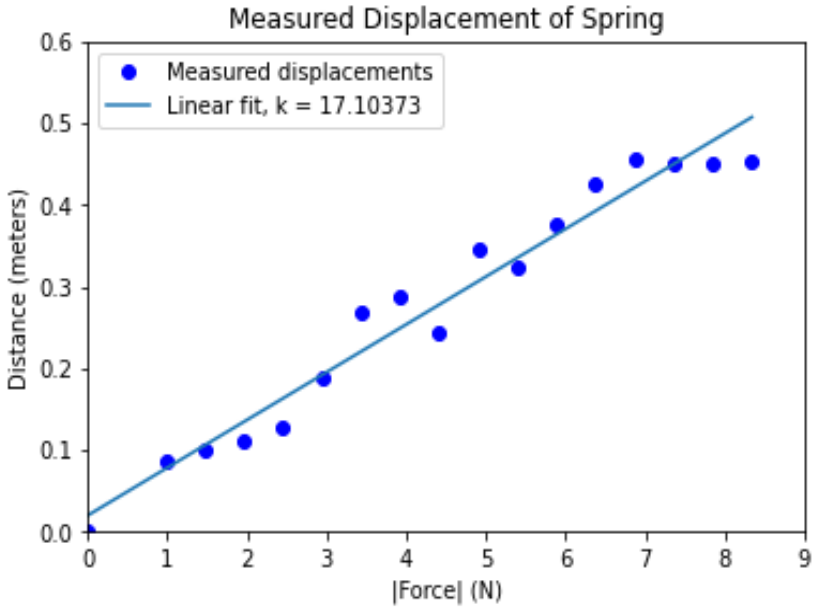

FIGURE 2.2: Row data and model of Hooke's law

The results go in the direction of Hooke: the points are globally aligned, highlighting the fact that the elongation is proportional to the tension exerted on the spring. The directing coefficient of the line, k, was named after the coefficient found by Young in 1802 whose name is **Young's modulus**. We will use it later in this paper where it will be written Y.
One could assume that this linearity will be found in the case where the mass should increase significantly. However the experiment does not go in this direction:

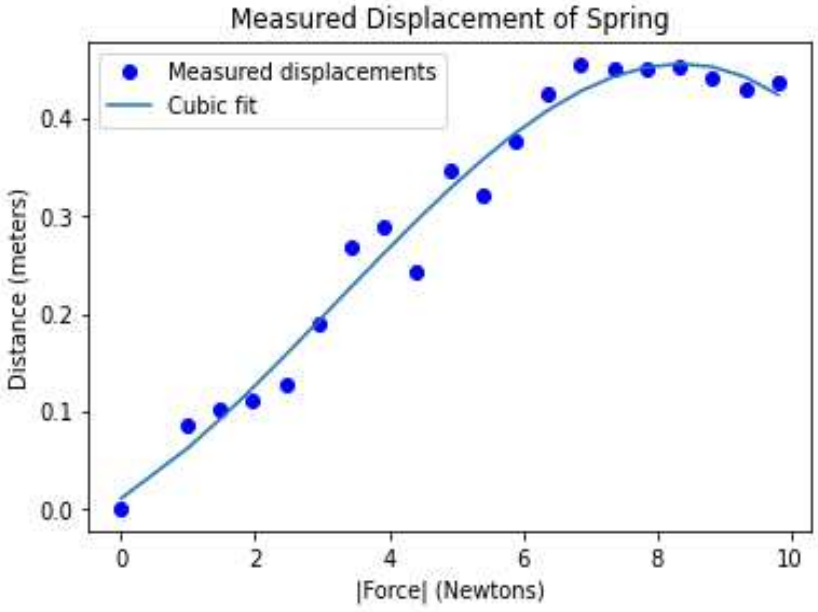

FIGURE 2.3: Domain of non linearity of Hooke's law

Those results show that, with **larger forces**, the length of the spring doesn't evolve and the spring, at rest, doesn't go back to its initial length. This part of the graph is called the plastic part.

The study of bio filaments will restrict us to the elastic domain.

Home made experiments with strings

In order to study a continuous macroscopic object with properties close to those of a biological filament, we need to look at stretchable wires that could undergo the same type of stress. The goal is to show that these wires behave like springs, having two domains (elastic and plastic). I choose to use horse-hair and fish-wire.

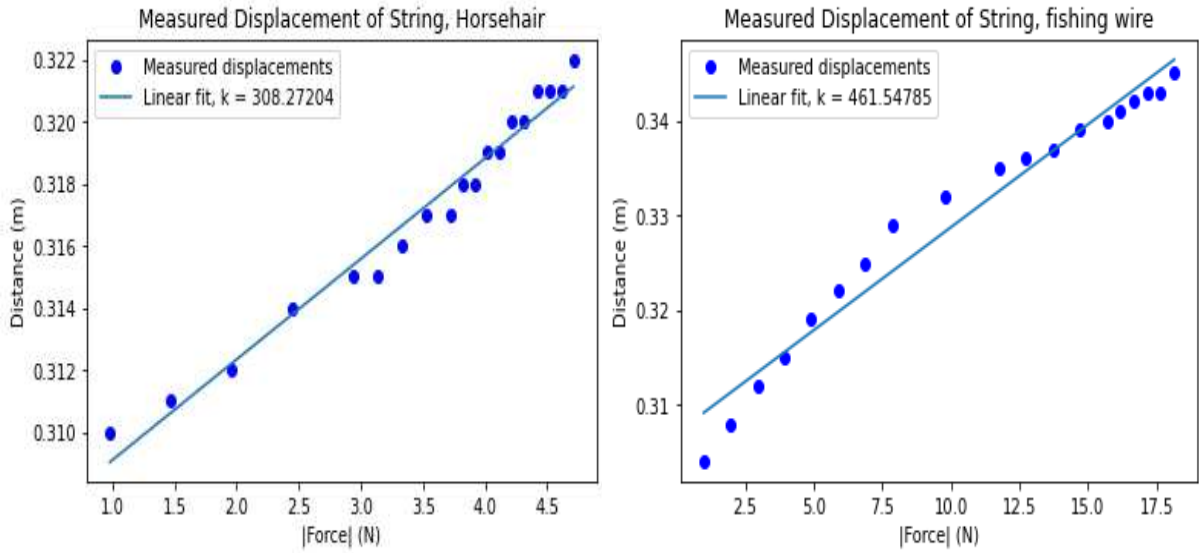

(A) Hooke's law for horse-hair

(B) Hooke's law for fishing-wire

As expected we clearly observe the elastic behavior of the two studied wires.

In this thesis we are interested in solid bodies and wish to define the changes in shape and volume resulting from the application of forces on the studied solid. We will thus rely on the contents of the theory of elasticity.

2.2 Hooke's law, general formula

Within the framework of the theory of elasticity, we will define (using [1]) the mathematical relationship between the stress tensor and the strain tensor which must be of the same type as the one obtained in the first part with a relationship of proportionality between the applied force and the elongation of the body studied. We will continue to work in the elastic domain of Hooke's law, i.e. with small deformations.
With this in mind, we will express the elastic energy in terms of the deformation tensor. This equation will then be used to link stress and strain tensors.

2.2.1 Elastic energy

The components of the strain tensor and the stress tensor are, respectively ε_{ik} and σ_{ik}. We study a body which is not deformed when no external force is applied, the temperature being constant throughout the whole body. First, we can show that, if the bar is not deformed (i.e $\varepsilon_{ik} = 0$), the internal stresses are also zero : $\sigma_{ik} = 0$. Since $\sigma_{ik} = \frac{\partial E}{\partial \varepsilon_{ik}}$ we can deduce that there will be no linear terms in the expansion of E in powers of ε_{ik}. We also know that the energy E is a scalar then each term in the expansion of E is also a scalar.
We can have two independents scalar using the symmetrical tensor ε_{ik} :the squared sum of the diagonal components, ε_{ii}^2, and the sum of the square of all the components, ε_{ik}^2. Thus E, **the elastic energy of a deformed isotropic body** can be written as :

$$E = E_0 + \frac{1}{2}\lambda\varepsilon_{ii}^2 + \mu\varepsilon_{ik}^2. \tag{2.1}$$

The quantities λ and μ are called *Lame coefficients*, they are factors which are typical of the elasticity of a material. We can not get them directly through experiments. Since any **deformation can be represented as the sum of a pure shear and a hydrostatic compression**, the strain can be given by :

$$\varepsilon_{ik} = (\varepsilon_{ik} - \frac{1}{3}\delta_{ik}\varepsilon_{ll}) + \frac{1}{3}\delta_{ik}\varepsilon_{ll}. \tag{2.2}$$

Indeed, it is more convenient to decompose any deformation into a pure shear and a hydrostatic compression. That is also why we will change (2.1) by taking, as independent scalars of second degree, the sum of the squared components defined in (2.2).
The equation of elastic energy becomes :

$$E = \mu(\varepsilon_{ik} - \frac{1}{3}\delta_{ik}\varepsilon_{ll})^2 + \frac{K}{2}\varepsilon_{ll}^2, \tag{2.3}$$

with

$$K = \lambda + \frac{2}{3}\mu. \tag{2.4}$$

2.2.2 Stress tensor

The components of the stress can be found using E, more precisely by differentiating this energy:

$$\sigma_{ik} = \frac{\partial E}{\partial \varepsilon_{ik}}, \tag{2.5}$$

then, all the $\frac{\partial E}{\partial \varepsilon_{ik}}$ must be calculated.
In order to do so, first we write the total differential dE and try to bring out $d\varepsilon_{ik}$

$$dE = 2\mu(\varepsilon_{ik} - \frac{1}{3}\delta_{ik}\varepsilon_{ll})d(\varepsilon_{ik} - \frac{1}{3}\delta_{ik}\varepsilon_{ll}) + K\varepsilon_{ll}d\varepsilon_{ll}. \tag{2.6}$$

In the first term, $d(\varepsilon_{ik} - \frac{1}{3}\delta_{ik}\varepsilon_{ll})$ can be split into two parts : $d\varepsilon_{ik}$ and $-\frac{1}{3}\delta_{ik}\varepsilon_{ll}$. If we multiply $(\varepsilon_{ik} - \frac{1}{3}\delta_{ik}\varepsilon_{ll})$ by δ_{ik}, we will always get zero. Then (2.6) becomes :

$$dE = 2\mu(\varepsilon_{ik} - \frac{1}{3}\delta_{ik}\varepsilon_{ll})d\varepsilon_{ik} + K\varepsilon_{ll}d\varepsilon_{ll}, \tag{2.7}$$

as $d\varepsilon_{ll}$ can also be written $\delta_{ik}d\varepsilon_{ik}$, we get :

$$dE = [2\mu(\varepsilon_{ik} - \frac{1}{3}\delta_{ik}\varepsilon_{ll}) + K\delta_{ik}\varepsilon_{ll}]d\varepsilon_{ik}. \tag{2.8}$$

Then we see the stress tensor σ_{ik} defined as the ratio $\frac{\partial E}{\partial \varepsilon_{ik}}$

$$\sigma_{ik} = 2\mu(\varepsilon_{ik} - \frac{1}{3}\delta_{ik}\varepsilon_{ll}) + K\delta_{ik}\varepsilon_{ll}. \tag{2.9}$$

The relation between σ_{ik} and ε_{ik} is determined only by μ (rigidity or shear modulus) if the deformation is a pure shear and by K (compression or bulk modulus), if the deformation is a pure hydrostatic compression.

2.2.3 Strain tensor

The final step is to find the equation of the strain tensor in terms of stress tensor, i.e, ε_{ik} in terms of σ_{ik}. The sum of the diagonal terms σ_{ii} is, using (2.9) :

$$\sigma_{ii} = 3K\varepsilon_{ii} + 2\mu(\varepsilon_{ii} - \frac{1}{3} \times 3\varepsilon_{ii}), \tag{2.10}$$

where we use the fact that $\delta_{ii} = 3$, leading to :

$$\sigma_{ii} = 3K\varepsilon_{ii}, \tag{2.11}$$

because the second term is zero. Then :

$$\varepsilon_{ii} = \frac{\sigma_{ii}}{3K}. \tag{2.12}$$

If we substitute (2.12) into (2.9), we get

$$\sigma_{ik} = 2\mu(\varepsilon_{ik} - \frac{1}{3}\delta_{ik}\frac{\sigma_{ll}}{3K}) + K\delta_{ik}\frac{\sigma_{ll}}{3K}. \tag{2.13}$$

Now we can isolate ε_{ik} in order to express it in terms of σ_{ll} and σ_{ik} :

$$\varepsilon_{ik} = \frac{(\sigma_{ik} - \frac{1}{3}\delta_{ik}\sigma_{ll})}{2\mu} + \frac{\delta_{ik}\sigma_{ll}}{9K}. \tag{2.14}$$

Consequences

- Relative change in volume (ε_{ii}) only depends on the sum of the diagonal components of the stress tensor, according to (2.12), ε_{ii} and σ_{ii} are linked together with K (modulus of hydrostatic compression)
- In hydrostatic compression the stress tensor is $\sigma_{ik} = -p\delta_{ik}$ so that (2.12) becomes

$$\varepsilon_{ii} = -\frac{p}{K} \tag{2.15}$$

Eq (2.14) shows that the strain tensor ε_{ik} is a linear function of the stress tensor σ_{ik} meaning **that deformation is proportional to the applied force**, we thus find Hooke's law.

2.3 The worm-like chain model

The worm-like chain or semi-flexible chain model is the basic model for any theoretical study of biological filaments. It has proven to be particularly valid for the interpretation of micromanipulation experiments on the DNA molecule. We will see that the experimental results on microtubules and intermediate filaments present anomalies that require the development of more complex models that include internal degrees of freedom of the subunit coupled to the elasticity of filaments (see chapter 6). But, for now, we start our road with the description of filament's shapes.

2.3.1 Elasticity of non extensible filaments

The Frenet-Serret base and its extension, the director frame, are the essential elements for the description of three dimensional curves.

The Frenet-Serret frame

The shape of an elastic rod can be described by the spatial evolution of the orthonormal vectorial Frenet-Serret frame $(\mathbf{n}, \mathbf{b}, \mathbf{t})$ attached to the centerline of the rod.

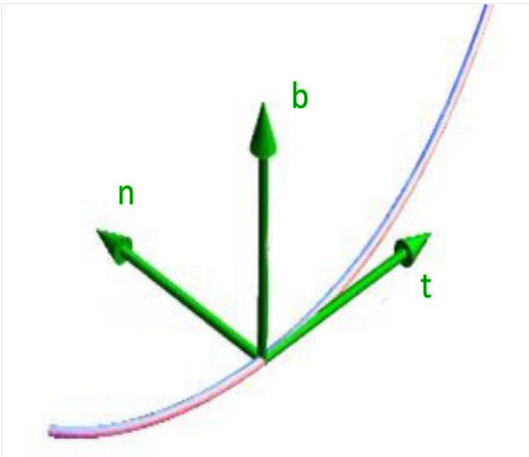

FIGURE 2.5: Local Serret-Frenet frame $(\mathbf{n}, \mathbf{b}, \mathbf{t})$ attached at a position s of the centerline of the rod.

The spatial position of the centerline is given by a vector $\mathbf{r}(s)$ with respect to an external frame, where s is the arc-length along the curve. The curve's tangent vector $\mathbf{t}$ of the Frenet-Serret frame is obtained by differentiating the position vector

$$\mathbf{t} = \frac{d\mathbf{r}(s)}{ds} \equiv \mathbf{r}'(s) \tag{2.16}$$

where $(')$ denotes the derivative with respect to s. Since s is the arc-length of the rod it satisfies the relation $ds^2 = d\mathbf{r} \cdot d\mathbf{r}$ resulting in the condition $\mathbf{t}^2 = 1$. By differentiating this relation we obtain that $\mathbf{t}'$ is normal to the tangent vector :

$$\mathbf{t}'(s) = \kappa(s)\,\mathbf{n}(s) \tag{2.17}$$

where κ, the magnitude of $\mathbf{t}'$, is also **the curvature at position** s and the unit vector $\mathbf{n}$ is called the normal vector. The third unit vector $\mathbf{b}$ called the binormal vector is defined as

$$\mathbf{b} = \mathbf{t} \times \mathbf{n} \tag{2.18}$$

and is perpendicular to the plan defined by $\mathbf{t}$ and $\mathbf{n}$, called the osculating plane. Note that the radius of curvature, $R = 1/\kappa$, corresponds to a circle in the osculating plane that is tangent to the curve at the position $\mathbf{r}(s)$.
Since $\mathbf{b}^2 = 1$ we deduce that $\mathbf{b}'$ belongs to the osculating plane. Since $\mathbf{b}$ and $\mathbf{t}$ are orthogonal we have :

$$0 = (\mathbf{b} \cdot \mathbf{t})' = \mathbf{b}' \cdot \mathbf{t} + \mathbf{b} \cdot \mathbf{t}' \tag{2.19}$$

thus

$$\mathbf{b}' \cdot \mathbf{t} = -\mathbf{b} \cdot \mathbf{t}' = -\kappa \mathbf{b} \cdot \mathbf{n} \tag{2.20}$$

and consequently $\mathbf{b}'$ is orthogonal to $\mathbf{t}$, and thus parallel to $\mathbf{n}$,

$$\mathbf{b}' = -\tau \mathbf{n} \tag{2.21}$$

where τ is called the local torsion of the curve and the minus sign is a convention. For a planar curve, the torsion τ is zero, **therefore the torsion is a local measurement of how much a curve deviates from being planar**.
For a full description of the variation of the Frenet-Serret triad $(\mathbf{n}, \mathbf{b}, \mathbf{t})$ along the filament we consider the variation of the principal normal vector $\mathbf{n}$. Since $\mathbf{n}$ and $\mathbf{t}$ are orthogonal we have :

$$0 = (\mathbf{n} \cdot \mathbf{t})' = \mathbf{n}' \cdot \mathbf{t} + \mathbf{n} \cdot \mathbf{t}', \tag{2.22}$$

thus

$$\mathbf{n}' \cdot \mathbf{t} = -\mathbf{n} \cdot \mathbf{t}' = -\kappa, \tag{2.23}$$

and in the same manner

$$0 = (\mathbf{n} \cdot \mathbf{b})' = \mathbf{n}' \cdot \mathbf{b} + \mathbf{n} \cdot \mathbf{b}', \tag{2.24}$$

thus

$$\mathbf{n}' \cdot \mathbf{b} = -\mathbf{n} \cdot \mathbf{b}' = \tau, \tag{2.25}$$

and we conclude that

$$\mathbf{n}' = -\kappa\mathbf{t} + \tau\mathbf{b}. \tag{2.26}$$

The evolution the Frenet-Serret triad $(\mathbf{n}, \mathbf{b}, \mathbf{t})$ is often written in a matrix form :

$$\frac{d}{ds}\begin{pmatrix} \mathbf{n} \\ \mathbf{b} \\ \mathbf{t} \end{pmatrix} = \begin{pmatrix} 0 & \tau & -\kappa \\ -\tau & 0 & 0 \\ \kappa & 0 & 0 \end{pmatrix}\begin{pmatrix} \mathbf{n} \\ \mathbf{b} \\ \mathbf{t} \end{pmatrix} \tag{2.27}$$

An alternatively way to express the Frenet-Serret frame evolution is by the introduction of the Darboux vector :

$$\mathbf{D} = \kappa\mathbf{b} + \tau\mathbf{t} \tag{2.28}$$

such that

$$\begin{aligned} \mathbf{n}' &= \mathbf{D} \times \mathbf{n} \\ \mathbf{b}' &= \mathbf{D} \times \mathbf{b} \\ \mathbf{t}' &= \mathbf{D} \times \mathbf{t} \end{aligned} \tag{2.29}$$

This formulation is analog to the description of the time evolution of a solid where vector $\mathbf{D}$ is the instantaneous angular velocity. From its definition it rotates with velocity τ and κ around the vectors $\mathbf{t}$ and $\mathbf{b}$ respectively.
In order to find the evolution of the triad as it moves along curve, we can integrate Eq.(2.29) knowing the initial conditions $(\mathbf{n}(s_0), \mathbf{b}(s_0), \mathbf{t}(s_0))$ and the darboux vector $\mathbf{D}(s)$ for all values of the arc length s. The profile of the curve is then given by integrating $\mathbf{t}(\mathbf{s}) = \mathbf{r}'(s)$ with initial condition $\mathbf{r}(s_0)$.

The director frame

The Frenet-Serret frame of an Euler rod has an intrinsic limitation. It cannot describe the internal twist degree of freedom of a rod. Indeed if you rotate the end of a straight rod that is attached at the other end, the rod twists around its center line axis. It means that at each position s the material cross-section itself rotates around the tangent vector $\mathbf{t}$. To keep track of the rotation of the material cross section around $\mathbf{t}$ another orthonormal frame $(\mathbf{e}_1, \mathbf{e}_2, \mathbf{e}_3)$ which rotates with the material is generally introduced.

This **material frame or director frame** $(\mathbf{e}_1, \mathbf{e}_2, \mathbf{e}_3)$ can be written in terms of the Frenet-Serret frame as :

$$\begin{aligned}\mathbf{e}_1 &= \mathbf{n}\cos\psi + \mathbf{b}\sin\psi,\\ \mathbf{e}_2 &= -\mathbf{n}\sin\psi + \mathbf{b}\cos\psi,\\ \mathbf{e}_3 &= \mathbf{t}\end{aligned}$$

where ψ is called the twist angle. While torsion τ describes the rotation of the Frenet-Serret frame about $\mathbf{t}$ for a non-planar shape, the twist defined as ψ' describes the rotation of the material frame about $\mathbf{t}$.

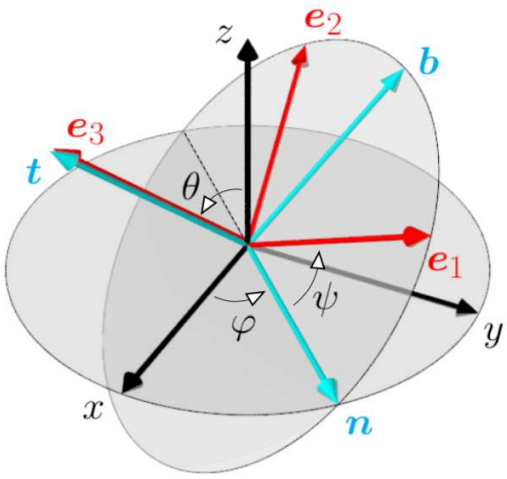

FIGURE 2.6: Adapted from [2]. Representation of the Frenet-Serret basis, the director basis and the Euler angles at a position s of the centerline of a twisted rod.

The vectors $\mathbf{e}_1, \mathbf{e}_2$ belong to a cross-section plane and they rotate with the material along the rod. The director frame is defined relative to some arbitrary reference configuration given by a chosen constant value of $\psi = \psi_0$. Although it is arbitrary, the reasonable choice for the reference configuration is the stress-free one, i.e. the configuration in the absence of external force and torque. The evolution of this basis along the centerline, described by the arc length s, is given by the twist equations :

$$\mathbf{e}_i' = \mathbf{\Omega} \times \mathbf{e}_i \tag{2.30}$$

where $\mathbf{\Omega} = (\Omega_1, \Omega_2, \Omega_3)$ is the strain vector function.
The components of $\mathbf{\Omega}$ are [3]:

$$\Omega_1(s) = \kappa(s) \sin \psi(s) \,, \tag{2.31a}$$
$$\Omega_2(s) = \kappa(s) \cos \psi(s) \,, \tag{2.31b}$$
$$\Omega_3(s) = \tau(s) + \psi'(s) \,, \tag{2.31c}$$

where $\kappa(s) \geq 0$ and $\tau(s)$ are the local curvature and torsion, respectively.
The local curvature is thus $\kappa^2(s) = \Omega_1^2 + \Omega_2^2$ and the twist density $\Omega_3(s)$ is the sum of the torsion and the excess twist ψ'.

$$\Omega_1 = \kappa \sin \psi \,, \tag{2.32a}$$
$$\Omega_2 = \kappa \cos \psi \,, \tag{2.32b}$$
$$\Omega_3 = \tau + \psi' \,. \tag{2.32c}$$

Elastic energy in Hooke's regime

The elastic energy of a rod whose shape is described in the director frame can be obtained by a Ginzburg-Landau type expansion

$$E = \sum B_{ij} \Omega_i \Omega_j + \sum A_{ijk} \Omega_i \Omega_j \Omega_k + ..., \tag{2.33}$$

the elastic constants being allowed by looking at the symmetries. The stress vectors on the rod are defined by the derivative of the energy as

$$T_i = \frac{\delta E}{\delta \Omega_i}. \tag{2.34}$$

As we have seen in the previous section, linear elasticity or Hooke's elasticity is a regime where stresses are proportional to the strains, i.e.;

$$T_i = \sum B_{ij} \Omega_j. \tag{2.35}$$

In this chapter we will only consider the linear regime of small deformations (see chapter 8 for the nonlinear elastic regime) and therefore limit ourself to the quadratic terms in the expansion of Eq. (2.33) :

$$E = \sum B_{ij} \Omega_i \Omega_j. \tag{2.36}$$

As an example, in the linear elasticity theory, an isotropic cylindrical rod, the straight, untwisted rod ψ', minimizes the elastic energy

$$E = \int_0^L \left(\frac{B}{2}\kappa^2(s) + \frac{C}{2}\tau^2(s) \right) ds, \tag{2.37}$$

with a **bending modulus** (or bending stiffness) **B** and **torsion modulus C**. The ground state is the shape that minimizes the elastic energy, Eq. (2.37), and is the shape of the filament at zero temperature (purely elastic). In a finite temperature environment the filament will fluctuate around the ground state shape. The study of the thermal properties of elastic filament is done in the frame of the statistical mechanics.

Another example is provided by the helical rod, whose shape is obtained by minimizing the following energy

$$E = \int \frac{B}{2} \left((\Omega_1 - \omega_1)^2 + (\Omega_2 - \omega_2)^2 \right) + \frac{C}{2} (\Omega_3 - \omega_3)^2 \, ds \, , \tag{2.38}$$

The positive constant parameters ω_1 and ω_2 are the principal intrinsic curvatures and ω_3 the intrinsic twist.
This ground state is a helix of radius R and pitch H with

$$R = \frac{\omega_1}{\omega_1^2 + \omega_3^2} \qquad \text{and} \qquad H = \frac{2\pi\omega_3}{\omega_1^2 + \omega_3^2} \, , \tag{2.39}$$

satisfying the preferred curvature and twist everywhere.

The worm-like chain used as a model for biofilaments is based on the theory of inextensible thin rods where the elastic deformations are thermally induced by an external environment. An extensible filament which can be stretched or compressed is very conveniently modeled by considering the linear theory of elasticity of a straight rod.

2.3.2 Extensible filament

The general definition of the elastic energy is

$$E = \frac{1}{2}\int dV \sigma_{ij}\varepsilon_{ij}, \tag{2.40}$$

where σ_{ij} is the stress tensor and ε_{ij} the strain tensor of the elastic object considered. We consider a homogeneous isotropic rod of constant cross-section, **initially straight,** and in the absence of twist, we expect two contributions to the stress : a **bending contribution, with local curvature κ and an extension/compression contribution due to a stress σ.**
Therefore a good ansatz seems to be:

$$\sigma_{zz} = Y\kappa x + \sigma, \tag{2.41}$$

with Y the Young modulus and σ a constant and uniform stress. We have introduced a fixed frame where z is parallel to the rod's centerline and the bending of the rods is supposed to be done in the x-direction. All other components of the stress are zero. The strain tensor is thus given by

$$\begin{aligned}\varepsilon_{zz}(x,y) &= \sigma_{zz}/Y = \kappa(z)x + \varepsilon(z)\\ \varepsilon_{xx} &= -\nu\kappa(z)x - \nu\varepsilon(z)\\ \varepsilon_{yy} &= -\nu\kappa(z)x - \nu\varepsilon(z)\end{aligned}$$

where we introduced $\varepsilon = \frac{\sigma}{Y}$, a stretching strain and ν, Poisson ratio. The energy of the rod reads then :

$$E = \frac{1}{2}\int dV \sigma_{zz}\varepsilon_{zz} = \frac{1}{2}Y\int dV \varepsilon_{zz}^2 = \frac{1}{2}Y\int dxdydz(\kappa x + \varepsilon)^2 \tag{2.42}$$

or

$$E = \frac{1}{2}Y\int\left(\kappa^2\int dx x^2\int dy\right)dz + \frac{1}{2}Y\int\left(\varepsilon^2\int dxdy\right)dz + Y\int\left(\kappa\varepsilon\int xdx\int dy\right)dz \tag{2.43}$$

Introducing the notations

$$B = Y \int dx x^2 \int dy$$
$$A = Y \int dx dy$$
$$D = Y \int x dx \int dy$$

and choosing a symmetrical cross-section $D = 0$, the energy reads

$$E = \frac{1}{2} B \int_0^L \kappa^2 dz + \frac{1}{2} A \int_0^L \varepsilon^2 dz \tag{2.44}$$

As a practical example, let's consider a rod with a circular cross-section of radius R. The coordinates, in a polar frame, are $x = r\cos\phi$ and $y = r\sin\phi$ with $\phi \in [0, 2\pi]$ we obtain for the bending stiffness the expression

$$B = \frac{\pi}{4} Y R^4 \tag{2.45}$$

and

$$A = \pi R^2 Y \tag{2.46}$$

for the compressional modulus A.
The energy Eq. (2.44) of the elastic rod is not the same as the energy of the worm-like chain, Eq. (2.37) with $C = 0$, in that it contains a stretching contribution in addition to the bending one. Such a stretching term is not possible neither in the Frenet-Serret nor in the director frame approach as the tangent vector satisfies the inextensibility constrain of the rod $|\mathbf{t}| = 1$. Therefore, from Ginzburg-Landau type expansion one has to add by hand a stretching energy term if we want to study a semi-flexible stretchable filament. If we go back to the director frame approach, another expression of the energy can be obtained by introducing the local displacement $u(s)$ as an additional variable.
If $u(s) = u_0$ is constant, then the rod is translated as a whole for free. The constant translation mode is a zero mode. By definition the local strain is related to the displacement u by :

$$\varepsilon = u'(s). \tag{2.47}$$

The energy of an extensible worm-like chain Eq. (2.44) can also be written:

$$E = \frac{1}{2}B\int_0^L \kappa^2 ds + \frac{1}{2}A\int_0^L (u')^2 ds \tag{2.48}$$

The filament conformation that minimizes this energy is obviously the relaxed $\varepsilon = 0$ straight state $\kappa = 0$. In the next section we review the statistical physics of an inextensible ($\varepsilon = 0$) semi-flexible chain under tension as a model for the study of the extension of DNA. The statistical properties of the full model Eq. (2.48) with an additional external force has been studied in [4].

2.3.3 Statistical physics of a semi-flexible chain (DNA) under tension

The DNA molecule is a double helix molecule that codes the genetic information of all cells. But DNA also has specific mechanical properties that allow the protein machinery to work efficiently during transcription, replication, repair and condensation of DNA [5]. In the past decades, progress on single DNA experiments allowed biophysicists to probe the elastic properties of DNA [6]. In these micromanipulation experiments, one uses several types of techniques (atomic force microscopes (AFM) [7],magnetic beads [8], [9],optical traps [10][11], hydrodynamic flows [12]) to measure the extension of a molecule as a function of the applied force. Thus, interactions between DNA and protein's complex were proven [13].

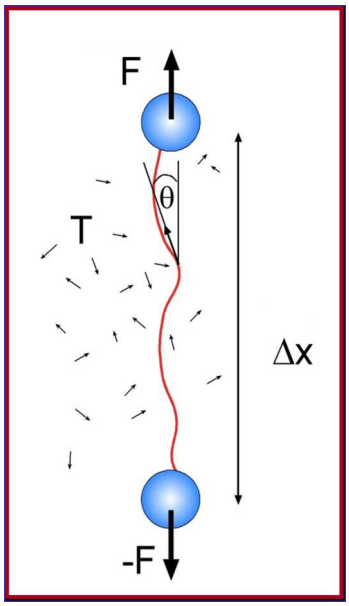

FIGURE 2.7: A single DNA molecule under external force in an environment at finite temperature.

Using the semi-flexible chain model [14] (also called the worm-like chain) was the best way to describe and interpret these experiments involving DNA [15]. With this model we have a hyper-simplified representation of DNA : all microscopic details are eliminated in favor of **the persistence length** $l_p = B/k_BT$ where T is the temperature and k_B is the Boltzmann constant. **This length gives an idea of the rigidity of the molecule** and depends on the temperature. At low enough T, thermal fluctuations are suppressed, l_p tends to grow and the filament straightens. In this regime, one can use the semi-classical approach where only small fluctuations around the ground state configuration are taken into account in the evaluation of the partition function as large fluctuations are suppressed by the Boltzmann weight. Instead high temperature induces large elastic fluctuations of the chain, l_p shrinks and the Boltzmann weight is dominated by deformations with large amplitudes with respect to the ground state. The semi-flexible chain behaves then like a flexible polymer.

The worm-like chain is the basic model for the theoretical interpretations of DNA and most biofilaments in micromanipulation experiments. For instance DNA shows an extensional force curve characteristic of this model. The measured extension- force curve can be understood in terms of the suppression of entropic fluctuations (temperature dependent) of the chain with increasing applied tension and allow to determine the persistence length of biomolecules.

We will see later that the worm-like chain is not relevant for the interpretation of experiments with microtubule. The partition function of a DNA strand under tension can be written as follows [16]:

$$Z(\mathbf{F},L,T) = \int \delta\left(\underline{\mathbf{t}}^2 - 1\right) \mathcal{D}^3\left[\underline{\mathbf{t}}\right] e^{-\beta E[\underline{\mathbf{t}}]}, \tag{2.49}$$

with for the elastic energy of (inextensible) DNA of length L stretched by an external force $\mathbf{F}$:

$$E\left[t\right] = \int_0^L \left(\frac{B}{2}\left(\frac{d\mathbf{t}}{ds}\right)^2 - \mathbf{F}\cdot\mathbf{t}\right) ds, \tag{2.50}$$

with $\mathbf{t}\left(s\right) = \frac{d}{ds}\mathbf{r}\left(s\right)$ is the tangent vector to the curve $\mathbf{r}\left(s\right)$ which describes the position of the DNA filament. The delta function imposes the condition $\mathbf{t}^2\left(s\right) = 1$ in the partition function and ensures the inextensibility of the molecule. This condition sometimes complicates the evaluation of the partition function, but it turns out that it can be relaxed in the semi-classical approximation method. Note that we have not considered the twisting degree of freedom of DNA around itself. This is justified in the absence of external torsions exerted on the molecule. Micromanipulation experiments have determine that for DNA, $l_P \approx 50nm$ at room temperature while for the filaments of the cytoskeleton persistence lengths are much larger : for instance, for actin and intermediate filament $l_P \sim \mu m$ and for microtubules $l_P \sim mm$. The semi-classical evaluation of the partition function Z gives the following result:

$$Z(F,L,T) = \frac{\beta\sqrt{BF}}{2\pi} e^{\beta F L} \sinh^{-1}\left(L\sqrt{\frac{F}{B}}\right). \tag{2.51}$$

From the free energy of the system $G(F,L,T) = -\frac{1}{\beta}\ln Z(F,L,T)$ we can deduce the force-extension relation from :

$$\langle \Delta x \rangle = -\partial G/\partial F. \tag{2.52}$$

In the particularly interesting regime of large forces, $L/\lambda \gg 1$ results in the expression:

$$F \approx \frac{k_B T}{4 l_P} \frac{1}{\left(1 - \langle \Delta x \rangle / L\right)^2}. \tag{2.53}$$

This relation is of entropic origin as indicated by the proportionality in temperature. It is very important because it allows to determine directly and precisely the persistence length of DNA by micromanipulation experiments under various conditions [6].

2.4 The railway track model

As already mentioned biofilaments of the cytoskeleton have a high bending stiffness with persistence lengths l_p varying from μm to mm in sharp contrast to synthetic polymers where usually $l_p \sim nm$. In article [17], the authors were investigating if bundles of individual filaments could explain the high flexural rigidity of biomolecules. The model introduced by [17] is a planar shearable bundle with two identical semi-flexible filaments denoted 1 and 2 of length L and bending stiffness B that are cross-linked by an inextensible transverse materials, thus fixing the inter-filament distance a.

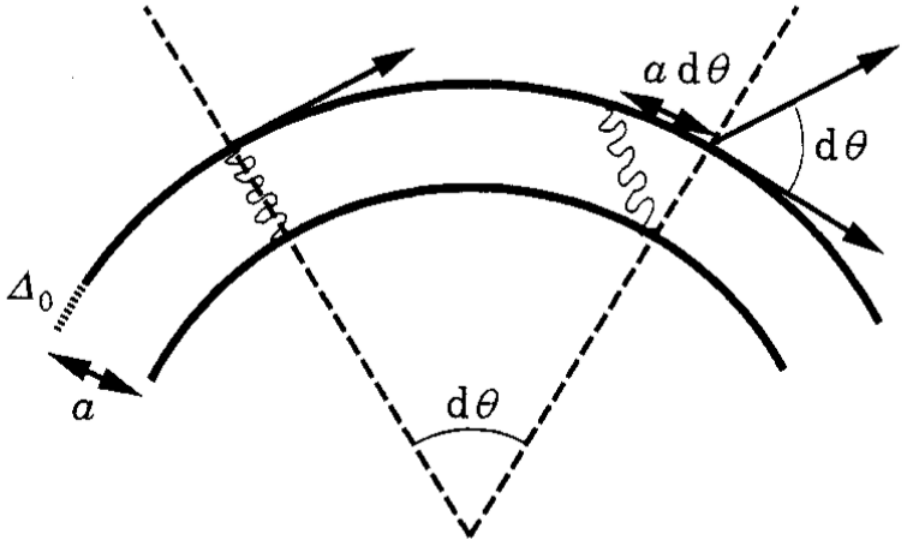

FIGURE 2.8: Railway track model with figure realized from [17] which shows the arc-length mismatch induced by bending of the bundle.

In this section we extend this so called railway-track model by considering extensible filaments. This model will be at the core of chapter 6. Since the bending energy for both filaments is the same during bending, the part of the filaments between the cross links having the same curvature, $\kappa_1 = \kappa_2 = \kappa$, the bending energy is two times the bending energy contribution of a single worm-like chain,

$$E_{bend} = B \int_0^L \kappa^2 ds. \tag{2.54}$$

In two dimensions we have (See Fig 2.8)

$$\kappa = \frac{d\theta}{ds}, \tag{2.55}$$

where θ is the angle with the tangent vector $\mathbf{t}$ and the bundle longitudinal axis. The bending energy therefore reads

$$E_{bend} = B\int_0^L \left(\theta'\right)^2 ds. \tag{2.56}$$

The energy term which accounts for the compression/stretching of the filament is (see section 2.3.2)

$$E_{stretch} = \frac{A}{2}\int_0^L (u_1')^2 ds + \frac{A}{2}\int_0^L \left(u_2'\right)^2 ds, \tag{2.57}$$

where A is the single filament compression/stretching stiffness. The third energy contribution results from cross-links-induced coupling of the filaments. The cross-links suppress the shear energy due to the relative sliding motion induced by bundle bending. This shear energy which can partially be compensated by filament stretching, is given by the following expression:

$$E_{shear} = \frac{K_s}{2}\int_0^L ds\Delta^2, \tag{2.58}$$

where K_s is the shear stiffness. The shear displacement Δ is related to the difference of filaments displacements $u_2 - u_1$ and a curvature induced additional displacement via

$$\begin{aligned}\Delta(s) &= u_2(s) - u_1(s) + a\int_0^s \kappa(s)ds \\ &= u_2(s) - u_1(s) + a\left(\theta(s) - \theta(0)\right),\end{aligned}$$

where a is the interdistance between the filaments.

2.4.1 Statistical properties

At finite temperature the statistical properties of this model are very interesting. We introduce the Fourier transform of $\theta(s)$ and $u_i(s)$ with $i = 1, 2$:

$$\theta(s) = \sum_n \theta_n \sin\left(\frac{n\pi s}{L}\right) \quad \text{and} \quad u_i(s) = \sum_n u_{i,n}\sin\left(\frac{n\pi s}{L}\right), \tag{2.59}$$

and compute the partition function Q by first integrating on the Fourier mode $u_{i,n}$ which leads us to the following expression

$$Q = \int D\theta_q \exp\left(-\frac{1}{k_B T}\left(\frac{L}{2}\sum_q G^{-1}(q)\theta_q^2\right)\right), \tag{2.60}$$

where we introduced the wave vectors $q = \frac{n\pi}{L}$. In Eq. (2.60) the propagator is given by

$$G^{-1}(q) = \left(\widehat{B} q^2 + \frac{q^2 a^2 \widehat{K}_s}{q^2 + \widehat{K}_s / \widehat{A}} \right), \tag{2.61}$$

where we have introduced the renormalized constants $\widehat{B} = 2B$, $\widehat{A} = A/4$ and $\widehat{K}_s = K_s/4$. To get some insight of the physics of this model we consider the limiting cases.

- In the inextensible limit, $\widehat{K}_s / \widehat{A} << 1$, the propagator simplifies to

$$G^{-1}(q) = \widehat{B} q^2 + a^2 \widehat{K}_s = \left(\widehat{B} + \frac{a^2 \widehat{K}_s}{q^2} \right) q^2, \tag{2.62}$$

and from this expression we can define an apparent mode dependent bending stiffness as :

$$\widehat{B}_{app}(q) = \widehat{B} + \frac{a^2 \widehat{K}_s}{q^2}, \tag{2.63}$$

this B_{app} diverges for small wave vectors indicating that the persistence length of the bundle is infinite at large scale. Therefore this two filaments bundle looks very rigid at long distance even if the individual bending B is negligible. It is the suppression of the relative sliding that straightens the bundle and the term $a^2 \hat{K}_s$ can be formally be understood as an intrinsic self-tension straightening the bundle at large scales. Accordingly we see on Eq. (2.63) that $\widehat{B}_{app}$ can not vanish and thus there is no spontaneous symmetry breaking that would lead to a curved ground state in this model. For large wave vectors, $\widehat{B}_{app} \simeq \widehat{B}$ meaning that the bundle behaves like a standard semi-flexible chain at small scale.

- In the zero shear limit, $\widehat{K}_s / \widehat{A} >> 1$, the propagator simplifies to

$$G^{-1}(q) = \left(\widehat{B} + a^2 \widehat{A} \right) q^2 \tag{2.64}$$

and the apparent bending stiffness is simply shifted by a constant :

$$\widehat{B}_{app} = \widehat{B} + a^2 \widehat{A} \tag{2.65}$$

In this limit of small shear the bundle behaves like a semi-flexible chain at all scales.

In conclusion, this analysis shows that in presence of shear, the bundle has two different behaviors depending on the scale of observation. While it behaves like a semi-flexible chain at short distance it displays a very large apparent bending stiffness at a larger scale and can thus be seen as an elastic rod with suppressed thermal fluctuations. This particular property of the model implies that its persistence length is actually L dependent, i.e.; $lp = lp\,(L)$. This result was very attractive as experiments probing the bending stiffness of clamped microtubules have precisely shown such a behavior [18]. It was therefore tempting to model a microtubule as a cylindrical bundle of shearable protofilaments [19]. We will return to this point in chapter 5 but we can already mentioned that the main drawback of this approach is the impossibility of a spontaneous symmetry breaking.

Chapter 3

Buckling and self-buckling

In chapter 2, we saw that microscopic semi-flexible chains seen as thin elastic rods immerged in a thermic bath can model real bio-macromolecule like DNA. The aim of this thesis is to convince the reader that this model is an over simplification when it comes to the study of the filaments of the cytoskeleton. One fundamental question we try to answer all along this thesis is : how can we explain that rigid isotropic filaments do form very persistent curved conformations at the length scale of observation $(L \lesssim l_p)$, being clear, that these curved states can not be thermally activated ? Chapter 6 to 8 are devoted to this question. One answer comes form the topic of confotronics which is summarized in chapter 5. A second answer relies on a new idea which stems on the concept of self-buckling that results from an elastic instability called auto-coiling. It is proposed that a new instability can be induced by stresses on the surface of the filament. Both approaches, confotronics and auto-coiling, rely on the very essential physical concept of spontaneous symmetry breaking. Before launching our research in this direction, we propose a very visual introduction to buckling and self-buckling of macroscopic objects. We will finish this chapter with a recall of the buckling of the worm-like chain model.

3.1 Buckling: Generalities

3.1.1 Examples

The situations of buckling are common in our daily life and sometimes confused with situations of bending, we will specify what differentiates these two phenomena. The best known example is that of bridges where the columns (pillars) must remain vertical despite the load. Another example is the change in the shape of an arrow when it is shot: at first, it is straight, but then it bends under the action of the string, which pushes it out of the bow.

(A) Bridge

(B) Arrow

FIGURE 3.1: Buckling examples

We are interested in the causes of this buckling that's why we study the importance of the type of material and its intrinsic properties, the type of load causing the buckling and the temperature.

3.1.2 Buckling or bending

To make the difference between a bending situation and a buckling situation it is sufficient to observe **the direction** in which **the load** is applied to the bar. When transverse load is acting perpendicularly to the neutral axis of structural members, the situation is called bending. The bending of a beam can be of two types: sagging and docking. Take the example of a horizontal beam supported by two piers, when the load is applied perpendicular to the beam (See Fig 3.2), it will experience a positive bending moment and bend in the concave face down structure. In concave face we find three layers : first a compression layer, then a neutral axis (middle layer), and, finally, a tension layer. We will use the structure of three layer later in chapter 6.

Bending is a state of stress when the direction of the load applied is perpendicular to the one of the neutral axis, the structure (rod, beam) can experience negative bending moment (in downward direction) and positive bending moment (in upward direction).

Buckling is the state of stress when load and neutral axis have the same direction.

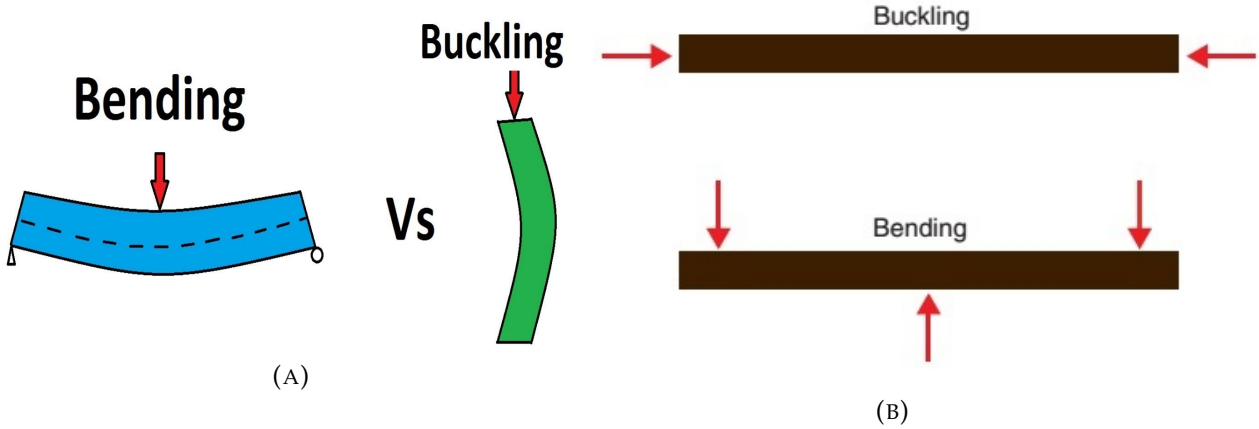

(A) (B)

FIGURE 3.2: Bending versus buckling

In engineering, an object which is unable to sustain the load will suddenly collapse : this what we call buckling. Buckling can therefore be defined as the sudden change in shape under the action of an axial load (the direction of the neutral axis). Axial loading on a column could cause significant and unforeseeable deformation and could lead to a complete loss of the capacity of the column to carry any load.

3.1.3 Columns and buckling

For a system, buckling corresponds to a passage from a stable state to a new stable state in which the shape of the system has to adapt to the load undergone. It is therefore a state of instability. We will both describe this state of instability and determine the load required to move to the new stable state. The previous paragraphs do not allow us to specify to what extent it is necessary to increase the load to observe a transition.

Euler's formula

We consider an ideal column i.e. perfectly straight and made of a homogeneous material. We also considered a slender column. Mathematician Leonhard Euler investigated the theory of the behavior of columns under loads. He found a formula giving the maximum load that an ideal column could carry without buckling. When the applied load reaches the critical load, the column comes to be in a unstable state.

The formula derived by Euler for long slender columns reads :

$$F = \frac{\pi^2 Y I}{(KL)^2}, \tag{3.1}$$

with :

- F, maximum load
- Y, modulus of elasticity
- I, area moment of inertia of the cross section of the column
- L, the column's length
- K, the effective length factor of the column

That can be used to give the critical buckling stress of the column, using the fact that $I = Ar^2$:

$$\sigma = \frac{F}{A} = \frac{\pi^2 Y}{(\frac{l}{r})^2}, \tag{3.2}$$

with:

- σ, stress at the origin of the buckling
- $l = KL$, the effective length of the column

We must note that buckling appears for any direction as explained : it's just about an axial load, parallel to the neutral axis.

Self buckling

Sometimes, the column doesn't need any external load to buckle: it could buckle due to its own weight. For most buckling situations, self-buckling is way smaller than buckling due to external loads.

Greenhill (in 1881) found that a bar (or column) would buckle if its length is larger than the following length :

$$l_{max} = (7.8373\frac{YI}{\rho g A})^{\frac{1}{3}}. \tag{3.3}$$

First, this length was used to calculate the maximum height trees can reach before buckling. This was a model assuming trees are prism-shaped and branches are neglected. Appendix B tells us how he found this equation.

Self buckling of home made gels column

I stacked gelatin bricks to observe the evolution of the curvature of the formed column as a function of the weight of the column and thus study the appearance of instability. Between each brick laying, I patiently waited for the stabilization of the system and made sure to lay each brick as precisely as possible.

I first made a vertical column composed of parallelepiped bricks, added one after the other (3.3). The goal is not to observe the oscillation frequencies of these bars but to verify the appearance of self buckling from a critical height. After repeating the same procedure, I observed each time the appearance of a slope from the installation of the fifth brick (figures 3.3c and 3.3d). It was never possible to lay a sixth brick, the column did not hold.

As announced in [20], with the use of a similar gelatin, I observe that from 10 cm heigh (5 experiments, with bricks having the same dimensions, 3x2 centimeters for the base) the tower collapses spontaneously.

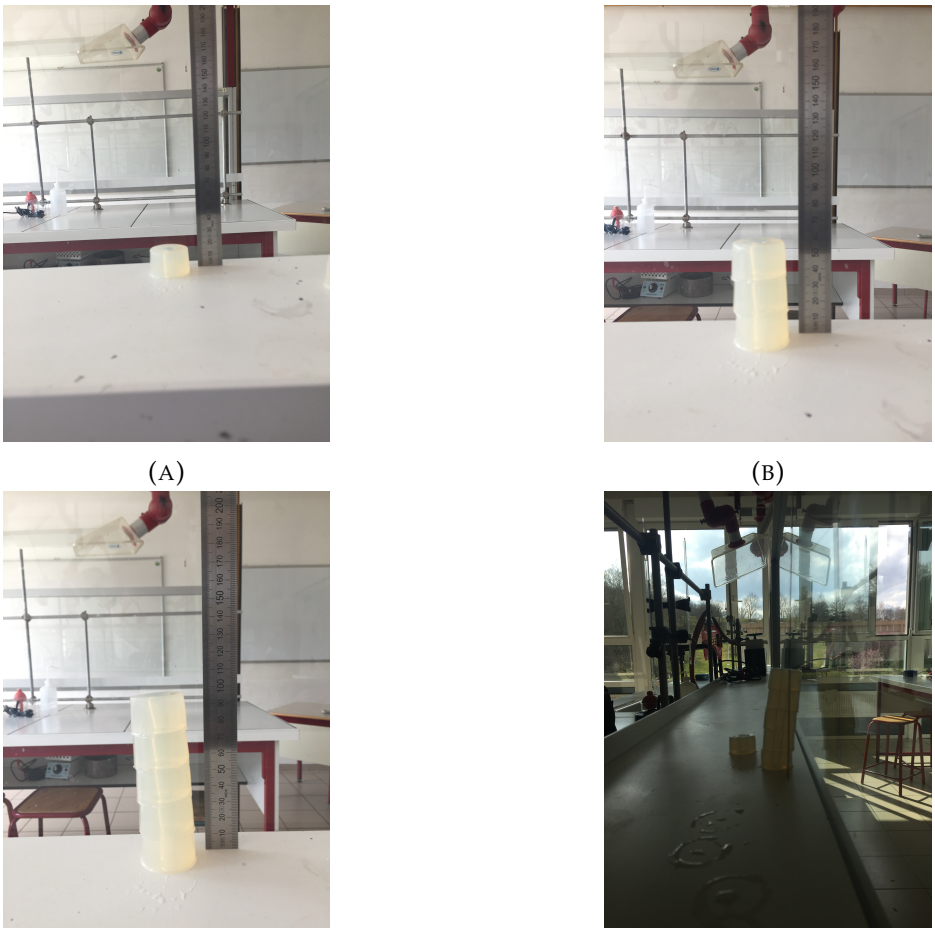

(A) (B)

(C) (D)

FIGURE 3.3: Column and self-buckling

3.2 Buckling of biopolymers

For the case of biopolymers, we will consider a compressive force with a chain whose length is always smaller than the persistence length. I will study the influence of thermal fluctuations on the buckling transition which is usually neglected in the high number of studies about buckling of biopolymers. In the article [21], a quantitative study of the buckling of a semi-flexible chain has been performed. Here we will limit ourselves to deduction of the classical buckling transition as was done at the macroscopic level (See Appendix C).

In the regime $l_p < L$, thermal fluctuations are small and a semi-classical approach can be applied. The elastic energy of a filament of length L under a compression force $\mathbf{F}$ is the same as the energy of DNA under tension but with an external force changed in sign:

$$E[t] = \int_0^L \left(\frac{B}{2} \left(\frac{d\mathbf{t}}{ds} \right)^2 + \mathbf{F} \cdot \mathbf{t} \right) ds, \tag{3.4}$$

where $\mathbf{t}(s) = \frac{d}{ds}\mathbf{r}(s)$ is the tangent vector to the curve $\mathbf{r}(s)$ that describes the position of the filament. Let's assume that the force is in the z direction and for simplification the filament fluctuations are in the (x, z) plane (filament confined in two dimensions), then the energy becomes

$$E = \int_0^L \left(\frac{B}{2} (\theta')^2 + F \cos\theta \right) ds, \tag{3.5}$$

where θ is the polar coordinate with respect to z-axis. We consider now the ground state before the buckling : this state corresponds to $\theta = 0$ and so the energy of the fundamental is $E(0) = FL$.

3.2.1 Semi-classical approximation

In order to determine when this state becomes unstable, one consider small fluctuations $\delta\theta$ around the solution $\theta = 0$. The energy at the quadratic order of fluctuation becomes

$$E \approx FL + \frac{1}{2} \int_0^L \left(B (\delta\theta')^2 - F\delta\theta^2 \right) ds. \tag{3.6}$$

Consider a molecule that has its two ends clamped at fixed orientations $\delta\theta(0) = \delta\theta(L) = 0$ with ends being able to move freely in the plane perpendicular to the force (See Fig. 3.4).

(A) Before transition (B) After transition

FIGURE 3.4: Adapted from [21] - Euler transition

The Fourier decomposition is written

$$\delta\theta(s) = \sqrt{2}/L \sum_{n=1} \sin\left(\frac{\pi n s}{L}\right) \theta_n, \tag{3.7}$$

and thus the quadratic fluctuations

$$\delta^2 E = \frac{1}{2} \sum_{n=1} \left(B\frac{\pi^2 n^2}{L^2} - F \right) \theta_n^2 ds, \tag{3.8}$$

lead to an instability when the external force reaches a minimum force F_c (critical force) given by the condition $n = 1$, i.e.;

$$F_c = B\frac{\pi^2}{L^2}. \tag{3.9}$$

This is the famous Euler buckling condition. This buckling condition varies according to the conditions imposed on the filament's two ends but in all cases the law scales as

$$F_c \sim B\frac{\pi^2}{L^2}, \tag{3.10}$$

and only the numerical coefficient can change with boundary conditions.

Introducing the wave vectors $q = \frac{n\pi}{L}$, with $n > 0$, we see that the propagator reads

$$G^{-1}(q) = Bq^2 - F = \left(B - \frac{F}{q^2}\right) q^2.. \tag{3.11}$$

As we did for the railway-track model (chapter 2), this suggests to introduce an apparent mode dependent bending stiffness:

$$B_{app} = B - \frac{F}{q^2}. \tag{3.12}$$

Consequently, the buckling instability can be interpreted as the consequence of vanishing apparent bending stiffness, i.e.;

$$B_{app} = 0. \tag{3.13}$$

We will use this essential criteria for the determination of self-buckling instability later on. It is interesting to compare with the propagator of the railway-track model which is

$$G_{rwt}^{-1}(q) = \widehat{B}q^2 + a^2\widehat{K}_s, \tag{3.14}$$

to see that $a^2\widehat{K}_s$ acts like an extensive force and no instability is possible in this model.

3.2.2 Circular arc approximation

Another approximation that we will be useful in chapters 6 to 7 is the circular arc approximation where we assume the filament's shape is a circular arc

$$\theta(s) = \kappa s.$$

The boundary conditions are now $\theta''(0) = \theta''(L) = 0$ and this ansatz is obviously not the true ground state. Nevertheless, this method will allow to determine a transition of Euler's type in more complicated models.

The energy Eq. (3.5) becomes

$$E = \int_0^L \left(\frac{1}{2}B\kappa^2 + F\cos(\kappa s)\right) ds = \frac{1}{2}\kappa^2 LB + \frac{F}{\kappa}\sin(\kappa L) \tag{3.15}$$

and for a small curvature $\kappa L << 1$ we have approximately

$$E \approx FL + \frac{1}{2}\kappa^2 L\left(B - F\frac{L^2}{3}\right). \tag{3.16}$$

Therefore the solution $\theta(s) = \kappa s$ has a smaller energy than the trivial solution $\theta(s) = 0$ for a force that satisfies the condition:

$$F \gtrsim 0.3B\frac{\pi^2}{L^2}. \tag{3.17}$$

This solution for the Euler transition is not exact but has the same scaling as Eq. (3.9). An even better match can be obtained if we compare Eq. (3.17) to the critical force $F_c = 0.25B\frac{\pi^2}{L^2}$ of filament buckling with one end clamped while the other is free.

Conclusion : we have presented the buckling of semi-flexible chain under an external compressive force. The force contributes negatively to the apparent bending modulus resulting in an elastic instability called Euler transition when $B_{app} = 0$. This criteria will be the essential tool to determine the auto-coiling instability of more complex biomolecules like microtubules and intermediate filaments in later chapters. Beyond the critical force i.e. for forces $F > F_c$, the ground state is not straight but is a buckled conformation, solution of the non-linear Lagrange equations of the exact energy Eq. (3.5). Contributions of thermal fluctuations to the force-compression relation, which allows to go beyond the classical Eulerian buckling transition into the non-linear regime, were studied in [21] .

Chapter 4

Bio-macromolecules of the cytoskeleton

4.1 Cells and cytoskeleton

The main component of living things is the cell. But what people usually don't know is that cells are not like blobs i.e. having zero structure to hold them ([22]). Actually, like our bodies, they are highly structured : they have a "skeleton". The difference with our bodies is that they have no bones.
Indeed, they are made of bio-filaments forming the "cell skeleton", also called cytoskeleton. This cytoskeleton will play many roles in cells' lifes : give a shape, hold the membrane that surrounds it, allow them to move, etc.

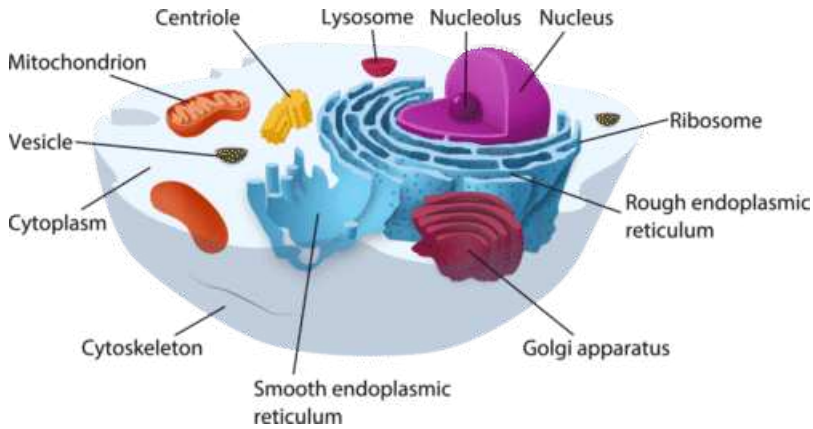

FIGURE 4.1: Cell and cytoskeleton

This cytoskeleton contains three types of biofilaments or protein fibers : microfilaments, intermediate filaments and microtubules.

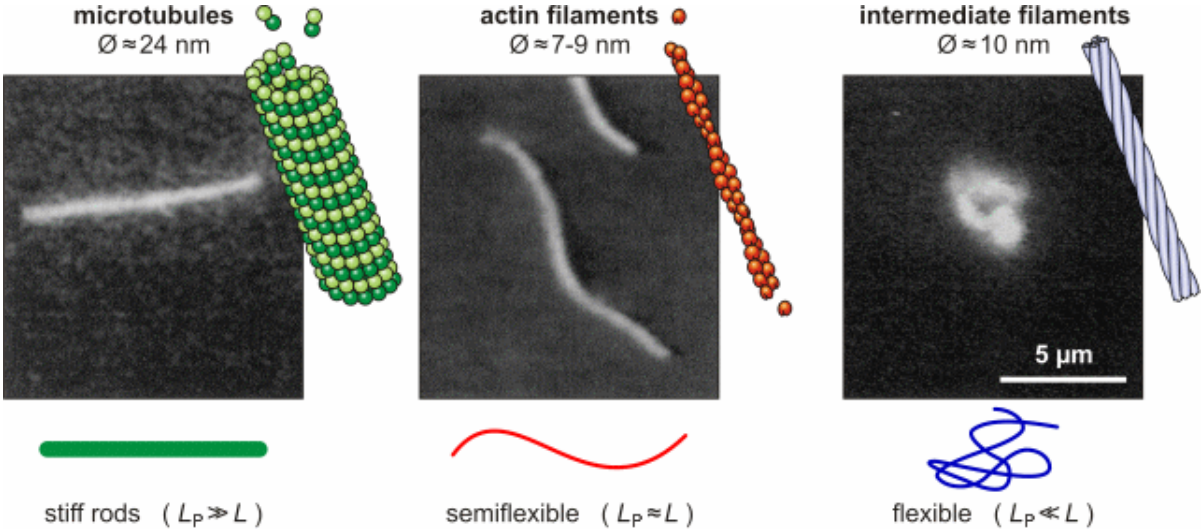

FIGURE 4.2: Biofilaments of the cytoskeleton

4.1.1 Microfilaments

Composition

Also called actin filaments, they are the narrowest biofilaments. They have a diameter of about $7nm$ and are made up of many linked monomers of actin (a protein). These monomers are combined in a structure looking like a double helix. They are also called actin filaments because of the protein constituting its basic monomers. They have two different ends, that is why we say that these filaments have directionality.

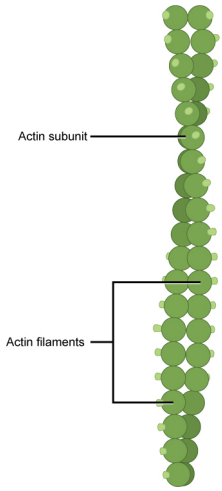

(A) Microfilament

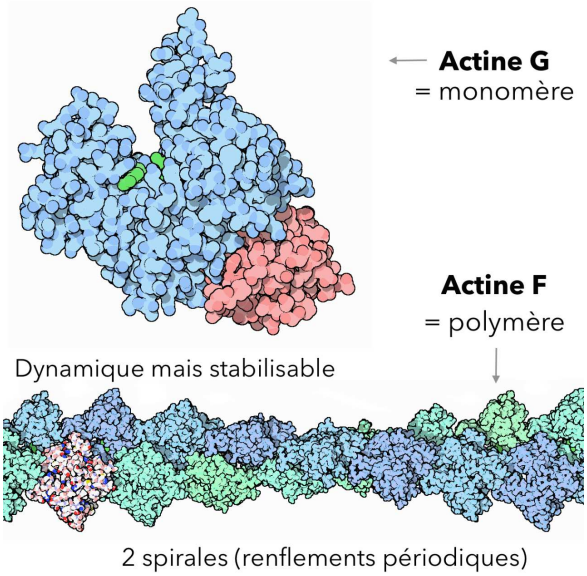

(B) Actin

FIGURE 4.3: Microfilaments and actin

Roles

The cell is a dynamic system able to do many things and where various process occur. In most animals, microfilaments form a network at the edge of the cell, giving its shape. Moreover, they are used in different process with myosin, they are also often involved in events requiring motion. Indeed, they serve as tracks for the movement of myosin, which is a motor protein, in muscle cells, actin and myosin form organized structures in sarcomers where their common motions make the muscles contract; microfilaments can assemble/disassemble quickly allowing them to play a role in the movement of cells; a ring made of actin filaments (and myosin) squeeze one cell apart to get two cells, etc.

4.1.2 Intermediate filaments

Intermediate filaments are made of multiple strands of fibrous proteins wound together. They are cytoskeletal components found in cells of animals. They are called "intermediate" because they have an average diameter of 8 to 10nm, in between the ones of microfilaments and microtubules.

Composition

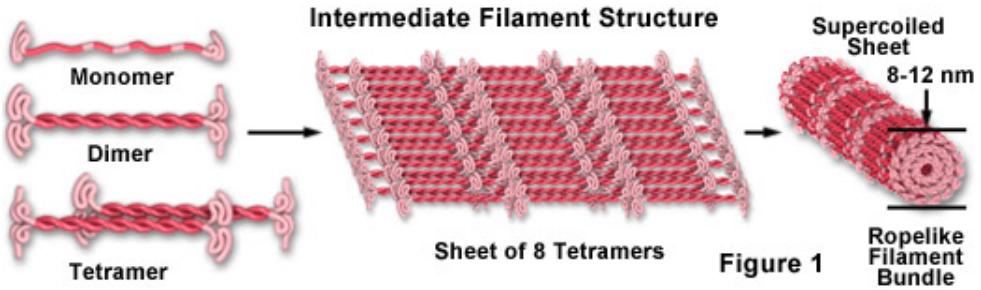

FIGURE 4.4: Interfilament

There are many types of intermediate filaments, each one made up of a different kind of protein. One well-known example of protein that forms intermediate filaments is keratin : this a famous protein in our bodies (hair, skin, nails).

Role

Intermediate filaments are more stable than actin filaments: they play an essential role in the structure of the cell. Their main activities are to be specialized to bear tension, to maintain the shape of the cell and anchor the nucleus.

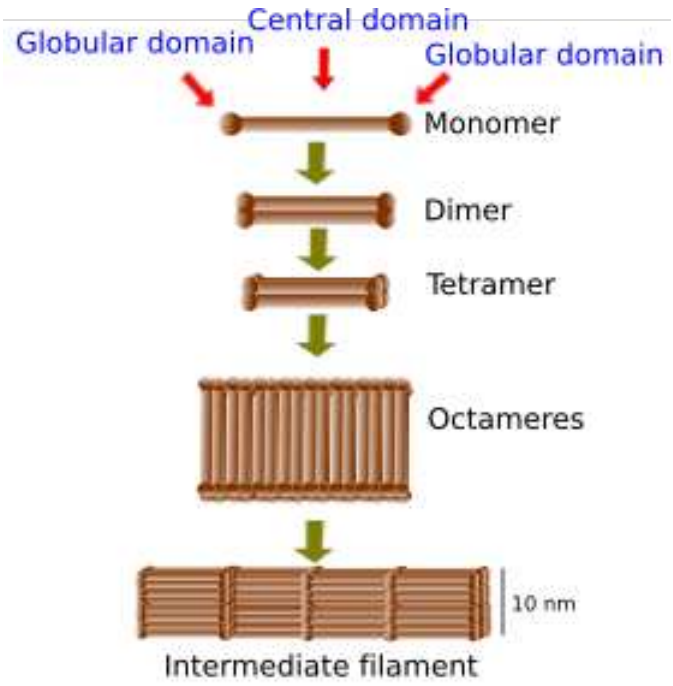

FIGURE 4.5: Interfilament

Key experiments

They are tons of experiments realized on filaments of the cytoskeleton in general. Here we summarize some experiments on intermediate filaments that are of interest with the topic studied in this thesis. Some of these experiments show the elastic response of intermediate filaments : they highlight that these filaments are the most flexible and extensible among the ones of the cytoskeleton [23][24][25][26]. The purpose of several other experiments was to determine the persistence length, all are in agreement on a persistence length around a few microns , $l_p \sim \mu m$ [23][27][28]. The experimental micrographs of refs. [23][27][28] show shapes resembling curved forms such as arcs or loops. (See Fig 4.6). These shapes look very much like three-dimensional helices confined on a two-dimensional substrate. [29][2][30]. Since intermediate filaments interact strongly with the substrates, the conclusions about the shapes and physical properties do also depend on the substrate properties.

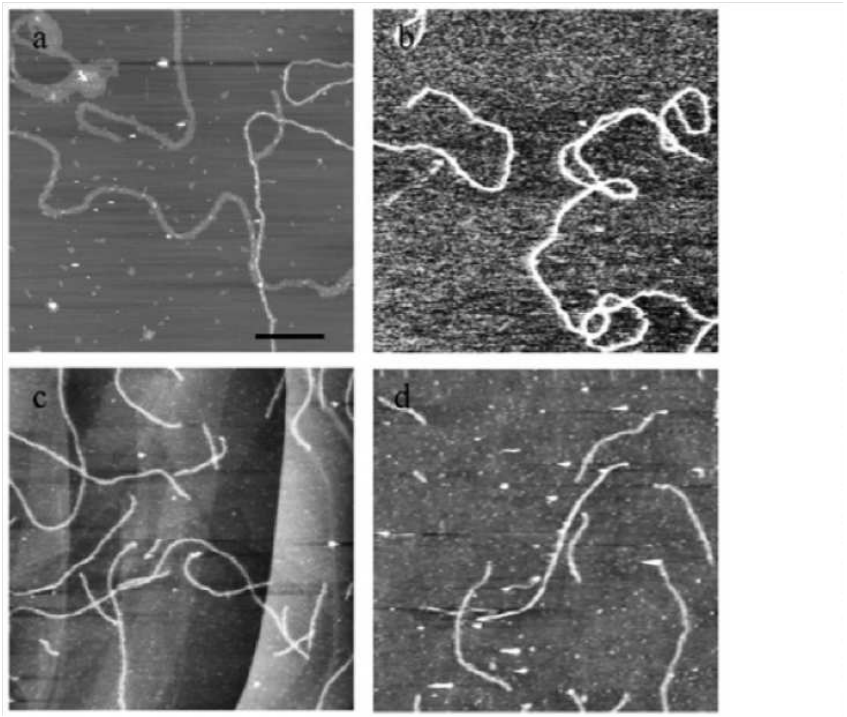

FIGURE 4.6: Adapted from [23]. Intermediate filaments adsorbed on different substrates. The black bar in a. represents 1μ m

To avoid this drawback, experiences on individual vimentin filaments, a prominent member of the intermediate filament family, where realized in quasi-two-dimensional microfluidic channels [31]. They have revealed several anomalous behaviors with respect to the usual semi-flexible polymer. For example, it was observed the transient formation of rings and loops which is, again, the behavior of confined helices in two dimensions.[30]. But certainly the most significant anomaly is the observation of strong oscillations in the tangent-tangent correlation function that appear in the presence of an additional lateral confinement (See Fig 4.7). Without entering into details it was shown that these anomalies can be explained by assuming that intermediate filaments behave like super-helical filaments subject to both a $2D$ and a lateral confinement [30]. These results suggest that vimentin filaments have a three-dimensional super helical structure whose origin is not yet known.

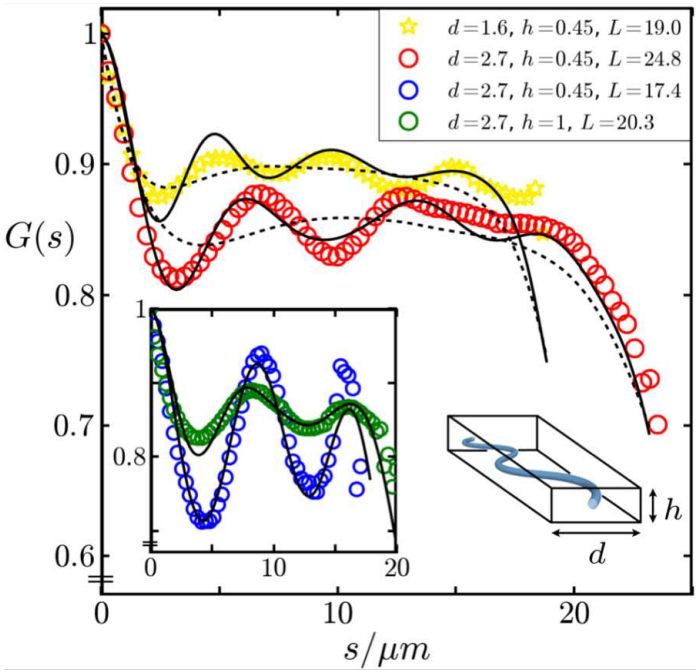

FIGURE 4.7: Adapted from [30]. Oscillatory tangent-tangent correlation function of vimentin filaments confined in a quasi-two-dimensional microfluidic channel.

4.1.3 Microtubules

Microtubules is the stiffest of the three types of cytoskeletal fibers with an average persistence length millimeter long, i.e.; $l_p \sim mm$

Composition

To determine the structure of microtubules, three-dimensional electron microscopy reconstruction was used [32][33]. They can be considered as hollow cylindrical filaments, with outer and inner diameters of $\sim$ 25 nm and $\sim$ 15 nm, respectively. The wall of the microtubule is made up of (on average) 13 parallel protofilaments. To be more precise, it is important to note that cryo-electron microscopy showed that microtubules can assemble in vitro in different configurations (N_s) where N and s are the numbers of protofilaments (between 12 and 16) and helix turns respectively [34][35][36]. Each of these protofilaments is made up of $\alpha\beta$-tubulin dimers whose structure is known from electron crystallography [37][38]. It' is also important to note that the microtubule is a dynamic polymer : it grows by polymerization of GTP-bound $\alpha\beta$-tubulin dimers or is undone by depolymerization of $\alpha\beta$-tubulin-GDP. In the article [32], a conformational transition of the tubulin dimer from a curved non-polymerized

conformation to a straight conformation upon binding to the microtubule was predicted. This transition between the straight and the curved state induces a pre-stress in the microtubule. A phenomenon can lead to the disassembly of the microtubule: if the stored energy is released, the dimers create a dislocation by taking their curved conformation. The transition from growth to shrinkage is called a catastrophe while the return to polymerization is called "rescue". Fortunately, this dynamic instability can be regulated with specific proteins, the MAPs (for Microtubules Associated Proteins), in vitro or in vivo.

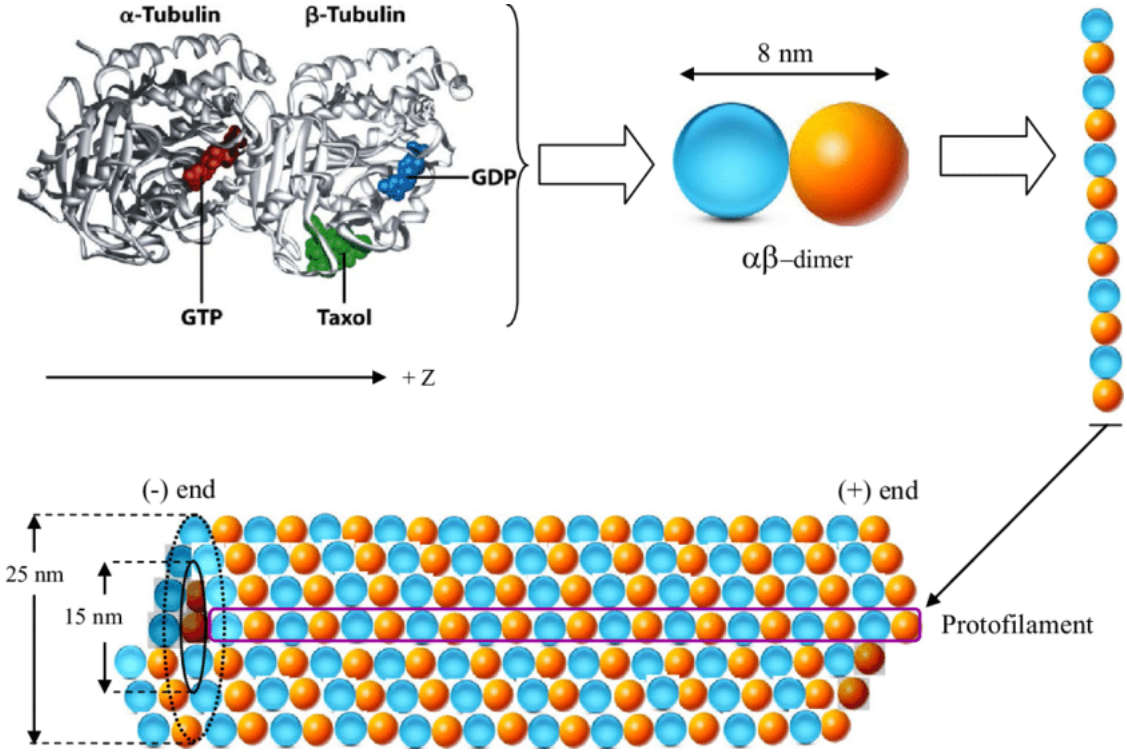

FIGURE 4.8: Microtubules

Roles

Like actin filaments, microtubules also have two different ends, then they also have directionality. Microtubules play an important structural role in cells : they help the cell resist compression forces. The microtubules provide a structural support, and also play the role of tracks for motor protein which are allowed to travel on their surface. These motors proteins (kinesins and dyneins) transport hormones or other molecules within the cell. They also play a role in cell division where they pull the chromosomes apart. Microtubules are also involved in three more specialized eukaryotic cell structures: flagella, cilia and centrosomes. You may remember that the

prokaryotes also have structures like flagella, which they use to move. The ones we are about to discuss have pretty much the same role, but a very different structure.

Key experiments

The understanding of the physical properties of microtubules is at the heart of many biological problems ranging from cell mechanics to information transport of material in the cell. Among the mechanical properties of interest, the persistence length l_p is here also, what has been most often measured. However, several methods such as the measurement of thermal fluctuations, or atomic force microscopy (AFM) for taxol-stabilized microtubules lead to values that vary in a wide range. Moreover, an analysis of thermal fluctuations of a bead attached to the end of stabilized microtubules of different lengths provide evidence that l_p is a function of the total length L [18] (See Fig 4.9 and 4.10). Then, we must conclude that the complex fluctuations and elastic properties can not be explained by the previous model considering the microtubule as a simple cylinder with a single modulus of curvature.

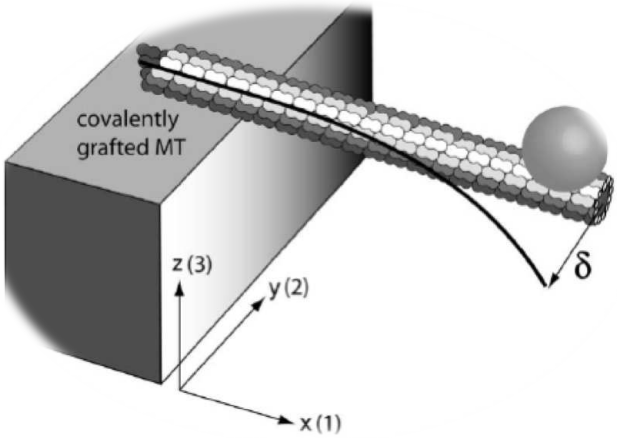

FIGURE 4.9: Adapted from [18]. Microtubule attached to a substrate at one end. The thermal fluctuations of the beads are measured to extract the persistence length.

In a recent article microtubules polymerization in the presence of MAP6, a neuronal associated protein, was studied [39]. Contrary to previous MAPs it was found that MAP6 localizes in the lumen of microtubules and induces the microtubules to coil into a left-handed superhelix (See Fig 4.11). One must add a model with a frustrated core-shell, where tubulin dimers can switch between a long and a short state, to explain the induction of microtubule curvature by MAP6.

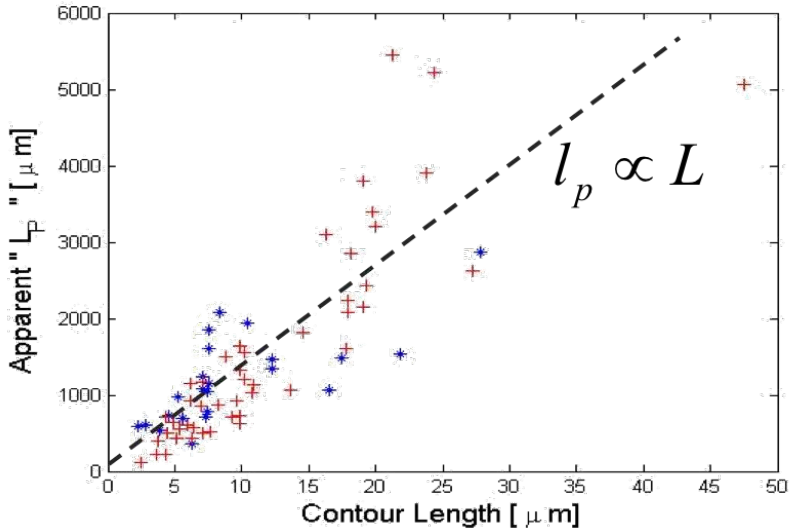

FIGURE 4.10: Adapted from [40]. Effective persistence length $l_p$as a function of position of the bead on the clamped microtubule showing that l_p scales linearly with L.

Remarkably, this model is based on the mechanism of symmetry breaking and is an illustration of the concept of confotronics. Both aspects will be discussed in the next chapters.

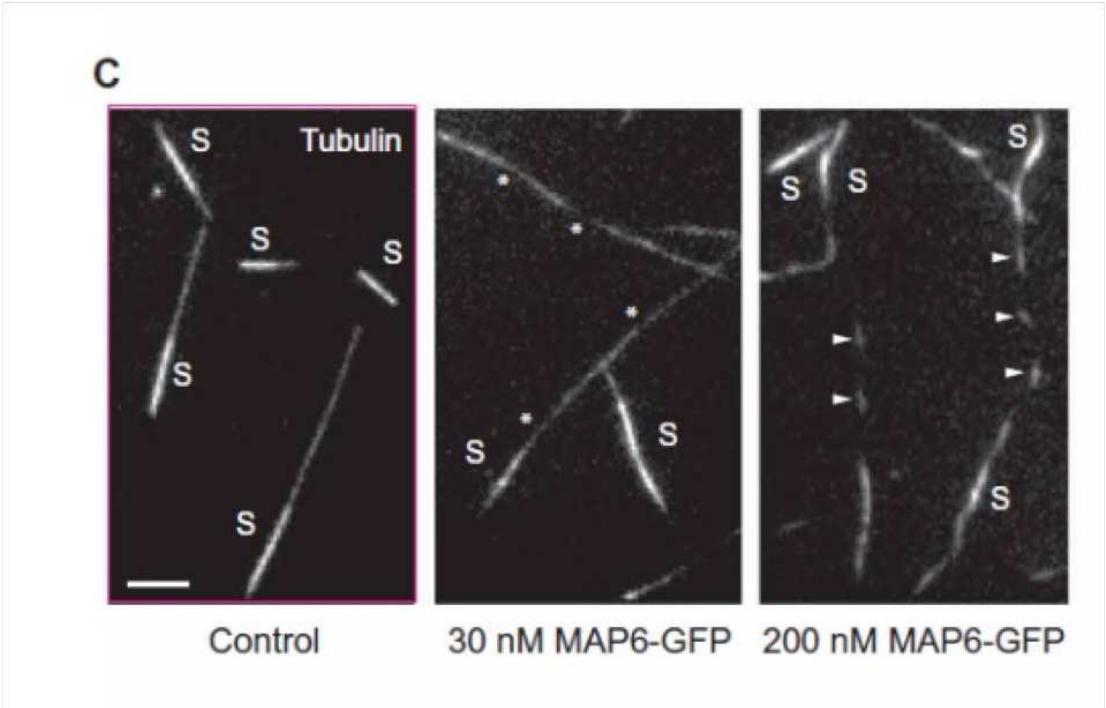

FIGURE 4.11: Adapted from [39]. Pictures of microtubules grown with increasing concentration of MAP6 from the left to the right showing the progressive formation of helices.

Chapter 5

Ground state, confotronics and symmetry breaking

5.1 Ground state and symmetry breaking in physics

The ground state of a physical system is the **state of minimum energy**. If this state has less symmetries than the Hamiltonian of the system we say that there is a symmetry breaking. We have seen, for example in chapter 3, the planar buckling of both an elastic rod and of a worm-like chain. For deformations constrained in a plane, the energy which depends only on the angle of deviation θ from the vertical axis, is invariant with respect to the symmetry $\theta \to -\theta$, called Z_2 symmetry.
Before the Euler transition of buckling, the rod is straight $\theta = 0$. But for a compressive force greater than a critical force (Euler force), $F > F_c$, the rod buckles, the ground state looks curved $\theta \neq 0$ and breaks the Z_2 symmetry. The ground state is actually twofold degenerated with two buckled conformations symmetric with respect to the vertical axis. The system randomly chooses one of the two possible ground states in a process called **spontaneous symmetry breaking**.
If the deformation is not constrained in a plane but allowed to evolve in a three dimensional space, then the system is rotational invariant and there is an infinite number of possible buckled states obtained by rotation around the vertical axis. We will go back to this important point when we will discuss the zero mode energy of microtubules and potentially of all biofilaments that results from the rotational invariance breaking during a process of self buckling.

Another well known example is provided by solid state physics. Although physical interactions between atoms do not break translational invariance, the ground state of a solid breaks this invariance since the atoms are organized on a regular lattice (supposed of infinite size). An important result is that the breaking of any continuous symmetry (such as translational invariance), leads to the existence of modes that have

zero energy and which are called zero modes. It is also said that the elementary excitations (or pseudo particles) have zero mass or a zero energy gap between the ground state and the first excited state of the systems. In solids these zero modes of vibration are the acoustic phonons.

Spontaneous symmetry breaking is strongly connected to **concept of phase transition** in statistical physics. In this case, what we call the ground state is **the state of lowest energy at zero temperature**. As already said, the ground state can have a degeneracy. Some of those systems can exhibit a phase transition at a critical temperature T_c of the medium that separates a symmetric phase ($T > T_c$) from a symmetry broken phase ($T < T_c$). In these systems, phase transitions can be described by the powerful concept of spontaneous symmetry breaking. On the other hand, there are several examples of matter that have no broken symmetries but are nevertheless distinct phases of matter. One can think of topologically ordered phases of matter, such as fractional quantum Hall liquids, topological insulators and spin-liquids. Unlike systems which exhibit spontaneous symmetry breaking, there is no general framework for describing such states. Here we do not consider these situations, and assume that **phase transition and spontaneous symmetry breaking are synonymous**.

It is important to note that a phase transition can only happen in the limit of infinite size of the system. If the size is finite, the energy barriers between the different ground states are always finite. The ergodicity property of statistical physics applies so that the system will, in limit of infinite time, explore all its allowed states. But even in the thermodynamics limit of infinite size, strong fluctuations might destroy the order resulting form symmetry breaking. For instance, a famous theorem tells us that there can't be any spontaneous symmetry breaking of a discrete symmetry for unidimensional infinite systems. The best known example is the one dimensional Ising model [41] of magnetism at finite temperature in which the magnetization is either M or $-M$ at temperature $T = 0$ (a Z_2 symmetry breaking) but the average magnetization cancels out, $\langle M \rangle = 0$ is in the limit of infinite size $L \to \infty$ as soon as the temperature T is non zero. In this case, it is the strong entropic contribution that destroys the magnetic order and breaks the ergodicity. Nevertheless a magnetic phase transition at a critical temperature $T_c \neq 0$ takes place for the Ising model but in higher dimensions of space. The Ising model in two dimensions was solved analytically in a mathematical tour-de-force [42].

What does the previous discussion tell us about a phase transition for a single filament ? Well, phase transitions are not possible because a filament has a finite length, so this is the same for spontaneous symmetry breaking. What is the point of this thesis, which is all about spontaneous symmetry breaking of single biofilaments ? For filaments, spontaneous symmetry is the property of the ground state only. It means that, at finite temperature, the full symmetry of the Hamiltonian has to be restored in some way. It is the manner the symmetry is restored by thermal fluctuations that can select a model among several others in various experiments.

Let's go back to buckling of a semi-flexible filament (chapter 3). Below the Euler transition and for a planar deformation, there is definitively a two fold ground state degeneracy. Since the Z_2 symmetry is a discrete symmetry there can't be a zero energy mode of deformation. Therefore, at finite temperature, if one waits long enough, thermal fluctuations will allow the filaments to elastically deform radially from one ground state to the other, as a consequence of the finite energy barrier between the two symmetric ground states and ergodicity of the system. On average we have $\langle\theta\rangle = 0$. Obviously this process can take a very long (almost infinite) time especially at low temperature. Of course, in an actual situation there are also fluctuations in the third dimension, a related situation can be found in graphene, the trendy $2D$ material. It turns out that it is theoretically impossible to realize a two-dimensional solid by virtue of a theorem of Mermin and Wagner [43]. In a $2D$ solid, low energy elastic fluctuations (long wavelength acoustic mode or also infrared mode) are supposed to destroy any regular structure and therefore graphene should not exist. However this theorem applies for a $2D$ lattice in a $2D$ space. In real life graphene exists in a $3D$ space and the elastic fluctuations are both in the graphene plane and perpendicular to it. In this case the Mermin-Wagner theorem does not apply. It is possible that this misunderstanding has delayed the discovery of two-dimensional solid materials.

Now what happens for the buckling of a filament in a three dimensional space ? Without the ends clamped the filament can rotate in space. In this case the system has an infinite ground state degeneracy. Each of the buckled states breaks the invariance by rotation around the vertical axis and the system, by picking one conformation, breaks the symmetry. But, as established, there can't be a phase transition. The thermally induced elastic deformations can have two modes: a radial mode, like for planar buckling, and a zero energy mode that, ignoring friction, can freely rotates the rod around, displacing the ground state in time. Actually, since no direction of rotation

is preferred, the curved conformation diffuses randomly around the vertical axis so that on average $\langle\theta\rangle = 0$ and the rotational symmetry is restored. For clamped rod, the rotational zero energy mode is blocked as the ends must be twisted for the rotation to occur. In the section devoted to microtubules we will discuss a new type of self buckling that allows an energy free rotation even when the microtubule is clamped. In conclusion, symmetry breaking of a continuous symmetry of a finite elastic system can't have a phase transition but the existence of the continuous zero energy mode of deformation can induce a large movement in order to restore the broken symmetry.

As a general principle in physics, we first search for the state of lowest energy and its eventual degeneracy, and then the energy states "above this fundamental state". For low energy phenomena the knowledge of the ground state is essential as the low energy modes are very dependent of the lowest energy state. For instance, in a solid, the vibrational modes depend on the periodic structure of the solid's ground state. However it is not always necessary to identify the ground state. At high energy, perturbation theory around a trivial ground state can be safely applied as the energy modes being far above the ground state are almost independent of it. A famous example which combines these two scales is given by quantum chromodynamics (QCD). The ground state of strongly interacting quarks in atomic nuclei is yet not known. However, for high energy processes far above the energy of the ground state (high energy collisions), perturbation theory based on a trivial zero particle ground state predicts results reproducible experimentally and led to the discovery of asymptotic freedom (Nobel prize 2004). On the other hand for low energy processes like quark confinement, the knowledge of the ground state is essential and is still under intense research.

What does this mean for macromolecules ? For semifexible filaments of length L, the persistence length $l_p = B/k_BT$ distinguishes two scales. If the persistence length is very small compared to the total length, $l_p << L$, polymer's fluctuations are large and in some way disconnected from the structure of the fundamental. Regarding the biofilaments of the cytoskleton, their persistence lengths are often of order or larger than their length L, i.e. $l_p \gtrsim L$. The strong fluctuations are suppressed and the physics is very much dependant on the nature of the ground state. Therefore any serious attempt to fully understand the complexity of actins, intermediate filaments and microtubules cannot avoid the question of their ground states. In the next sections we will discuss in details how symmetry breaking of biofilaments can be crucial for the understanding of their properties in key experiments.

5.2 Confotronics and symmetry breaking

The simplistic view of biological macromolecules like those of the cytoskeleton considered as simple semi-flexible filaments is not acceptable anymore. The last decades has provided many experimental (often single molecule micro-manipulations) results that can not be understood in the context of the statistical physics of elastic filaments. Since the biological filaments of the cytoskeleton are macromolecules, they are also made of subunits (complex proteins). Therefore it has been suggested that the subunits could get different conformational states and, then, undergo rearrangements. Moreover, these multisatble subunits could interact cooperatively all along the protofilaments (for microtubules) and lead to specific behaviors of the whole filament. These systems combine cooperative polymorphism of subunits and global elasticity of the whole structure and could perform biological tasks that a single unit cannot. These subtle observations bring individual biofilament into the world of complex systems.

Switchable multistable filaments are found everywhere in living nature. We mention, FtsZ (protein "Filamenting temperature sensitive mutant Z") [44],[45], Mrb [46], bacterial flagella [47],[48] and also DNA whose bases can flip, tilt and interact with the orientation of its backbone, giving rise to discrete A, B and Z forms of DNA. As we will see, the filaments of the cytoskeleton belong also to this category of switchable multi-stable filaments. For example, microtubules can form helical structures with zero mode energy motion [51] thanks to their subunits (tubulin dimers) which act as curvature switchable elements. The same way, actin filaments (see references [49],[50]) are able to switch their inter-unit twist. Recently, it has been shown that intermediate filaments, confined in microchannel, have a helical superstructure nature [30].
In these cases, the multistability is a consequence of their monomer's molecular complexity. Their exists other situtations where multistability is induced by geometrical constraints like the closure constraint on filaments [52]. Even though switchable biological systems are mainly found in macromolecules, switchability also seem to exist for microorganisms thanks to the properties of their constituent filaments [53],[54].

The study of conformational states of large groups of soft switchable units systems in biology [55] was named **confotronics**. As we will see the confotronics of biofilaments is intimately linked to the concept of symmetry breaking and the existence of a nontrivial ground state. How does multistability emerge is the first question one might ask.

5.2.1 Multistability, non linearity and frustration

To be concrete, let's take the example of the railway-track model, the bundle of double stranded polymers studied in [17] and reviewed in chapter 2. This model has very unique elastic properties and its generalization to the microtubule has lead to the soft shear model of microtubule [19]. Take two elastic monomers of two identical strands that are opposite to each other and separated by a fixed distance $2d$.

This pattern is the basic element of **confotronics**, it is the simplest bistable structure we can study.

Both monomers are monostable units, they are not supposed to be switchable. But, when sticked together, they can collectively become bistable. Moreover, when these two units bend together to one side with a curvature κ of the centerline : the monomer on the "outside" of the curvature undergoes a positive (tensile) strain $\varepsilon = \kappa d$ while the monomer on the "inside" of the curvature undergoes a negative (contractile) strain $\varepsilon = -\kappa d$.

Since monomers are identical, let us assume they have a bending energy per length given by $f_{unit}(\varepsilon)$. The total energy is thus:

$$f_{tot}(\kappa d) = f_{unit}(\kappa d) + f_{unit}(-\kappa d) \tag{5.1}$$

Because of the symmetry of the situation, the total energy density f_{tot} only depends on even terms of κ. Thus we expect the system to have three equilibrium configurations: two symmetrical bent states and a straight state. The straight ground state becomes instable when

$$\left.\frac{\partial^2 f_{tot}}{\partial \kappa^2}\right|_{\kappa=0} = 2 \left.\frac{\partial^2 f_{unit}}{\partial \kappa^2}\right|_{\kappa=0} < 0, \tag{5.2}$$

leading to two equivalent bent ground states. The system formed by these two monomers is thus bistable. Note that a bi-stability of f_{unit} is not necessary, contrary to its convexity around zero which will be necessary, i.e.;

$$\left.\frac{\partial^2 f_{unit}}{\partial \kappa^2}\right|_{\kappa=0} < 0. \tag{5.3}$$

It is also clear that a bistability can not emerge from monomers with "linear" elastic properties, i.e. a quadratic energy in the curvature: $f_{unit}(\kappa) \sim \kappa^2$. The function $f_{unit}(\kappa)$ must have a global minimum at $\kappa = \kappa_m$ corresponding to the monomer's intrinsic curvature. For instance, one can take a monomer energy density of the form

$$f_{unit}(\kappa) = A\kappa - \frac{B}{2}\kappa^2 + \frac{C}{4}\kappa^4, \tag{5.4}$$

with positive elastic constants A, B and C. The constant A represents a structural asymmetry of the monomer unit. The total energy density

$$f_{tot} = -B\kappa^2 + \frac{C}{2}\kappa^4, \tag{5.5}$$

then has a minimum at

$$\kappa = \pm\sqrt{B/C}. \tag{5.6}$$

Consequently this system has two symmetrical bent ground states: the system is bistable.
Although neither monomer can minimize its energy $f_{unit}(\kappa)$ as $\kappa \neq \kappa_m$, the contractile side is energetically less frustrated than the tensile one. Non linearity of the units and frustration of the system are two common features of confotronics.

Later on, in chapter 6, we will address the question of the bistability induced by linear elastic monostable units, but for the moment we assume that confotronics requires some nonlinearity properties of the elementary units.

5.2.2 Tubular multistability, quasi-particle and zero energy motion

For switchable tubular systems (See Fig.5.1), like microtubules [51],[55] and bacterial flagella ([54],[56],[57],[58]), one uses, as a basic motif, the symmetry breaking and multi-stability presented aforesaid.

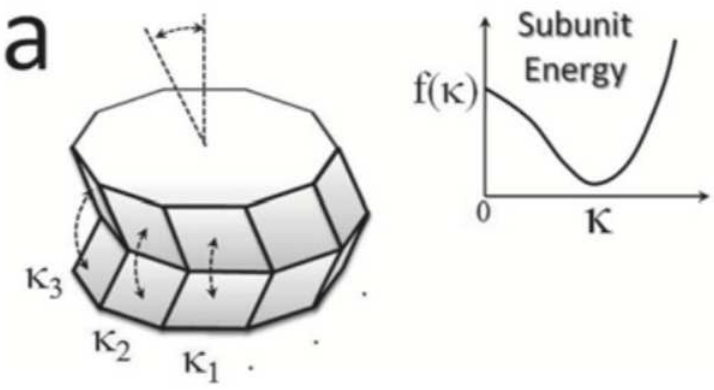

FIGURE 5.1: Adapted from [52]. Tubular cross-section showing coupled bendable nonlinear units with their curvature κ_i and bending energy $f(\kappa)$.

By generalizing the previous reasoning we can get a multi-stable tubular system, if the N monomer units are mechanically coupled in the plane perpendicular to their bending axis, they form a short section of a tube of circular cross-section. These monomers will adapt accordingly if the tube section bends in a direction orthogonal to the cross-section with a curvature κ. If the curvature, $\kappa > 0$, is chosen to point in the direction of the $i = N$ monomer the other units become curved with

$$\kappa_i \approx \kappa \cos\left(\frac{2\pi i}{N}\right) \qquad i = 1..N.. \tag{5.7}$$

The previous equation of the curvature κ_i of the monomer i is the result of the geometric projection of the tube's curvature on each monomer unit.
The strains of the monomers are thus $\varepsilon = \kappa_i d$ with d the distance of the monomer to the center of the tube. The total elastic energy density of the tubular cross-section in this geometry is then :

$$f_{tube}(\kappa) = \sum_{i=1}^{N} f_{unit}\left(\kappa \cos\left(\frac{2\pi i}{N}\right) d\right). \tag{5.8}$$

A similar reasoning gives the condition

$$\left.\frac{\partial^2 f_{tube}}{\partial \kappa^2}\right|_{\kappa=0} = \sum_{i=1}^{N} \left.\frac{\partial^2 f_{unit}}{\partial \kappa_i^2}\right|_{\kappa=0} < 0, \tag{5.9}$$

for the instability of the straight ground state to occur. For concreteness, let's consider again the same $f_{unit}(\kappa_i)$ with a global minimum at $\kappa = \kappa_m$. This choice leads for the tube energy density to the following expression (even in κ as expected by symmetry)

$$f_{tube}(\kappa) = -\frac{BN}{4}\kappa^2 + \frac{NC}{8}\kappa^4, \tag{5.10}$$

whose minimum is given

$$\kappa = \sqrt{\frac{B}{C}}. \tag{5.11}$$

Note that, for a curve evolving in a three dimensional space, the curvature κ is positive (but the κ_i can be negative). Interestingly, the cylindrical symmetry applies that the tubular system has actually N degenerated ground states. The tube can indeed bend in any of the N equivalent directions and is therefore N multistable. Eq. 5.7 shows that a group of neighboring dimers on one side of the ring is switched to the curved state and so creating a negatively curved depression that gradually decreases towards the opposite side of the tube. This makes that the opposite side of the tube will bulge outwards. This ring structure was called a partial confoplex in ref. [55] (See Fig.5.2). The (discrete) rotational invariance of the N ground states leads to a remarkable property, the zero energy mode motion. At finite temperature, the cylinder should be able to explore all its equivalent N states if the thermal energy is high enough to overcome the energetic barrier (friction) between these states. Thus, a partial confoplex can be considered as a dynamic object able to rotate around the lattice as a localized discrete object. This is the reason we can refer to it as a quasiparticle. In this manner the system will, on long time scale, restore the rotational symmetry around the tube's axis. It is clear that switchable tubular filaments with this property will have a radically different dynamics than a simple semi-flexible filaments.

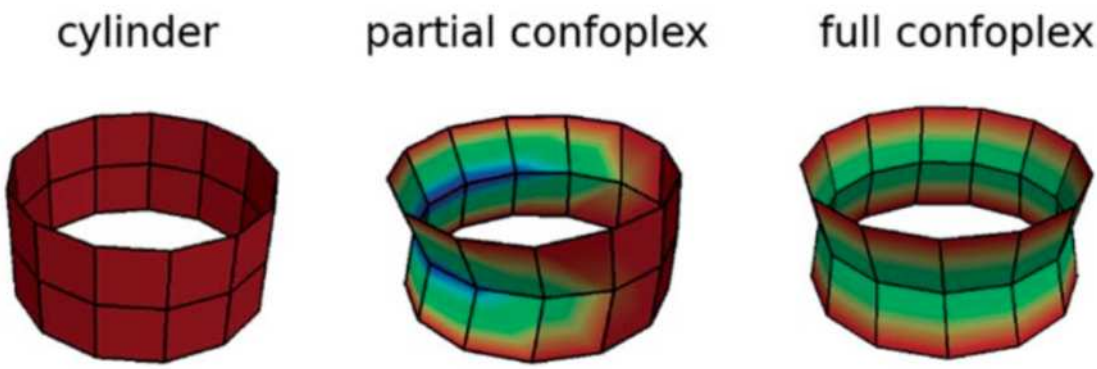

FIGURE 5.2: Adapted from [55]. Three tubular cross sections in different conformations : the straight cylinder with all subunits in their straight state, a partial confoplex, and a full confoplex for which all dimers are in the curved state.

5.2.3 Cooperativity in filaments

In general we don't want that the multi-stability become averaged out on relevant scales. On the contrary we want this property to influence the biological system on a large scale. But, this implies a ne cessary positive cooperativity between the unit conformations. For instance, in a tubular filament, the elastic interaction between two successive confoplexes turns out to be repulsive [55] and the ground state looks straight at large scale (See fig.5.3a). A global symmetry breaking of the filament can therefore only occurs when neighboring confoplexes interact cooperatively via allosteric interactions (See Fig.5.3b). Microtubules seem to be the paradimatic biofilaments showing multi-stability and cooperativity on a large scale. We notice that cooperativity might be due to the tubulin's built-in long amorphous polymer tails that can span to their nearest neighbors [59].

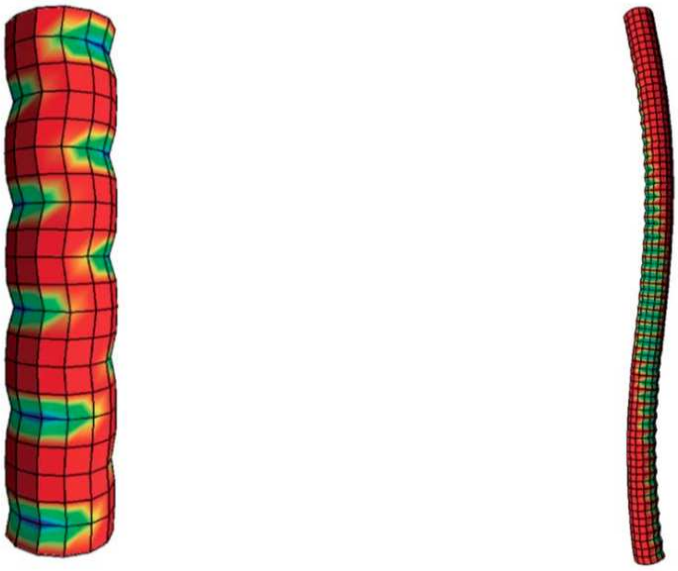

(A) (B)

FIGURE 5.3: Adapted from [55]. (A) Polymorphic tube without cooperative interaction. Repulsive partial confoplexes form a zigzag pattern on the tube. (B) Simulation snapshots of a polymorphic tube with cooperativity forming a superhelix in space.

5.2.4 Anisotropy (The railway-track model)

We have seen that for a symmetry breaking at the scale of a filament to occur, the monomers must have some nonlinear elasticity and a positive cooperativity between them. Here we look again at **the railway-track model** to see if an elastic anisotropy can lead to large scale elastic interactions within a filament and thus to some long range curvature cooperativity [17],[60],[19].

We remind that the model is a bundle of two glued together, semi-flexible filaments that are cross-linked by soft spring connections that are compliant along the bundle axis but are inextensible laterally, thus fixing the filaments interdistance. This structure makes the bundle anisotropic. For simplicity we consider the bundle in two dimensions only and neglect the axial stretching of the two filaments [17]. This corresponds to the limit of infinite stretching modulus $A \to \infty$ in the model of chapter 2. In addition to the bending energy per length, which depends on the bending stiffness B (twice the one of a single chain), one must add an inter-filaments shear deformation $\Delta(s)$ giving a shear energy depending on the shear modulus K_s.

The total energy can then be written as:

$$E = \frac{1}{2}\int_0^L \left(B\theta'^2 + K_s\Delta^2\right) ds \tag{5.12}$$

The shear deformation $\Delta(s)$ can be expressed as

$$\Delta(s) = \theta(s) - \overline{\theta} \tag{5.13}$$

with the average angular orientation

$$\overline{\theta} = \frac{1}{L}\int_0^L \theta(s)\, ds$$

and L the contour length. The energy (5.12) with the constraint (5.13) can be interpreted for weak angular deformations as semi-flexible filament under an "internal self-tension" K_s that acts with respect to the mean internal orientation [19]. This model has an apparent Fourier mode dependent bending stiffness

$$B_{app}(q) = 2B + \frac{1}{4}\frac{K_s}{q^2} \tag{5.14}$$

which divergences for small wave vectors q even for vanishing individual bending stiffness B. By gluing together two soft worm-like chains one get a bundle with very large stiffness and an obviously straight ground state.

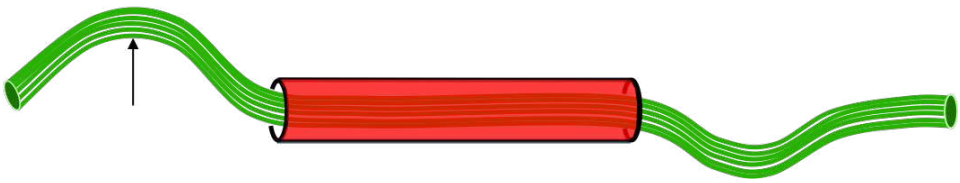

FIGURE 5.4: The curvature - anticurvature long range interaction of the soft shear model of microtubules constrained in a tube. The soft shear model is a tubular generalization of the railway-track model (see section 5.3.1)

Conclusion : at short scale a local curvature induces a sliding and thus a length mismatch between the two (inextensible) filaments that has to be compensated with an opposite shear and thus an opposite curvature at a proximal region (See Fig. 5.4). This long range negative curvature-curvature interaction is responsible for the absence of symmetry breaking and the apparent high rigidity of the bundle. An extension of this $2D$ model was proposed for the modeling of microtubules [18][19].

5.3 Microtubules

As we know, microtubule is the stiffest cytoskeletal component. Its elementary building blocks, tubulin dimers, polymerize head to tail into linear protofilaments that associate side by side to form the hollow tube structure. Despite the knowledge of its structure and numerous experiments probing its elastic properties [18] [61][62][63] [64], understanding the microtubule mechanics still poses challenging problems. A remarkable one is the observation of the unusual dynamic fluctuations of grafted taxol-stabilized microtubules [18]. These authors measured the lateral fluctuations of microtubules grafted to a substrate and found an intriguing "length-dependent stiffness", named persistence length $l_p(L)$, that depends on the total length L of the microtubule. These results do not fit with the worm-like chain model for which the persistence length is constant.

5.3.1 Anisotropic lattices (The soft shear model)

To explain this mechanical complexity, a first model, the so called "soft shear model" was introduced [65][18][60][19]. In this model the microtubule is considered as an anisotropic fiber-reinforced material where the tubulin protofilaments are strong fibers weakly linked by easily shareable inter protofilament bonds (See Fig 5.5).

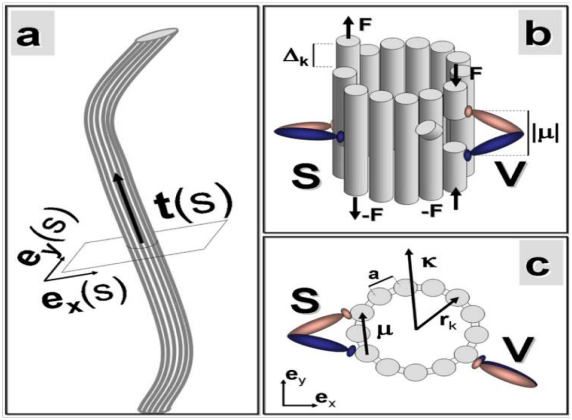

FIGURE 5.5: From [19]. (a). The soft shear model of microtubules. (b) tubular structure with shearable protofilaments. (c) Deformations induced by Katanin motors with internal force doublets between two PFs (S) and along the same PF (V).

This model is therefore a tubular generalization of the railway track model and has consequently similar properties like the long-distance curvature relaxation and the long-range interaction along the microtubule contour. Beside, the soft shear model is

in agreement with the observations of cooperative deformations induced by enzymes such as katanin [19]

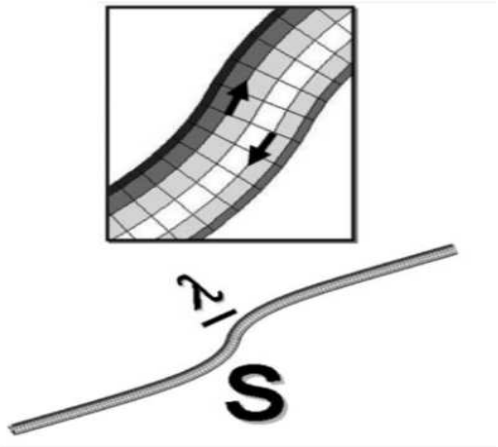

FIGURE 5.6: Adapted from [19]. The shear deformations induced by the katanin motor binding onto two different protofilaments produce an S-shaped over a length scale that depends of the lattice elastic constants.

Importantly, this model predicts a length-dependent persistence length $l_p(L)$ which approximately fits with the measured behavior [18][64] but also shows some inconsistencies. Especially, the ground state of the soft shear model is straight, in conflict with the observation of a superhelical ground state of taxol-stabilized microtubules (when taxol is in solution during microtubule polymerization) [63]. A helical ground state was also recently observed during the polymerization microtubule in the presence of the microtubule-associated proteins MAP6 [39]. One can now wonder how does an intact microtubule, which is a rigid tubular structure, change into a stable large-scale superhelix of micron-sized pitch and diameter? The soft shear model with its straight ground state can not be the solution. Note that there are many other inconsistencies discussed in detail in [40]. In fact a large body of experimental evidence points toward a higher degree of complexity with a cooperative curvature switch within the microtubule lattice [66][40].

5.3.2 Switchable lattices (The polymorphic tube model)

Superhelical ground states in various conditions (copolymerization with taxol or with MAP6) strongly suggests a general mechanism of symmetry breaking. If a confostack (name given to a block of several protofilaments in [55]) bends outwards, while keeping the tube unbroken, a superhelix could be formed. When protofilaments are parallel as for microtubules with $N = 13$ protofilaments, the tube bends in the direction of the bent protofilament's block and forms an arc. When protofilaments are twisted

(for instance for $N = 14$) around the tube with a given internal pitch, the microtubule adopts a superhelical shape (see Fig 5.3b).
The next step is to find the physical reason why the bloc of protofilaments could bend (or shorten). A first answer could be a change of conformation at the level of the tubulin dimer propagating along the protofilaments (see [66][40]), using the cooperativity property, and implying the global bending of the filament.
In the microtubule's model introduced in [66][40] the tubulin monomers (actually the GDP tubulin) are bistable and can fluctuate between a straight and a curved conformation. In support to this assumption their is an empirical evidence for tubulin bistability as a single taxol stabilized protofilament can coexist in a straight and a slightly curved state [67]. At the level of a microtubule's cross section, it can be explicitly proven that switched dimers induce elastic deformations that result in an attractive interaction energy of the form $E_{int} \sim -\cos(\alpha)$ with α the angle separating two switched dimers (See [68] for supplementary materials). This energy therefore favors the formation of switched blocks.

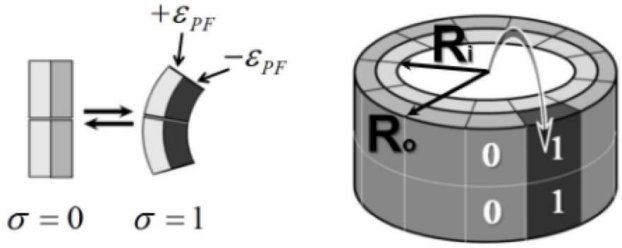

FIGURE 5.7: Adapted from [66]. Cross-section of the polymorphic tube model. Each tubulin dimer with intrinsic curvature κ_{PF} can fluctuate between a straight state $\sigma = 0$ and a curved state $\sigma = 1$. This creates a positive prestrain on the inner part and a negative prestrain on the outer part of the tubulin dimer.

With no cooperative interaction on the same protofilament between succesive dimers, we would have independent choices of the sides of the curved states so that microtubule would be locally curved but at large scales the microtubule would have a straight ground state. But, considering the cooperativity along the protofilaments, the confostacks prefer to stack on top of each other and get the same orientation. What would happen in the case of a change of conformation in a block on one side of the microtubule lattice while the rest of the protofilaments stay straight? This would result in a lattice frustration and, then, an additional stress. This additional stress will

be reduced by a microtubule bending and helical reshaping.

The mystery of the superhelix ground state is solved. But there is another question we must answer : in which direction will this filament bend? Indeed the rotational symmetry allows all the directions. The choice taken by the microtubule can only result from the process of spontaneous symmetry breaking. The superhelical ground state is thus highly degenerate with ground states given by the N different orientations of the helix. If the thermal energy is high enough to overcome the energy barriers between the ground states, the microtubules can hop between them with some friction (see Fig 5.8). The (almost) zero energy motion restores the rotational symmetry and the long time average shape is actually straight (movies of this zero energy motion can be seen in the supplementary of ref [55]). This is expected for a finite system where ergodicity can not be broken. This model with multi-degenerated ground states was called the **polymorphic tube model**.

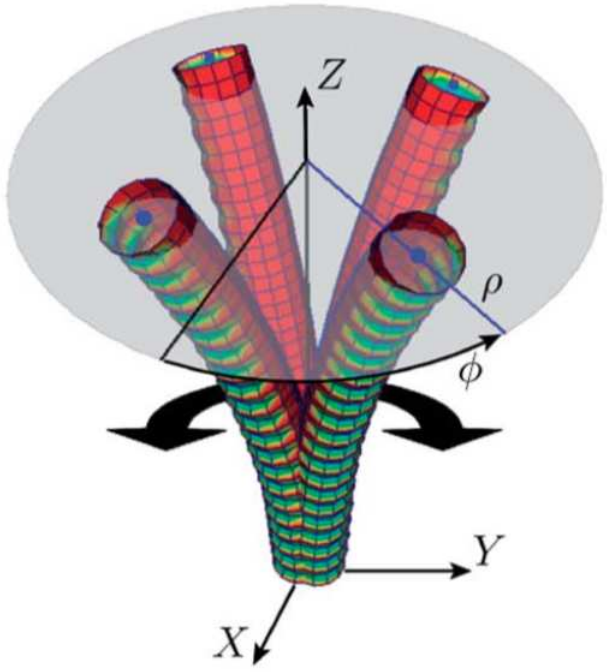

FIGURE 5.8: Adapted from [55]. Simulation snapshots of the zero energy rotationnal mode of circular portion of polymorphic tube. The rotating confostack at finite temperature diffuses randomly around a fixed axis

5.3.3 The ground state matters

Consider again the experiment with a microtubule grafted on one end to a substrate [18][64]. If the clamped tube was not polymorphic, but had the shape of a static superhelix instead, its elastic fluctuations are decomposed into a radial and an azimuthal elastic mode describing the dynamic behavior of a classical wormlike chain without rotation. In contrast, the polymorphic microtubule will still be able to reach the N equivalent orientations leading. This situation will lead to a random rotary motion caused by a confostack that moves around the lattice.
Therefore the main contribution to the dynamics is not the thermally induced elastic fluctuations around a fixed ground state, but instead thermally induced switching between the equivalent ground states. These microtubules, clamped on one side, looks like a "rigid conical rotor" (see Fig 5.9). In this "model", the elastic fluctuations become negligible compared with polymorphic ones.

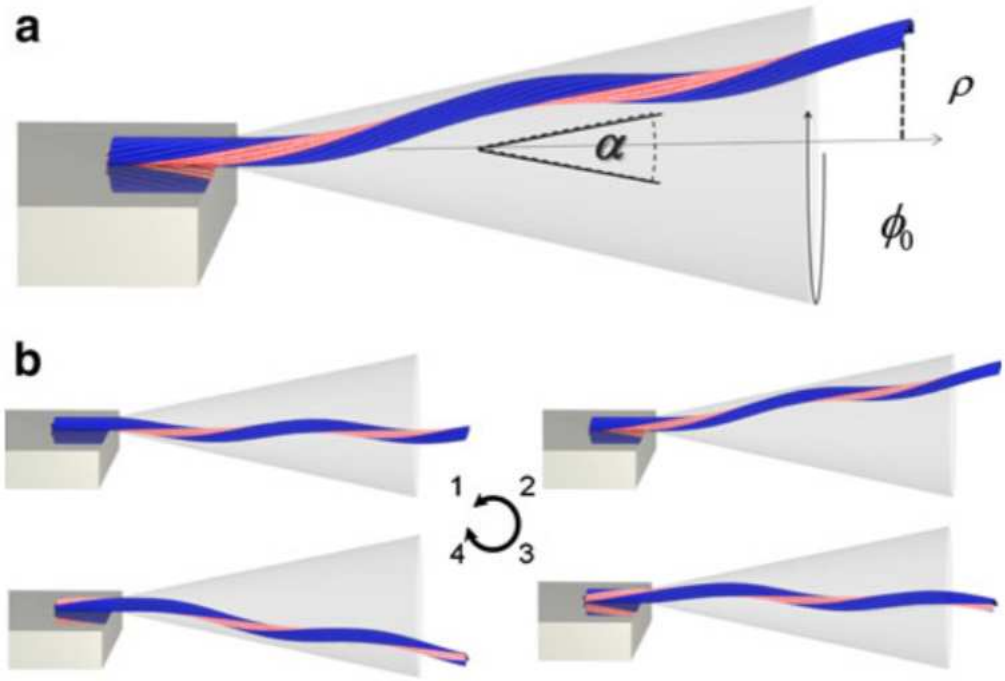

FIGURE 5.9: Adapted from [40]. A clamped polymorphic superhelical microtubule switches between its N degenerate ground states at no energy cost. The approximately conical motion leads to anomalous lateral fluctuations radically different from all other semi-flexible filaments.

For this rotor, the transverse displacement ρ of the microtubule end is proportional to its length L. In order to interpret these observations, we use the usual worm-like

chain definition of persistence length [18],

$$l_p = \frac{L^3}{3\left\langle \rho^2 \right\rangle} \tag{5.15}$$

(where $\langle\rangle$ is the ensemble average) and the fact that $\left\langle \rho^2 \right\rangle \propto L^2$, we see that

$$l_p \propto L \tag{5.16}$$

This scaling is in agreement with the experimental results of refs [18] [64] (see chapter 4). Comparing the soft shear model and the polymorphic model of microtubule, both give length dependent persistence length $l_p(L)$ but with different scalings and both can nevertheless approximately resemble the measured behavior. But the physics of the two models is completely different. The soft shear model has a straight ground state and the data are reproducible with an extremely small shear modulus K_s [18][64] [19] (10^5 times smaller than the Young's modulus). A significant shearing would then appear in bent microtubule structures, but we must note that this is not supported by other experimental observations [34]. Moreover, anomalous slow thermal dynamics [18] [64] show up with a relaxation time different from the worm-like chain : respectively $\tau \sim L^3$ against $\tau \sim L^4$. The soft shear model doesn't lead spontaneously to this anomaly because it needs to add another internal dissipation whose origin isn't known yet [64].

What about the polymorphic model? In this case, the zero energy motion and the helical ground state of the filament lead to more consistent interpretations of statics and dynamics. Indeed, if we look at the frictions for a thin rod (length L) rotating along a conical surface, we found that $\xi \propto L^3$ and, then, a diffusional equilibration time precisely given by

$$\tau \propto \xi / k_B T \propto L^3 \tag{5.17}$$

This model also predicts the equation giving the diffusional equilibration time τ (details can be found in [66] [40]).

This section highlights the importance of knowing the ground state of biofilaments. A wrong ground state could lead to results numerically compatible with observations, but to wrong physical interpretations and a misunderstanding of the physics. Good numerics does not mean good understanding.

5.3.4 Switchable metastable lattices

A beautiful consequence of switchable lattices is that microtubules can be forced to switch from a straight into a curved state by external forces and torques that can be due to molecular motors for instance. A more elaborate model of polymorphic microtubules, now subject to external forces and torques, shows that a straight microtubule (for instance when taxol or MAP6 are added after the microtubule formation and not during polymerization), if bent by an external torque for a short time, can convert to metastable curved conformations [68]. A remarkable manifestation of this effect is found in microtubule gliding assays [69][70][71]. Actually, it was observed ([70]) the formation of arcs for microtubules driven by kinesin motors on a glass surface. These arcs continue to glide for important times before suddenly coming back to a straight conformation (See Fig 5.10). An interesting consequence of the metastability property of switchable lattices is that these systems have a memory of their induced deformations and can then be classified as tunable shape memory materials.

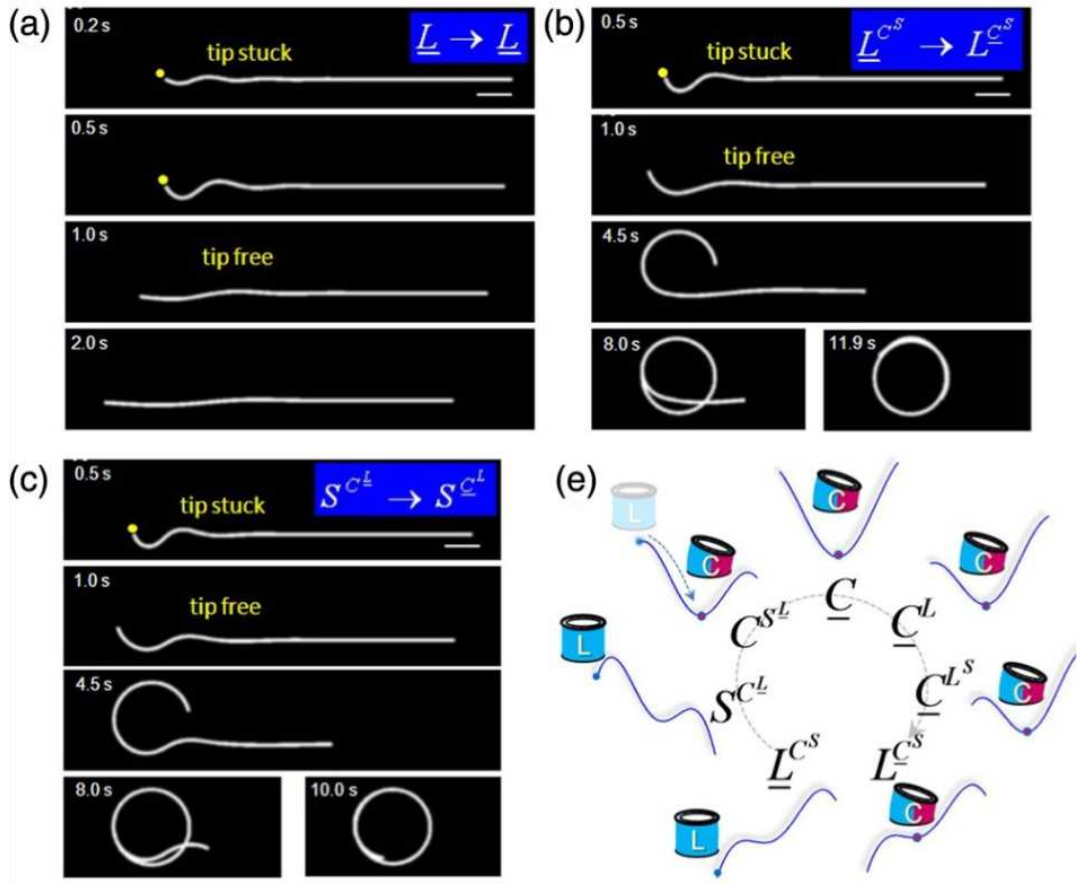

FIGURE 5.10: Adapted from [68]. Curvature switching and hysteresis of gliding polymorphic microtubules on kinesin motor carpets.

5.3.5 The frustrated core-shell model

Symmetry breaking of microtubules was also observed when MAP6 (Microtubules Associated Protein 6) is present during microtubule polymerization. It was discovered that MAP6 localizes in the lumen of microtubules and induces the microtubules to coil into a left-handed superhelix [39]. In order to explain the curvature induced by the presence of MAP6, one's used a frustrated core-shell built on the switchable lattice model. Concretely, a co-polymerization between MAP6 and non-hydrolyzed long GTP tubulin was assumed. Afterwards, the MAP6 also binds to the inner microtubule wall before hydrolysis to form an elastic network. An initial long state of the tubulin dimers, that can either straight or curve, is stabilized thanks to this elastic network. But, after hydrolysis, the GDP-tubulin tends to shorten and is in contradiction with the elastic network leading to a frustrated prestressed lattice. The particularity of this model is that an additional internal spring is present. It restores the straight state and, thereby, avoids the switching to short state of the bistable tubulin dimer. Once again, the prestress will be minimized by a symmetry breaking mechanism. A curved ground state will relaxe the prestress due to both types of tubulin dimers : compact (red) on one side and elongated on the opposite side (illustrated in Fig. 5.11). Remark that the conformational switching of GDP-tubulin to the compact state propagates along the protofilament axis, thanks to cooperativity, and forms a superhelix with a built-in protofilament pitch.
Considering the absence of MAP6 or small values of spring constant K, a metastability of the helical state is the only one predicted by the frustrated core-shell model. This conclusion leads, in this case of low or zero K, to a straight ground state for the microtubule. Now, for large enough K, the ground state can be a superhelix with the characteristic experimentally observed [39]. The coiled helical structure makes sense from a biological point of view : this type of structure is more likely to resist small forces by uncoiling.

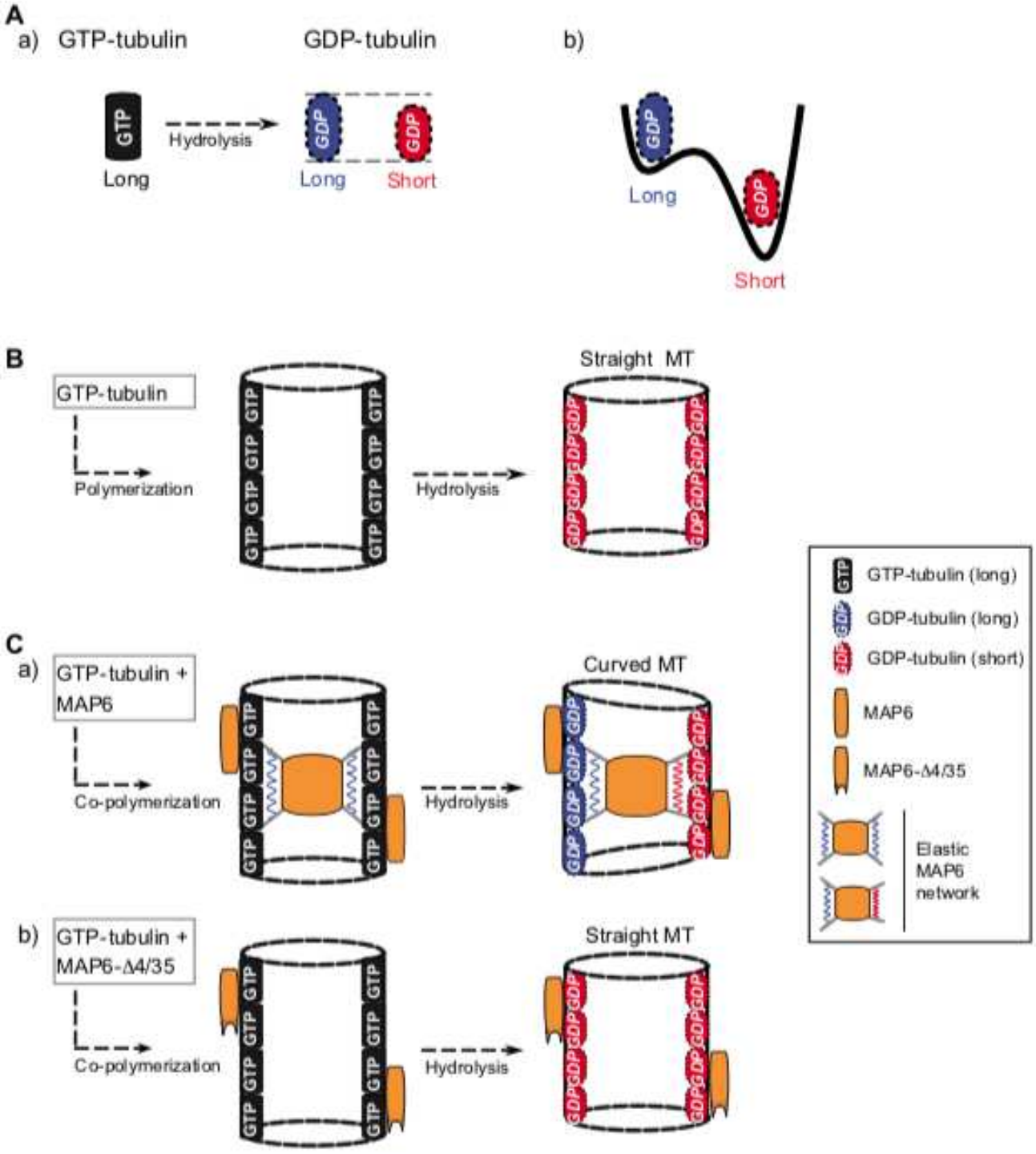

FIGURE 5.11: From [39]. The frustrated core-shell model of MAP6-microtubule.

Chapter 6

Symmetry breaking - Model with three filaments

6.1 Anisotropic lattice and symmetry breaking

The frustrated core-shell model of microtubule is an adaptation of the switchable, polymorphic lattice model, extended by the presence of an additional internal restoring spring force originating from the elastic MAP6 network. The presence of pre-stress in the model and frustration between external and internal preferred elastic states raises the question of the symmetry breaking by a simpler mechanism which does not require switchability.
Can the stress on the outside of a filament result in a mismatch with the stress on the inside of it, that leads to a conflict and a shape instability ? Such a surface-core instability was recently proposed for the curving instability of intermediate filaments and was called autocoiling [30].

In the following we will explore more precisely the feasibility of this symmetry breaking mechanism. Two methods come to mind to study the effect of surface stress on the filament's shape. **The first idea** is to use a mechanical approach which differentiates the physical properties of the surface and those of volume. **The second approach** is to use the generalization of the concept of surface tension of liquids to solids and in our case to elastic filaments.

6.2 Bundle of three filaments

The simplest mechanistic model consists of a tri-layered structure with two outer layers which individually prefer the same contracted length and a middle layer which has a different preferred length. This is a generalization of the railway track model [17] to three filaments that describes a bundle where the outside stress is different that in the inside, exactly the situation we want to probe. In these kind of models, filaments are irreversibly cross-linked to their nearest neighbors by discrete cross-links that are in general compliant in shear along the bundle axis but inextensible laterally [17][60].

At first sight, the analysis of the section anisotropic lattice in chapter 5 tends to show that this kind of models belongs to the category of linear elasticity models and can not lead to spontaneous symmetry breaking. Besides, the confotronics section shows that some non-linear elastic ingredient seems to be mandatory for an instability to occur. Therefore we ask the more general question : **can a bundle of elastic filaments without any non linearity have a non trivial ground state** ? We will see that, despite the previous discussion, this is indeed possible.

We consider three stretchable worm-like chains (6.1) that form a shearable bundle. For the simplicity of the analysis, we consider that this bundle can only deform in 2 dimensions.

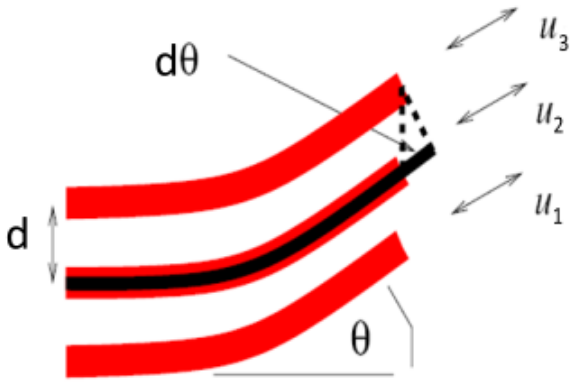

FIGURE 6.1: Fig. adapted from [60] Shearable bundle of three extensible filaments with a fixed interdistance d.

The total energy is the sum of three terms, the bending, stretching and shear energies,

$$E_{total} = E_{bending} + E_{stretch} + E_{shear} \tag{6.1}$$

- The bending energy $E_{bending}$ of the bundle is the sum of the standard worm-like chain energy of the individual filaments which we assume have the same bending modulus $\widetilde{B}$. Then

$$E_{bending} = \frac{B}{2}\int_0^L \theta'^2 ds, \tag{6.2}$$

where θ is the angular deviation with respect to bundle axis, and $s \in [0, L]$ is the arc length. All deformations will be measured with respect to the centerline of length L at rest that is our reference frame. As we consider three identical worm-like chains with regards to bending, the total bundle's bending stiffness is $B = 3\widetilde{B}$. As shown in chapter 2, the bending stiffness $\widetilde{B}$ of a filament considered as a rod with a circular cross-section of radius R is given by

$$\widetilde{B} = \frac{\pi}{4} Y R^4, \tag{6.3}$$

with Y the Young modulus.

- The second term $E_{stretch}$ accounts for filament stretching. Again we assume the same stretching stiffness

$$A = \pi Y R^2, \tag{6.4}$$

for all filaments but different individual lengths at rest (preferred lengths out of the bundle). Accordingly, the stretching energy reads

$$E_{stretch} = \frac{A}{2}\sum_{i=1}^{3}\int_0^L \left(u_i' + \varepsilon_i^0\right)^2 ds, \tag{6.5}$$

with ε_i^0 the intrinsic strain of the filament i.

The two external filaments $i = 1$ and 3 are assumed to be in prestressed state with the same preferred negative and thus contracting intrinsic strain

$$\varepsilon_1^0 = \varepsilon_3^0 = -\varepsilon_0. \tag{6.6}$$

Therefore the elastic energy of these filaments is minimized when their respective displacement fields are identical, $u_1(s) = u_3(s) = -\varepsilon_0 s$. The individual lengths at rest of these filaments are equal and shorter than L by construction :

$$L_1 = L_3 = L + u_1(L) = L(1 - \varepsilon_0).$$

On the contrary the filament $i = 2$ which is the bundle's centerline is chosen without intrinsic strain, thus $\varepsilon_2^0 = 0$. Its preferred length is its length at rest :

$$L_2 = L.$$

This system is therefore frustrated since the external filaments want to be shorter than the one in the middle. Can this frustration be minimized by a symmetry breaking mechanism leading to the curving of the bundle ? Before trying to answer this question we need to add the shear energy which results from the cross-link-induced coupling of neighboring filaments.

- We assume the same shear coupling k_s of neighboring filaments and a single interdistance. Accordingly the shear energy reads

$$E_{shear} = \frac{k_s}{2} \int_0^L \left((u_3 - u_2 + d\theta)^2 + (u_2 - u_1 + d\theta)^2 \right) ds \tag{6.7}$$

  where d is the interdistance between the filaments.

To minimize the cross-link energy, any relative filament slip induced by the deviation $\theta(s)$ must be compensated by filament stretching. This cross link shear energy suppresses the relative sliding motion of neighboring filament. The finite temperature statistical physics of this model would be an interesting exercise, but we are here mainly interested in finding the ground state of this frustrated model.

6.3 Straight ground state

Suppose that the bundle is clamped at one end chosen at the origin of the frame such that $\theta(0) = 0$ and that it forms a circular arc which is the simplest curved state we can imagine. Then the angular deviation reads

$$\theta(s) = \kappa s, \tag{6.8}$$

where κ is a constant curvature. Similarly we assume a constant (s independent) strain ε_i for each filaments:

$$u_i'(s) = \varepsilon_i, \tag{6.9}$$

for $i = 1; 2; 3$.

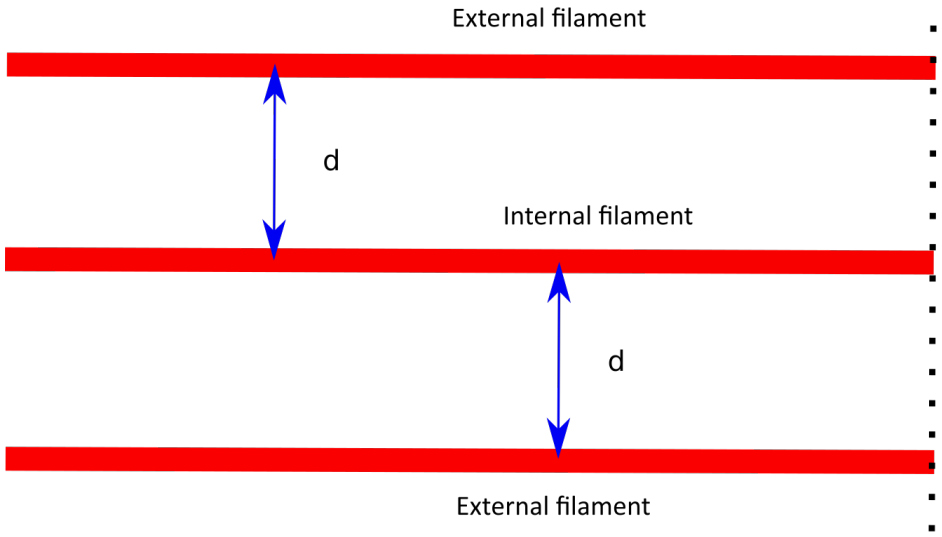

FIGURE 6.2: Bundle of three extensible filaments with a fixed interdistance d. When the rest lengths of the filaments are different this bundle is unstable.

The total energy density $e = \frac{E_{total}}{L}$ then becomes

$$e = \frac{1}{2}B\kappa^2 + \frac{A}{2}\sum_{i=1}^{3}\left(\varepsilon_i + \varepsilon_i^0\right)^2 + \frac{K_s}{2}\left((\varepsilon_3 - \varepsilon_2 + \kappa d)^2 + (\varepsilon_2 - \varepsilon_1 + \kappa d)^2\right), \tag{6.10}$$

where $K_s = \frac{k_s L^2}{3}$.

The minimization of this energy density gives a single solution, the straight state $\kappa = 0$ with

$$\varepsilon_2 = -\frac{2K_s}{A+3K_s}\varepsilon_0, \quad \text{and} \quad \varepsilon_1 = \varepsilon_3 = -\left(\frac{A+2K_s}{A+3K_s}\right)\varepsilon_0 \tag{6.11}$$

and the bundle density energy of this configuration is

$$e = \frac{AK_s}{A+3K_s}\varepsilon_0^2 \tag{6.12}$$

From Eq. (6.11) we see that all filaments have a shorter length than L but none is in its preferred state. The center filament is under a compressed stress as $\varepsilon_2 < 0$ while the external ones are under tension as they can not get fully contracted to their preferred strain $-\varepsilon_0$. This compromised situation depends on the ratio A/K_s, it is interesting to look at the limiting cases.

- In the limit of large $A/K_s >> 1$, stretching is not allowed and each filament reaches its preferred intrinsic state $\varepsilon_2 = 0$ and $\varepsilon_1 = \varepsilon_3 = -\varepsilon_0$ (see 6.3) In this case the sliding between the filaments is maximal and the cross-link between the filament is under maximal extension. The energy is given by

$$e = K_s\varepsilon_0^2, \tag{6.13}$$

  which depends now only on K_s .

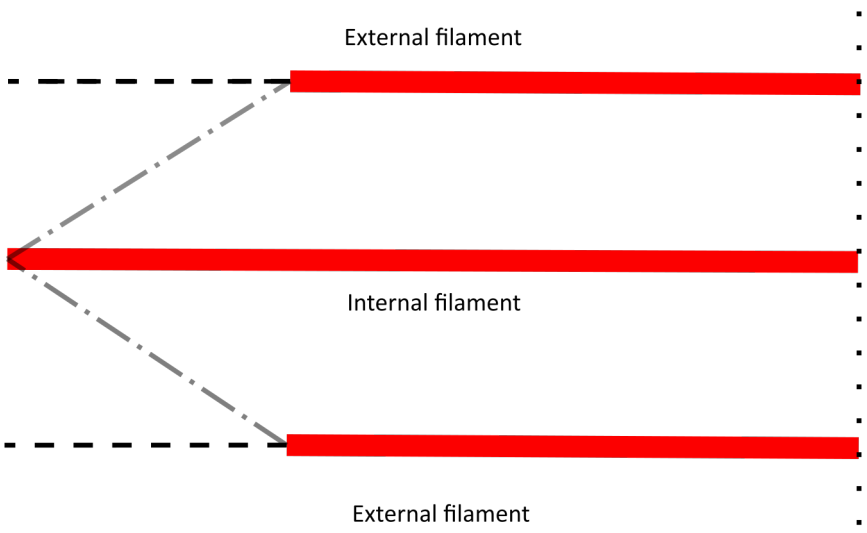

FIGURE 6.3: For inextensible filaments this bundle is unstable bundle and relaxes to a straight state with maximum shear with all filaments having their rest lengths.

- In the limit of small shear $K_s/A >> 1$ the sliding is forbidden and the three filaments have the same non-optimal strain $\varepsilon_2 = \varepsilon_{1/3} = -\frac{2}{3}\varepsilon_0$ and obviously the same length (6.4.) given by $L(1 - 2\varepsilon_0/3)$. The total energy density is in this case

$$e = \frac{A}{3}\varepsilon_0^2. \tag{6.14}$$

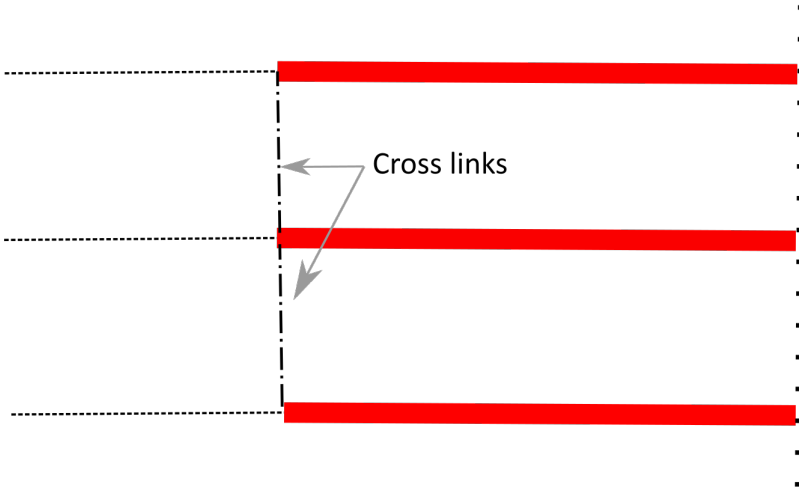

FIGURE 6.4: When shear is not allowed, the bundle relaxes to a shorter straight bundle where all filaments have the same shorter length.

In conclusion of this section, the model based on linear elasticity with asymmetric stresses between the surface and the interior of the bundle does not have a symmetry breaking and a curved ground state. We remind that in this model, as well as in the soft shear model of microtubule, the cross-links are supposed to be compliant in shear along the bundle axis with finite shear stiffness K_s but are assumed to be inextensible transverse to the bundle axis, thus fixing the interfilament distance d. This is a strong assumption, that we will relax in the next paragraph.

6.4 Straight ground state instability

To keep the discussion as simple as possible we consider the zero shear case ($K_s \to \infty$) but assume that the cross-links can now fluctuate around an equilibrium position. In other words, the filaments' interdistance can change. The distances between the central filament $i = 2$ (the reference frame) and the two external filaments $i = 1$ and 3 are written as

$$d_1 = d\,(1 + y_1) \quad \text{and} \quad d_3 = d\,(1 + y_3)\ . \tag{6.15}$$

We additionally model the cross-links as springs with a quadratic potential energy that suppress strong deviations of the cross-link from its preferred length d. Denoting δ the cross-links with mean axial spacing we thus have L/δ discrete cross-links.
We assume that each cross-links is extended by the same amount so that total potential energy of the cross-links is

$$W = \frac{Ld^2k_L}{2\delta}\left(y_1^2 + y_3^2\right). \tag{6.16}$$

With the notation

$$K_L = \frac{d^2k_L}{\delta}, \tag{6.17}$$

we then add the following density of cross-links energy

$$V(y_1, y_3) = \frac{K_L}{2}\left(y_1^2 + y_3^2\right), \tag{6.18}$$

to the energy density of the bundle. The limit of large K_L leads to the constrain $y_1 = y_3 = 0$ of fixed interdistances discussed above. In the absence of shear ($K_s \to \infty$) , the cross links are compressed/extended only in the orthogonal direction to the bundle axis while the longitudinal strains satisfy the constrains

$$\varepsilon_3 = \varepsilon_2 - \kappa d_3 \quad \text{and} \quad \varepsilon_1 = \varepsilon_2 + \kappa d_1$$

The total energy density simplifies greatly and reads

$$e\,(\kappa, \varepsilon_2, y_1, y_3) = \frac{1}{2}B\kappa^2 + \frac{A}{2}\left(\left(\varepsilon_2 - d\,(1 + y_3)\,\kappa + \varepsilon_0\right)^2 + \left(\varepsilon_2 + d\,(1 + y_1)\,\kappa + \varepsilon_0\right)^2 + \varepsilon_2^2\right) + \frac{K_L}{2}\left(y_1^2 + y_3^2\right) \tag{6.19}$$

Now, it only depends on four variables. The infinite shear limit is physically close to the continuum formulation: the bending of a rod which has no shear by construction.

6.4.1 Energy minimization

The minimization of the energy density equation 6.19 with respect to all variable leads to the following four coupled non-linear equations :

$$\kappa = \frac{A(y_3 - y_1)(\varepsilon_2 + \varepsilon_0)}{B/d^2 + A\left((1+y_3)^2 + (1+y_1)^2\right)} \tag{6.20}$$

$$\varepsilon_2 = \frac{1}{3}\left(-2\varepsilon_0 + d\kappa(y_3 - y_1)\right) \tag{6.21}$$

$$Ad^2\kappa^2\left(1+y_3\right) + y_3 K_L = Ad\kappa\left(\varepsilon_0 + \varepsilon_2\right)$$

$$Ad^2\kappa^2\left(1+y_1\right) + y_1 K_L = -Ad\kappa\left(\varepsilon_0 + \varepsilon_2\right)$$

These coupled equations seem very difficult to solve. We will discuss later on the results of the numerical minimization. But for now, we can use a different approach. Notice that the straight state defined by $\kappa = 0$, $y_1 = y_3 = 0$ and $\varepsilon_2 = -\frac{2}{3}\varepsilon_0$ is always a solution, we can look at its stability. Indeed we know that the straight state is the ground state for infinite value of K_L. By reducing K_L can the trivial ground state become unstable ?

6.4.2 Stability analysis

To look at the stability of the straight state solution, we compute the second derivative of the energy Eq.6.19 around $\kappa = 0$, $y_1 = y_3 = 0$ and $\varepsilon_2 = -\frac{2}{3}\varepsilon_0$ in order to determine the Hessian matrix H.
A simple computation gives

$$H = \begin{pmatrix} 2A + B/d^2 & 0 & -\frac{1}{3}A\varepsilon_0 & \frac{1}{3}A\varepsilon_0 \\ 0 & 3A & 0 & 0 \\ -\frac{1}{3}A\varepsilon_0 & 0 & K_L & 0 \\ \frac{1}{3}A\varepsilon_0 & 0 & 0 & K_L \end{pmatrix}. \tag{6.22}$$

This matrix has the following eigenvalues

$$\lambda_1 = \frac{1}{2}\left(2A + B/d^2 + K_L - \sqrt{\frac{8}{9}A^2\varepsilon_0^2 + (2A + B/d^2 - K_L)^2}\right)$$
$$\lambda_2 = \frac{1}{2}\left(2A + B/d^2 + K_L + \sqrt{\frac{8}{9}A^2\varepsilon_0^2 + (2A + B/d^2 - K_L)^2}\right)$$
$$\lambda_3 = 3A$$
$$\lambda_4 = K_L$$

The Hessian matrix has four eigenvalues but only one, λ_1, can be negative. The straight solution is stable if $\lambda_1 > 0$, that is for a spring constant K_L of the cross-links which is larger than a critical value $K_{L,critic}$, i.e.;

$$K_L > K_{L,critic}, \tag{6.23}$$

with

$$K_{L,critic} = \frac{2}{9}\frac{A^2\varepsilon_0^2}{2A + B/d^2} \tag{6.24}$$

When $K_L < K_{L,critic}$ the straight ground state is unstable and the actual one is curved.

6.4.3 Order of magnitude

From Eq.(6.17) we can estimate the value of the spring constant of a single cross-links. Eq. (6.24) can be rewritten

$$\frac{k_{L,critic}}{\delta} = \frac{8}{9}\frac{\pi R^2 Y}{8d^2 + R^2.}\varepsilon_0^2 \tag{6.25}$$

Assuming that R and d are of the order of nm we have

$$k_{L,critic} \sim Y\delta\varepsilon_0^2. \tag{6.26}$$

For a Young modulus Y between 10^6 to 10^9 Pa, and again $\delta \sim nm$ we have

$$10^{-3}\varepsilon_0^2 \lesssim k_{L,critic} \lesssim \varepsilon_0^2, \tag{6.27}$$

in units of N/m.
Note that for a protein of length L

$$k_{protein} \sim \frac{F}{L\varepsilon_0} \tag{6.28}$$

As the typical force are in *piconewton*, and for $L \sim \mu m$ we have the estimate

$$k_{protein} \sim \frac{10^{-6}}{\varepsilon_0}$$

which is of the same order of magnitude than $k_{L,critic}$.

6.4.4 Discussion

This elastic instability is easy to understand : Both filaments $i = 1$ and 3 want to shorten with respect to filament 2 . If, for instance, the bundle bends inwards with respect of filament 1 (with a bending energy $\sim B\kappa^2$ not too large), filament 1 is under compression and will obviously reduce its length with respect to filament 2 by curving but also by increasing d_1 as much as possible. On the opposite side, filament 3 is elongated due to bending but it can limit its elongation by getting closer to filament 2 i.e.; reducing d_3. Actually, if Eq.(6.23) is satisfied filament 3 will collapse on filament 2, i.e.; $y_3 = -1$ (see 6.5).

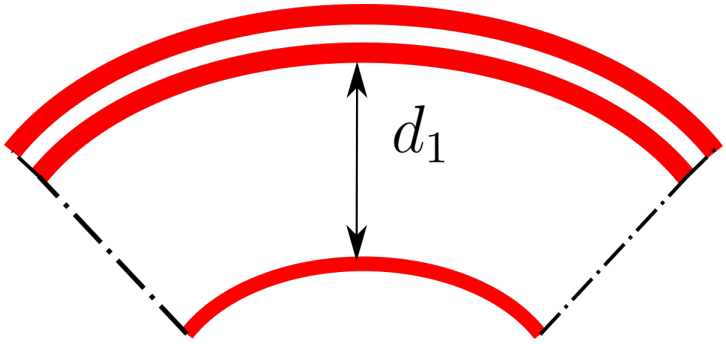

FIGURE 6.5: When the cross-links are laterally extensible the straight state of the bundle can become unstable. The quadratic potential energy of the cross-links can not stabilize the bundle and two filaments collapse onto each other.

One can numerically show that this collapse can be prevented by adding a quartic potential $V = \frac{1}{4}K_4\left(y_3^4 + y_1^4\right)$ which will stabilize the circular arc shape of the bundle. It seems that some non-linear elastic components are coming back to stabilize the curved state (see Fig.6.6).

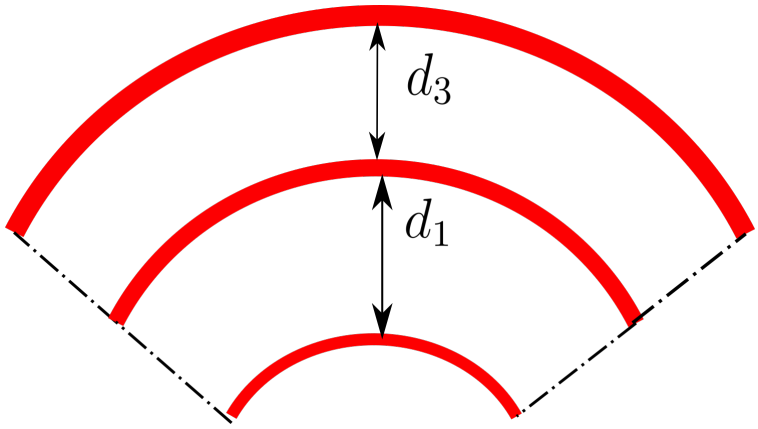

FIGURE 6.6: A quartic potential stabilizes the bundle in a curved state.

Conclusion : the lesson from this analysis is that a fully linear elastic bundle model can lead to curved ground state via a symmetry breaking induced by a surface-core instability if the bundle cross section can be elastically deformed. The previous frustrated core-shell model of microtubule without switchable dimers could not lead to such instability as the microtubule cross-section was maintained circular. It also seems that going beyond the instability, i.e. if we want to describe the actual ground state, requires to go beyond linear elasticity and consider non-linear elastic deformation. This is what we are going to see in the next chapter when we will consider surface tension as a source of instability.

Chapter 7

Symmetry breaking induced by surface tension : linear regime

In this chapter we adopt a sort of continuum version of the three filaments models presented in chapter 6. Here the effect of a surface stress on the shape of a filaments, seen as elastic rods, is investigated with the formalism of surface tension of solids. Then, the main question is : can the frustration induced by the mismatch between the surface elastic state, that is under stress, and the stressless core of the rod lead to an elastic instability ? In other word, can surface tension modify the bending modulus of the rod such that resulting apparent (or renormalized) bending stiffness can vanish for a critical value of the surface tension ? This is a fundamental importance as it could explain the observed recurrence of persistent curved conformations of biofilaments but can also have practical consequences like making biofilaments potentially actuating shape shifter fibers. Before embarking to this topic, as usual we will recall the concept of surface tension in liquids ([72]) but also in soft material like gels with visual examples and also home made experiments.

7.1 Surface tension

7.1.1 Surface Energy

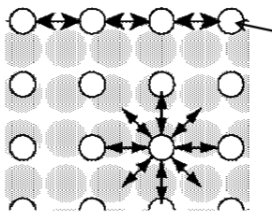

FIGURE 7.1: Arrangement of molecules on the surface of a liquid

As we can see on figure 7.1, , on the surface of this liquid, we can observe that some molecules can feel unhappy because they can not take advantage of some of the interactions a priori possible with other molecules of the surface. These molecules are "Unhappy" at the surface because they are missing half their attractive interactions : this situation generates an additional energy called **surface energy**. The existence of this surface energy helps explaining the change in the surface of liquids and the adaptation of these surfaces so that the exposed area is as short as possible. This excess energy corresponds to the energy necessary for the existence of a free surface, i.e. in contact with a medium different from the liquid concerned (air, usually). This phenomenon is visible in various everyday situations: soap bubbles, curling hair, etc.

Can this surface energy be associated with a surface force?

Let us assume we want to create on the free surface of a liquid a slit-shaped opening of length L and very small width Δx (fig. (7.2)): in order to do it we must exert forces T_i at several points of the opening, which must be tension forces.

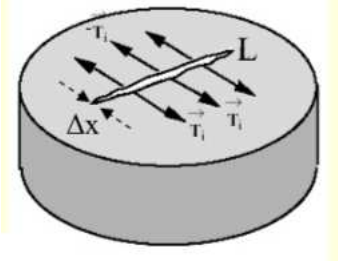

FIGURE 7.2

Indeed, the liquid tends to oppose this operation by developing a force so that

$$\vec{F} = -\vec{T}_i.$$

Then $\vec{F}$ can be written :

$$F = \gamma L,$$

where γ is given in N/m and called **Surface tension**.

Energy expression

To "open" the slit in the liquid surface, energy must be supplied to fight the force $\vec{F}$ that opposes this action. This energy is measured by the work of F during the increase in surface area : $\vec{F}$ is doing resistive work and this increases the energy of the liquid.

$$\Delta E = F.\Delta x = \gamma L.\Delta x,$$

then

$$\Delta E = \gamma.\Delta S.$$

The term γ also appears in the expression of the energy and will be central in the use we will make of the surface tension.

Helium (4K)	Ethanol	Acetone	Glycerol	Water	Water (373K)	Mercury
0.1	23	24	63	73	58	485

FIGURE 7.3: Surface tension of common liquids in mJ/m2

Mechanical definition, a capillary force

Surface tension (γ) can also be viewed as a force per unit length (N/m) The term “surface tension” is tied to the concept that the surface stays under a tension. Examples where surface tension manifests itself as a force : slider, capillary adhesion or objects floating on water.
The meniscus is the curve in the upper surface of a liquid close to the surface of the container or another object : it is caused by surface tension. It can be either convex or concave, depending on the liquid and the surface.

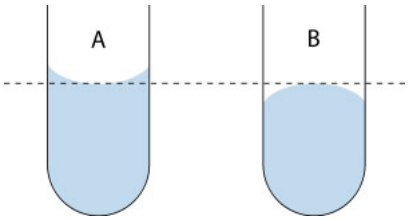

FIGURE 7.4: Meniscus

As shown on figure 7.4 (a), a concave meniscus occurs when the particles of the liquid are more strongly attracted to the container than to each other, causing the liquid to climb the walls of the container. This occurs between water and glass. Figure 7.4 (b) shows a convex meniscus that occurs when the particles in the liquid have a stronger attraction to each other than to the material of the container. Convex menisci occur, for example, between mercury and glass in barometers.

FIGURE 7.5: Menisci at the surfaces of water and mercury, respectively

7.1.2 Solids

The term surface tension is usually associated with the free surface of a liquid or the shape of a drop. Solids are also sensitive to these capillary forces and can be deformed under their influence. For example, a wet sheet of paper will deform. The same result can appear in the case of a bar, geometrical model mainly studied here ([73]).

The Elastocapillary Length

Although solids are, like liquids, sensitive to this type of force, the deformations observed will be different. Indeed, the solids are able to withstand the deformations, to respond in a less significant way. To what extent will a solid undergo deformation?

The Shuttleworth equation is an equation that links surface tension Υ and surface energy γ through the strain ε ([74]) :

$$\Upsilon = \gamma + \frac{\partial \gamma}{\partial \varepsilon}. \tag{7.1}$$

It would then be interesting to define a critical length, $\mathbf{l_s}$, from which the surface stresses become important ([75]). What could this length depend on? It is considered that a significant strain appears when the stress reaches the shear modulus of the solid (G). This stress can be given by Laplace Law :

$$\sigma = \frac{\Upsilon}{L}, \tag{7.2}$$

with L is a characteristic length of the solid studied. We use equation (7.2) to get the **Shear elastocapillary length** :

$$l_S = \frac{\Upsilon}{G}. \tag{7.3}$$

The following table gives an overview of l_S values for some examples of solids.

l_s for different material			
Material	Surface tension (N/m)	Shear modulus	Elastocapillary length
Glass	0.250	20 GPa	10 pm
Copper	1.8	50 GPa	40 pm
Biological tissues	0.01 - 0.1	0.1 - 1,000 kPa	10 nm - 1 mm

Rounding the angles of a solid

In the case of a liquid, the surface tension will cause a curvature on the surface. The same effect is visible on solids. Indeed, several studies [76] state that bars with initially right-angled corners tend to become rounded under the effect of surface tension. The rounding of the edges of a solid also induces more global deformations on the large scale of a thin object. Using (7.3), we can write the equation giving the radius of the deformation of an right angled corner, of the order of l_S : $R \approx \Upsilon / G$ (figure 7.6).

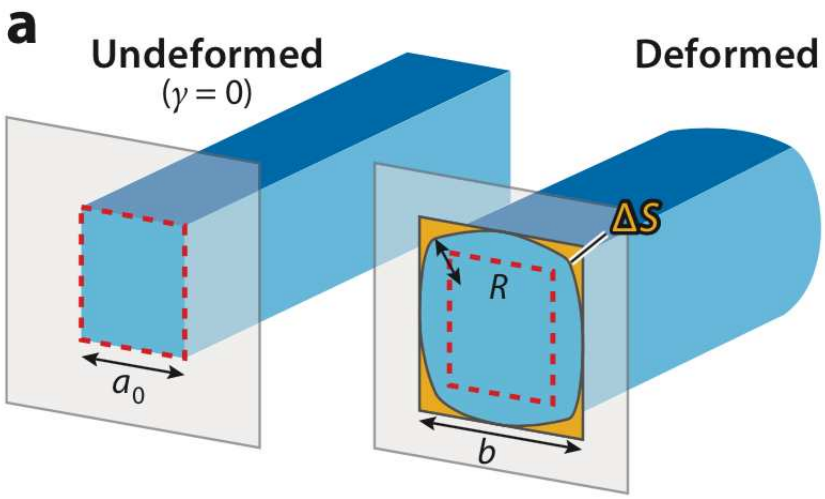

FIGURE 7.6: Deformation of the corners due to surface tension - Adapted from [73]

Home-made bar

Inspired by the work of [20] on how high a gelatin tower could be, I decided to replicate some of their experiments in the laboratory. In order to carry out a manipulation allowing to check the influence of the value of the surface tension on the shape of a bar, I chose to prepare and use a gel bar solidified after passage in the refrigerator. Then, in the continuity of the work done in chapter 3, a second manipulation consists in placing a continuous gelatin bar between two Plexiglas plates. The lower plate supports the bar while the upper plate covers it without pressing, this will allow us to observe the evolution of the bar over several days. During this period, the bar will dry, implying a modification of the surface tension value.

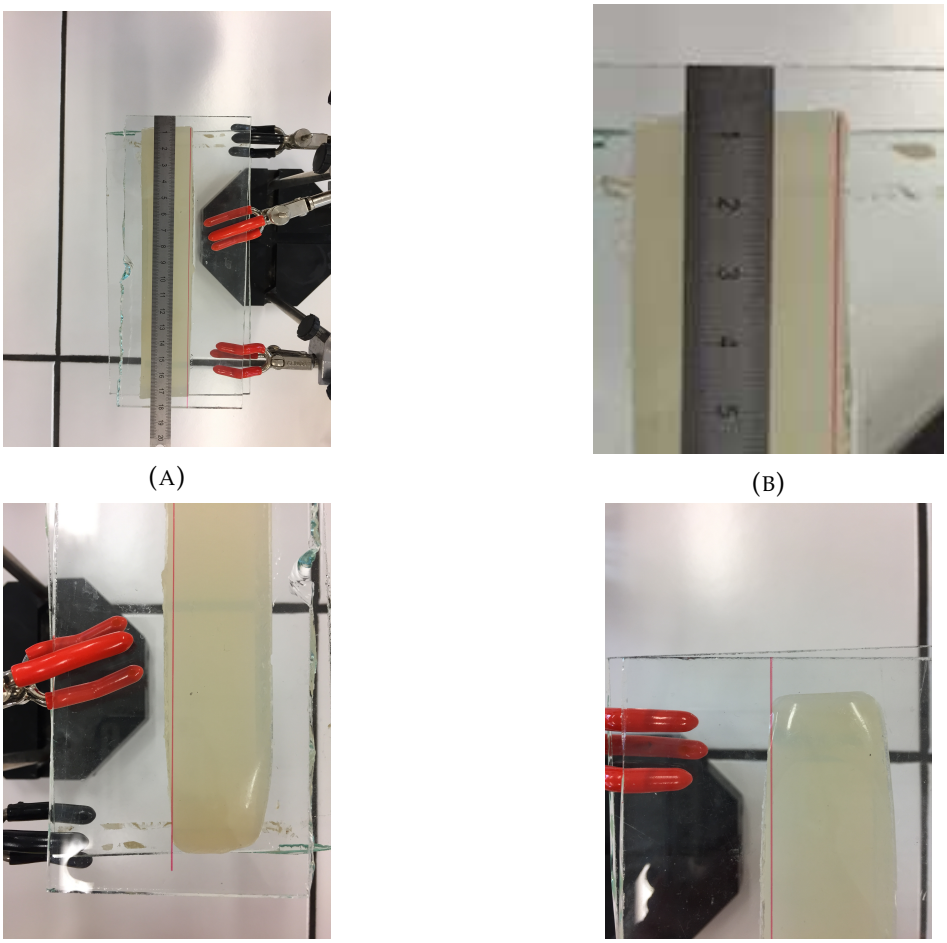

(A) (B)

(C) (D)

FIGURE 7.7: Gelatine bar between two plates

The idea was to let the bar dry in order to let the value of the surface tension change on the other four faces of the studied rectangular parallelepiped.

The experiment, which lasted five days, allowed me to observe the horizontal buckling of the bar under the effect of the surface tension variation. This experiment confirmed the observations of [77].

Indeed, we observe that the bar (7.7b and 7.7d) initially of straight section, sees its shape evolve with the appearance of curves on the part most exposed to the air thus having seen its surface tension significantly evolve.

7.2 Autocoiling instability

The extension of the mechanistic railway track model for more realistic systems with surface-core instability turns out to be very difficult. Here we use the approach of surface tension that was first used in the study of the elastic properties of nanotubes, nanofibers and nanowires. Surface tension is very significant for liquids but usually negligible for bulk materials, thus only for nanomaterials with large area to volume ratio do we expect surface effects become predominant and significantly modify the macroscopic properties. For instance, the experimental Young's modulus of carbon nanotubes [78] and of Ag and Pb nanowires [79] were found to increase dramatically with decreasing diameters. This increase of the apparent elastic modulus for smaller nanotube diameters is usually attributed to the surface tension effect [79][80]. In ref [79], a transversal force was applied at a beam midpoint inducing a deflection that increases the surface of the beam (See Fig.7.8). Adding to the elastic energy deformation of the beam $E_{elastic}$ a surface energy term $\gamma \Delta S$ with γ the surface tension of the material, gives an additive surface contribution to the beam bending modulus [79]. Similarly, the influence of the surface stress on the static deflection by a transversal force on nanowires clamped at one end was studied in [80] (See Fig.7.8).

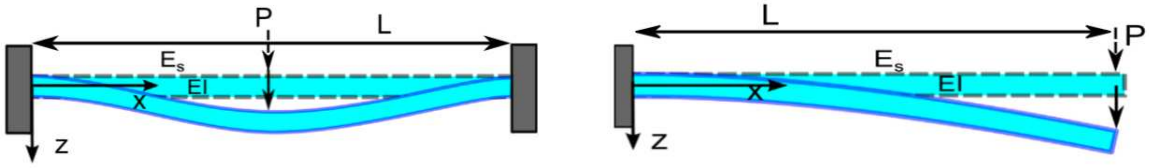

FIGURE 7.8: From fig 1 of [80]. By measuring the deflection of the beam one can deduce the apparent bending modulus which was found to increase dramatically with decreasing diameters.

In this work it was recognized that a negative residual surface stress that leads to a frustration between the surface which tends to shrink with respect to the core could lead to prebending of a beam with asymmetric cross section. For this reason a symmetric cross section such as rectangular and circular cross were assumed. But even in this case, these authors remarkably noted that a self-buckling could occur if the resultant force (similar to an axial compressive force) is large enough (when the apparent bending modulus is zero). They then excluded this case and only consider a regime where negative surface tension does not lead to buckling [80]. We instead consider the opposite point of view and infer if surface stresses on biofilaments could drive a self-buckling instability. Biofilaments, even in vitro-experiments, are materials which (like nanowires) can have mechanical properties very sensitive to surface coating and adsorbed molecules. A surface stress could be induced by any mismatch between the

surface and the bulk of the filament, like the surface tension between the ordered water and ions at the outer layers of the filament which display mismatched stresses (osmotic and Maxwell). This self-buckling mechanism was first motivated by the observation of important member of the intermediate filament, vimentin, displays conformational anomalies in narrow microfluidic channels [81]. The measured correlations function of confined intermediate filaments is strongly oscillating and this is not understandable with the usual semi-flexible chain theory. This anomaly was convincingly interpreted as the consequence of a previously undetected, large-scale helically curved superstructure [30]. As oscillations in the tangent correlation functions of individual actin filaments were also previously observed [82] helical microtubules as well [63][39] , the question of a more general physical mechanism arises.
Besides nanofilaments, other macroscopic filaments exposed to surface stresses can display broken symmetry via self induced curved states. For instance in a drying spaghetti, the outer layer dries faster than the inner layer. Then it also shrinks faster inducing a buckling stress on the more swollen core. Once all the water is evaporated, the dry spaghetti keeps frozen in a curved plastic state [30] (7.9a). In paper [83] an agar gel with a triangular isosceles cross section (prism) undergoes a large reversible bending when immersed into a silicone oil (see 7.9b)

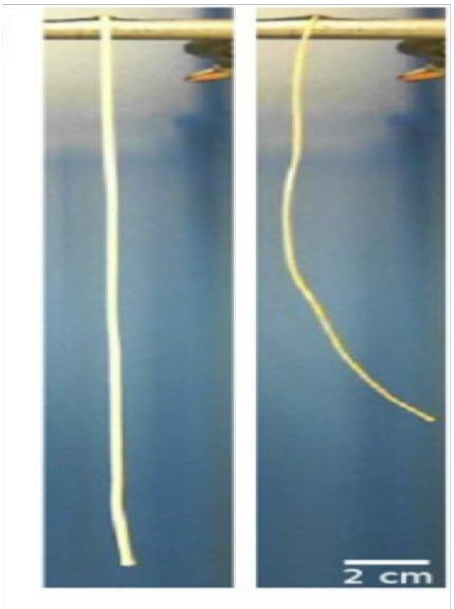

(A)

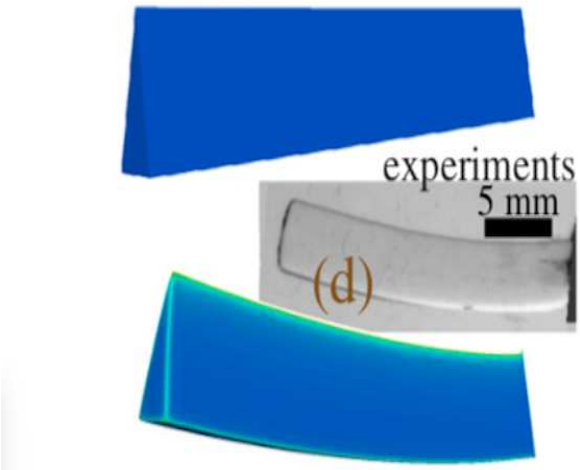

(B)

FIGURE 7.9: (A) Drying spaghetti becomes curved as a result of water evaporation creating a stress gradient [30]. (B) Surface tension in non isotropic gel induces a bending of the gel. This is no spontaneous symmetry breaking [83].

The surface energy γS, with γ the surface tension between the outer fluid and

the solvent and S the area of the boundary, is the driving term for the deformation of the gel against the gel restoring elasticity. Actually, a compressive resultant force and a non-zero bending moment are induced by the uniform surface stress on the triangular prism. These lead to a large curved conformation and, in this case, the self buckling is due to no symmetry breaking. Interestingly, bending disappears in the more symmetrical equilateral case, as well as for circular and square cross sections [83]. We see that surface tension has important consequences on filamentous structure but symmetry breaking might depends on the softness of the material.

7.2.1 Self buckling of a rod

As the simplest possible model for self-buckling under a surface stress, we consider an elastic filament with the highest possible symmetrical cross section, namely, circular cylinders.

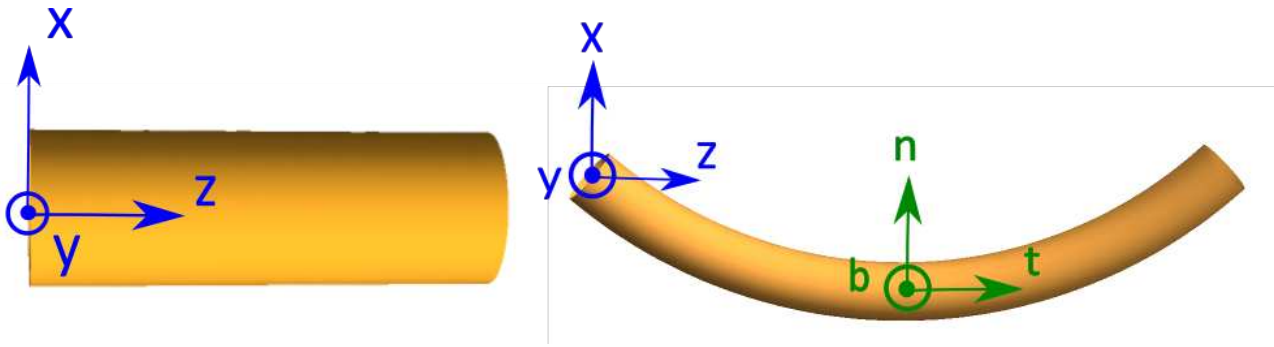

(A) Initial bar

(B) Deformed bar

FIGURE 7.10: Bars and frames

Energy

The energy in the linear elasticity approximation is

$$E = \frac{1}{2}\int dV \sigma_{ij}\varepsilon_{ij} + \gamma \Delta S, \tag{7.4}$$

where σ_{ij} and ε_{ij} are the bulk stress and strain tensor, respectively and dV is the differential volume of the rod. The constant γ is a positive isotropic surface stress or a surface energy density which favors surface shrinking and ΔS denotes the variation of the surface after deformation.

When negative, the term $\gamma \Delta S$ can compete with the positive elastic bulk energy and reduces the bending stiffness. A null apparent bending modulus would be the

signal that the straight state is unstable and that the true ground state is curved. Since surface tension can induce a compressive resultant elastic force as well as a bending moment we consider a stretchable rod.

To compute the deformation we need a reference frame (x, y, z) with basis vectors $(\overrightarrow{e_x}, \overrightarrow{e_y}, \overrightarrow{e_z})$ for the undeformed rod. **The z-axis** is chosen as the **longitudinal axis** of the rod that passes through the center of all cross sections. The positions $z = 0$ and $z = L$ correspond to the left and the right faces of the bar, respectively, so that origin of the coordinate axes is at the centre of the left end section (See Fig.7.10). Assuming a bending deformation of constant curvature κ in the x direction and a longitudinal strain ε, a good ansatz for the stress is :

$$\sigma_{zz} = Y\kappa x + Y\varepsilon,$$

with Y the Young modulus of the rod. All other components of the stress tensor are zero. The relation between stresses and deformations is given by constitutive Hooke's law which gives the following strains in the longitudinal direction:

$$\varepsilon_{zz} = \frac{\sigma_{zz}}{Y} = \kappa x + \varepsilon \tag{7.5}$$

and in lateral directions

$$\varepsilon_{xx} = \varepsilon_{yy} = -\nu\kappa x - \nu\varepsilon \tag{7.6}$$

where ν is the Poisson ratio which ensures that the rod is not laterally extensible. The elastic energy in Eq. 7.4 only depends on the stress and strain in the z direction and is easily computed (see chapter 2) to give

$$E = \frac{1}{2}BL\kappa^2 + \frac{1}{2}AL\varepsilon^2 + \gamma\Delta S \tag{7.7}$$

where

$$B = \frac{\pi}{4}YR^4, \tag{7.8}$$

and

$$A = \pi YR^2, \tag{7.9}$$

are respectively the bending and the stretching stiffness of the rod of length L.

The goal is now to compute the surface change ΔS in the bent conformation. To do so, we first need to search for the rod's conformation which will be deduced from the displacement field of the bent rod.

Displacement field

The shape of the rod is determined from the knowledge of the displacement field (u_x, u_y, u_z) defined by the strain - displacement equations, which, for small deformations, are approximately [1]

$$\partial_z u_z = \varepsilon_{zz}, \quad \partial_x u_x = \varepsilon_{xx} \quad \text{and} \quad \partial_z u_z = \varepsilon_{zz} \tag{7.10}$$

In our case $\partial_z u_z = \kappa x + \varepsilon$ can be easily integrated to give

$$u_z = (\kappa x)\, z + \varepsilon z + h(x, y)$$

Similarly, integrations of the lateral fields, $\partial_x u_x = -\nu\kappa x - \nu\varepsilon$ and $\partial_y u_y = -\nu\kappa x - \nu\varepsilon$, give

$$\begin{aligned} u_x &= -\frac{1}{2}\nu\kappa x^2 - \nu\varepsilon x + f\,(y, z) \\ u_y &= -\nu\kappa x y - \nu\varepsilon y + g\,(x, z)\,, \end{aligned}$$

where $h(x, y)$, $f\,(y, z)$ and $g\,(x, z)$ are function that we will determine.
In the absence of shear we also have the following relations [1]:

$$\begin{aligned} \partial_x u_z + \partial_z u_x &= 2\varepsilon_{xz} = 0 \\ \partial_x u_y + \partial_y u_x &= 2\varepsilon_{xy} = 0 \\ \partial_z u_y + \partial_y u_z &= 2\varepsilon_{zy} = 0 \end{aligned} \tag{7.11}$$

which lead to

$$\kappa z + \partial_x h(x, y) + \partial_z f\,(y, z) = 0 \tag{7.12}$$

$$-\nu\kappa y + \partial_x g\,(x, z) + \partial_y f\,(y, z) = 0 \tag{7.13}$$

$$\partial_z g\,(x, z) + \partial_y h(x, y) = 0 \tag{7.14}$$

The last equation imposes that g and h have the following forms :
$g\,(x, z) = \alpha_1 z + g_1(x)$ and $h(x, y) = -\alpha_1 y + h_1(x)$, where α_1 is a constant.
Then Eqs. (7.12) and (7.13) become

$$-\nu\kappa y + \partial_x g_1\,(x) + \partial_y f\,(y, z) = 0 \tag{7.15}$$

$$\kappa z + \partial_x h_1(x) + \partial_z f\,(y, z) = 0 \tag{7.16}$$

From Eq. (7.16) we see that f and h must be of the form :
$f(y,z) = -\frac{\kappa}{2}z^2 + f_1(y) + \alpha_2 z$ and $h_1(x) = -\alpha_2 x + \alpha_3$ with α_2 and α_3
Then Eq. (7.15) becomes

$$-\nu\kappa y + \partial_x g_1(x) + \partial_y f_1(y) = 0$$

which can be easily integrated to give : $g_1(x) = \alpha_4 x + \alpha_5$ and $f_1(y) = \upsilon\frac{\kappa}{2}y^2 - \alpha_4 y + \alpha_6$ with three other constants α_4, α_5 and α_6.
Collecting f, g and h we obtain the following displacements

$$\begin{aligned}
u_z &= \kappa xz + \varepsilon z - \alpha_1 y - \alpha_2 x + \alpha_3 \\
u_x &= -\frac{\kappa}{2}z^2 + \upsilon\frac{\kappa}{2}\left(y^2 - x^2\right) - \nu\varepsilon x + \alpha_2 z - \alpha_4 y + \alpha_6 \\
u_y &= -\nu\kappa xy - \nu\varepsilon y + \alpha_1 z + \alpha_4 x + \alpha_5
\end{aligned}$$

The various constant α_i depend on the boundary conditions.

Boundary conditions

We consider the following boundary conditions $u_x(0) = u_y(0) = u_z(0) = 0$ corresponding to a fixed origin. We also impose that the displacement of the end is possible only in the $z-$direction, i.e.; $u_x(0,0,L) = u_y(0,0,L) = 0$.
The first condition leads immediately to $\alpha_3 = \alpha_5 = \alpha_6 = 0$ while the second condition implies $\alpha_1 = 0$ and $\alpha_2 = \frac{\kappa}{2}L$. The displacement field then only depends on α_4. Assuming the additional condition $\partial u_x(0)/\partial y = 0$ we get $\alpha_4 = 0$ and finally we obtain

$$u_z = \kappa x(z - L/2) + \varepsilon z \tag{7.17}$$
$$u_x = \frac{\kappa}{2}z(L - z) + \nu\frac{\kappa}{2}\left(y^2 - x^2\right) - \nu\varepsilon x \tag{7.18}$$
$$u_y = -\nu\kappa xy - \nu\varepsilon y \tag{7.19}$$

We must keep in mind that the coordinates in these equations correspond to positions of points of the undeformed rod. We can check our results.
When $\kappa = 0$ we retrieve the expected result $u_z = \varepsilon z$, $u_x = -\nu\varepsilon x$, $u_y = -\nu\varepsilon y$ and when $\varepsilon = 0$ we get the results of pure bending [84]. In this case the central line is usually called the neutral line since $u_z = 0$ for all z if $\varepsilon = 0$.

Rod deformation

In order to apprehend the shape of the rod, we first consider the deformation of the rod center line, for $x = y = 0$.
Then the displacement field is :

$$\begin{aligned} u_z &= \varepsilon z \\ u_x &= \frac{\kappa}{2} z(L - z) \\ u_y &= 0 \end{aligned}$$

We see that bending induces on the longitudinal axis (the centerline of the rod) a resultant extensive or compressive force depending on the sign of ε. There is no displacement in the y direction for the centerline, meaning that the bending is planar (no torsion). The displacement $u_x(z)$ gives the deflection curve of the beam which is an arc with the two ends fixed i.e. $u_x(0) = u_x(L) = 0$. Note that at the mid-range cross section $z = L/2$, we have $u_z = \varepsilon z$ so the plane is shifted to the right (stretching) or to the left (compression) but stays vertical.
As there is no shear allowed here, each plane cross section remains a plane and are all identical after bending. They simply rotates by an angle given by $\sim du_z/du_x$. .

Cross section deformation

To compute the shape of the cross section it is wise to consider the displacement vector $\overrightarrow{\widetilde{u}}\ (\widetilde{u}_x, \widetilde{u}_y)$ that gives the displacement from the centerline and not from the z-axis.
We see that

$$\begin{aligned} \widetilde{u}_x &= \frac{1}{2}\kappa\nu \left(y^2 - x^2\right) - \nu\varepsilon x \\ \widetilde{u}_y &= -\nu\kappa xy - \nu\varepsilon y \end{aligned}$$

Along the outer surface $x = R\cos\phi$ and $y = R\sin\phi$ with $\phi \in [0, 2\pi]$ the polar angle we have for the displacement vector

$$\overrightarrow{\widetilde{u}}\ (\phi) = -\frac{1}{2}\kappa\nu R^2 \begin{pmatrix} \cos 2\phi \\ \sin 2\phi \end{pmatrix} - \nu R\varepsilon \begin{pmatrix} \cos\phi \\ \sin\phi \end{pmatrix}.$$

The contour of the deformed cross section is thus given by the coordinates

$$x' = x + \widetilde{u}_x \quad \text{and} \quad y' = y + \widetilde{u}_y$$

and the vector that describes the contour of the new, visibly non circular, cross section can be written as

$$\vec{C}(\kappa,\phi) = R\begin{pmatrix} (1-\nu\varepsilon)\cos(\phi) - \nu\delta\cos 2\phi \\ (1-\nu\varepsilon)\sin(\phi) - \nu\delta\sin 2\phi \end{pmatrix} \tag{7.20}$$

where we introduced the dimensionless parameter $\delta = \frac{\kappa R}{2}$ which will be, for small curvatures, a parameter for expansion later on.

Surface of revolution

Such a rod curving in the x direction with a constant curvature is actually a surface $S(R,\kappa;\phi,\theta)$ of revolution around the y-axis (See Appendix A). The centerline is a circular arc at a distance $1/\kappa$ from the origin of rotation, that we chose now at the origin of a new system of coordinates. In this way the contour of the cross section, as seen from this new origin, defines a new vector $\vec{C}_{shift}(\kappa,\phi)$

$$\vec{C}_{shift}(\kappa,\phi) = \vec{C}(\kappa,\phi) + \frac{1}{\kappa}\overrightarrow{e_x} \tag{7.21}$$

with new coordinates still denoted x and y are

$$\begin{pmatrix} x(\phi) \\ y(\phi) \end{pmatrix} = R\begin{pmatrix} (1-\nu\varepsilon)\cos(\phi) - \nu\delta\cos 2\phi + \frac{1}{R\kappa} \\ (1-\nu\varepsilon)\sin(\phi) - \nu\delta\sin 2\phi \end{pmatrix} \tag{7.22}$$

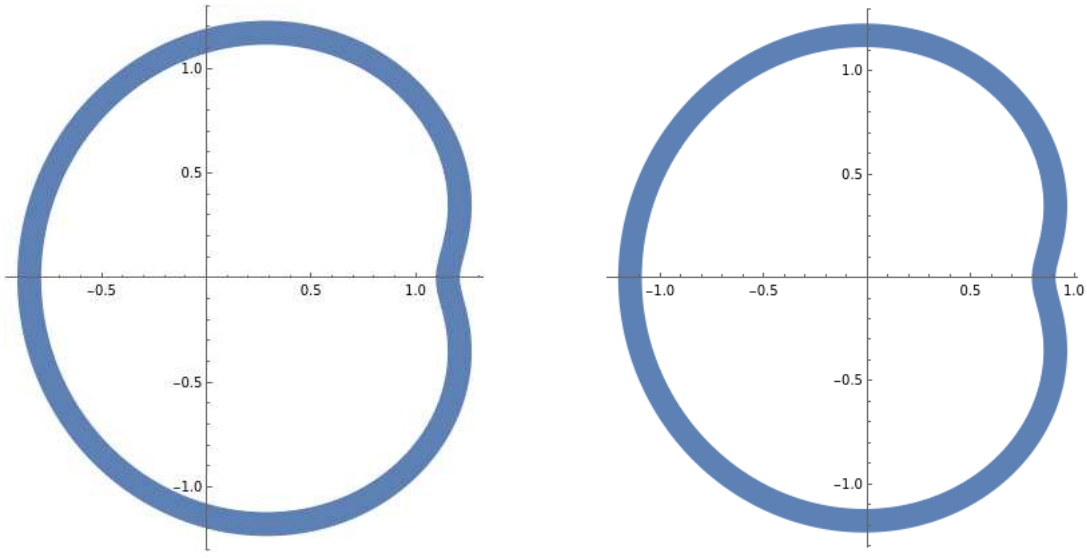

(A) $\kappa = 2$ (B) $\kappa = 5$

FIGURE 7.11: Cross section with shift of neutral line

Pappus theorem

To compute the area of the surface of revolution we use Pappus theorem : if a curve is parametrically described by $(x(t), y(t))$,and the surface area is obtained by rotating by an angle θ the curve about the y-axis for t in $[a, b]$, then the surface area is given by

$$S_y = \theta \int_a^b x\sqrt{x'(t)^2 + x'(t)^2}dt$$

In our case the angle of rotation is $\theta = \kappa L(1+\varepsilon)$ where we have taken into account the change in the length of the centerline and the formula becomes

$$S_y = L(1+\varepsilon)\kappa \int_0^{2\pi} x(\phi)\sqrt{x'(\phi)^2 + y'(\phi)^2}d\phi \tag{7.23}$$

As

$$\begin{pmatrix} x' \\ y' \end{pmatrix} = R \begin{pmatrix} 2\nu\delta\sin 2\phi - (1-\nu\varepsilon)\sin\phi \\ (1-\nu\varepsilon)\cos\phi - 2\nu\delta\cos 2\phi \end{pmatrix}$$

we obtain

$$S_y = LR(1+\varepsilon)$$
$$\int_0^{2\pi} \left(2\delta(1-\nu\varepsilon)\cos(\phi) - 2\nu\delta^2\cos 2\phi + 1\right)\sqrt{4\nu^2\delta^2 + (1-\nu\varepsilon)^2 - 4\delta\nu(1-\nu\varepsilon)\cos\phi}d\phi \tag{7.24}$$

Expanding this expression to quadratic order in $\delta = \kappa R/2$ and integrating over ϕ we obtain

$$S_y = 2LR\pi\frac{1+\varepsilon}{(1-\nu\varepsilon)}\left((1-\nu\varepsilon)^2 + \delta^2\nu\left(\nu - 2(1-\nu\varepsilon)^2\right)\right) \tag{7.25}$$

When $\delta = \varepsilon = 0$ we recover the surface of the undeformed rod : $S_0 = 2\pi LR$.

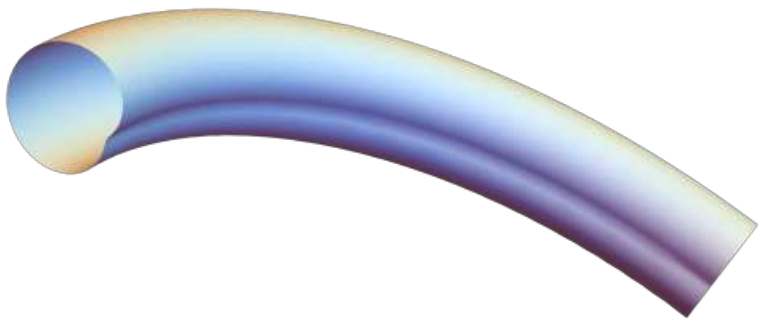

FIGURE 7.12: Bent bar with deformed section

7.2.2 Contribution of surface tension to the bending modulus.

The computation of ΔS at quadratic order in κ and ε gives

$$\frac{\Delta S}{S_0} \approx -\frac{1}{4}R^2\nu\,(2-\nu)\,\kappa^2 + (1-\nu)\,\varepsilon - \nu\varepsilon^2. \tag{7.26}$$

We see that the surface energy $\gamma\Delta S$ adds contributions to both bending and stretching modulus, so that the energy density $e = E/L$ can be written

$$e = \frac{1}{2}\widehat{B}\kappa^2 + \frac{1}{2}\widehat{A}\varepsilon^2 + C\varepsilon, \tag{7.27}$$

with the renormalized (apparent) modulus

$$\widehat{B} = \frac{\pi}{4}R^4(Y - \frac{4}{R}\gamma\nu(2-\nu)), \tag{7.28}$$

and

$$\widehat{A} = \pi R^2(Y - \gamma\frac{2\nu}{R}), \tag{7.29}$$

plus an additional positive modulus.

$$C = 2\pi R\,(1-\nu)\,\gamma. \tag{7.30}$$

As expected both $\widehat{B}$ and $\widehat{A}$ are reduced by the surface tension.
In linear elasticity, bending and stretching are decoupled and the optimal longitudinal strain is :

$$\bar{\varepsilon} = \frac{-C}{\widehat{A}}$$

For standard material $\nu < 1$ and the surface tension is equivalent to a compressive resultant force as $\bar{\varepsilon} < 0$ similarly to agar gel in [83]. The total energy density then reduces to a bending energy density

$$e = \frac{1}{2}\widehat{B}\kappa^2, \tag{7.31}$$

if we dismiss the constant energy term $e(\kappa = 0) = -C^2/(2\widehat{A})$ of the straight compressed state. When the surface tension γ reaches a critical value γ_c given by :

$$\gamma_c = \frac{RY}{4\nu(2-\nu)}, \tag{7.32}$$

the stiffness modulus $\widehat{B}$ vanishes and the rod becomes unstable. This is the signature

of a spontaneous broken symmetry of the rod also named self-buckling (Note that $\widehat{B}$ vanishes before $\widehat{A}$ for all values of γ).
To have an order of magnitude consider a microtubule with $R \simeq 25nm$, $\nu \simeq 0.5$ (inextensible) and $Y \simeq 1GPa$. We get $\gamma \simeq 8\ N/m$ of the same order of the nanowires [79] but much larger than for gels, $\gamma \simeq 0.01\ N/m$, which are very soft [83].

The detected helical superstructure of vimentin in [30] was based on the self-induced filament buckling via a surface stress located at the outside of the cross section. They suggested that the surface stress originates from the vimentin molecular structure and the maturation phase of its subunits during polymerization. The supposed elastic shape instability that leads to the vimentin helical state was called autocoiling [30].

This raises the question whether self-buckling discussed could, beyond the curvature, explain the observed helical torsion of vimentin. To settle this point, we compute the surface area S of an helical rod of length L with both a constant curvature κ and torsion τ (for simplification we will consider $\varepsilon = 0$)

7.2.3 Surface area in helical autocoiling

The centerline coordinate of the helix s is given by vector $\overrightarrow{R}(s)$ in the Frenet-Serret frame and the border of the cross section at position s is given by the coordinates $x(\phi)$ and $y(\phi)$ from the center of the cross section. With these choices the surface of the helical rod is parametrized by vector $\overrightarrow{F}(s)$ which is

$$\vec{F}(s,\phi) = \overrightarrow{R}(s) + \overrightarrow{n}(s)x(\phi) + \overrightarrow{b}(s)y(\phi),$$

where $\overrightarrow{n}(s)$ and $\overrightarrow{b}(s)$ are the normal and binormal vectors of the Frenet-Serret frame, respectively. The first fundamental form (of differential geometry)

$$I(s,\phi) = \begin{pmatrix} \overrightarrow{F}_s.\overrightarrow{F}_s & \overrightarrow{F}_s.\overrightarrow{F}_\phi \\ \overrightarrow{F}_s.\overrightarrow{F}_\phi & \overrightarrow{F}_\phi.\overrightarrow{F}_\phi \end{pmatrix}$$

where we have defined $\overrightarrow{F}_s = \partial\overrightarrow{F}/\partial s$ and $\overrightarrow{F}_\phi = \partial\overrightarrow{F}/\partial\phi$ allows to compute the area S of the rod with the following formula

$$S = \int \sqrt{\det(I(s,\phi))}dsd\phi$$

Using $\overrightarrow{R}'(s) = \overrightarrow{t}$ the tangent vector of the centerline and $\overrightarrow{t}' = \kappa\overrightarrow{n}$ as well as $\overrightarrow{n}' = \tau\overrightarrow{b} - \kappa\overrightarrow{t}$ (see chapter 2) we find that :

$$\vec{F}_s = (1-\kappa x)\overrightarrow{t} - \tau y\overrightarrow{n} + \tau x\overrightarrow{b}$$

and

$$\vec{F}_\phi = x'\overrightarrow{n} + y'\overrightarrow{b}$$

where $'$ means the derivative with respect to ϕ. The determinant of $I(s,\phi)$ at quadratic order in κ and τ is easily calculated and we obtain the following expression for the area of the helix

$$S = \int \sqrt{(1-\kappa x)^2(x'^2+y'^2) + \tau^2(yy'+xx')^2}dsd\phi \tag{7.33}$$

Regardless of the exact form of the cross section (i.e. x, y), the area can only grow with torsion τ. So there seems no way to reduce surface area with a helical shape with respect to a simple arc. Therefore the precise molecular origin of the helical torsion of vimentin remains currently unexplained. As previously mentionned, the ability of the intermediate filaments to support mechanical elements could be explained by the high compliance of the coiled structure of the filaments.

Conclusion : Surface tension contribution to the bending stiffness are likely ubiquitous among the filaments in biology and make biofilaments analogue to actuating elastic fibers whose elastic properties can fine tuned by changing the properties of the liquid in which fiber is immersed. But there is more.

Autocoiling instability gives rise to a zero elastic energy mode and an energy landscape that depends only on the magnitude of curvature and not on its direction displaying a continuously degenerated ground state.
Therefore not only are biofilaments potential actuating fibers but a zero energy mode can make them (randomly) rotate at finite temperature (see clamped microtubules). A beautiful macroscopic application of the geometric zero-energy modes to elicit a rotary motion in elastic materials can be found in [85]. There, a prestrained polymer fibres exhibit self-actuation and continuous rotation when placed between two heat baths. This opens the way to built functional machines composed solely from shape-changing materials.

The frustrated core-shell models at the level of linear elastcity demonstrates that spontaneous symmetry breaking is possible and actually may be the rules in biology. The determination of the true ground states of the filaments beyond the unstability threshold demands to consider the non-linear regime of elasticity.

Chapter 8

Symmetry breaking induced by surface tension: non linear regime

Models developed in chapters 6 and 7 are based on two different physical approaches. In chapter 6, the model was made to describe the elastic behavior in the plane of a bundle of discrete extensible semi-flexible filaments without any additional physical principle. This model is likely the simplest model one can imagine and it is appealing in demonstrating the origin of symmetry breaking of biofilaments. The physical principle stems from the elastic mismatch between the filaments on the boundary and the filaments in the interior of the bundle (in practice we have considered three filaments). The main result was that a self-buckling elastic instability can only occur when the interdistance between filaments is allowed to change. In other words, the deformation of the cross section of the bundle during buckling has to be taken into account in the model. Most models of buckling of biofilaments like microtubule for instance do not take into account this cross-section deformation [66][40]. We have mentioned that the curved ground state conformation beyond the instability threshold can be stabilized against collapse onto each other of the filaments on the opposite side of the curvature by adding a quartic elastic cross-links potential energy. This quartic potential stabilizes the interfilament distance. Therefore non-linearity is coming back in the description of the non-trivial ground state. This is a very common feature in physics that states in the regime of broken symmetry are solutions of non-linear differential equations. One can mention again the buckling of a rod where the buckled conformation beyond the Euler transition is "non-linear" [21].

The other model developed in chapter 7 is somehow a continuum version of the discrete bundle but is more adapted to the deformations in space. In this model the rod is continuous and the stress exerted by the surface on the core is modeled by a surface tension term. The physical principle of solid surface tension is then added in this theory. This approach was often used in the study of materials with large area to volume ratio like nanofibers [79][80] but also for gels in solvents [83]. In both cases it

was found that surface tension plays a significant role. We found that surface tension could contribute negatively to the bending modulus of a rod making the rod softer, to the point where the apparent bending vanishes. This is the analogue of the Euler transition in the usual rod buckling. In complete analogy with the discrete model, the surface tension contribution results from the deformation of the cross-section of the rod during bending. It was also found that the self buckling elastic instability of a rod can not lead to a helical ground state but only to a planar arc. The major limitation of the continuum model is that it can only describe the self-buckling elastic instability but not the shape (new ground state) of the rod in the broken phase. Indeed if we want to describe the regime after the self buckling we must determine the shape of the rod in the regime of non-linear elasticity which was developed for the study of finite deformations [86].

Unfortunately the resolution of the non-linear elastic equations of a bent rod with circular cross section turned out to be an extraordinary difficult mathematical problem. We therefore decided to revisit the classical flexure problem of non-linear incompressible elasticity of a rectangular beam which is the paradigmatic example for the study of the non-linear deformations of elastic materials.

In the first section of this chapter we review the principle of non-linear elasticity to facilitate the lecture of the following sections where surface tension effects on the non-linear elasticity of a rectangular beam is presented in details.

8.1 Principles of non-linear elasticity

As for linear elasticity of small deformation, it is necessary to define different physical quantities that will be useful for the study of plane strain bending. After having defined the tools for describing the motion in the case of a continuous medium, we will present different tensors allowing us to access the stress, the strain and the energy of the bar [87].

8.1.1 Continuum, description

Continuum mechanics is a branch of mechanics in which materials are treated as continuous, which is the case of the bar we will study. The volume studied is divided into sub-units, one speaks of an infinitesimal volume of material. One of these infinitesimal volume is also called particle of the continuum [87]. A body will evolve under the effect of a constraint, the particles of the continuum will change their position. The path line of a particle is described by a vector $\vec{r}$:

$$\mathbf{r} = \mathbf{r}(t)$$

The path line describing the motion from the initial position to the final position, we must use two set of coordinates to identify the particle before/after the motion :

- at a reference time t_0, we use the set of coordinates (X_1, X_2, X_3) to identify the particle;
- at a time t, we use (x_1, x_2, x_3).

More generally, the path line of one particle can be described by the following equation :

$$\mathbf{x} = \mathbf{x}(X, t) \tag{8.1}$$

8.1.2 Deformation tensor

The deformation gradient **F** transforms a vector of an undeformed body to that of the deformed one. It can be given by derivating each component of the deformed vector **x** with respect to each component of **X**. Since $x = x(X)$, the tensor can be written :

$$F_{ij} = \frac{\partial x_i}{\partial X_j} \tag{8.2}$$

That can also be written as a matrix :

$$F = \begin{pmatrix} \frac{dx_1}{dX_1} & \frac{dx_1}{dX_2} & \frac{dx_1}{dX_3} \\ \frac{dx_2}{dX_1} & \frac{dx_2}{dX_2} & \frac{dx_2}{dX_3} \\ \frac{dx_3}{dX_1} & \frac{dx_3}{dX_2} & \frac{dx_3}{dX_3} \end{pmatrix} \tag{8.3}$$

This tensor describes the possible deformations undergone by the body studied. These deformations can be simple displacements, simple rotations or a combination of both (See Fig.8.1).

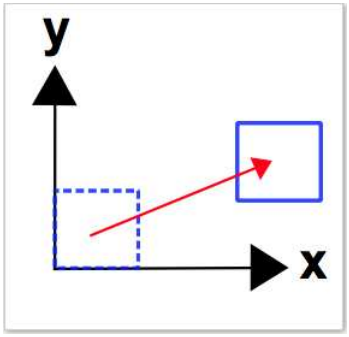

(A) Displacements

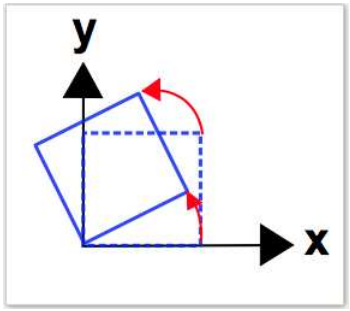

(B) Rotation

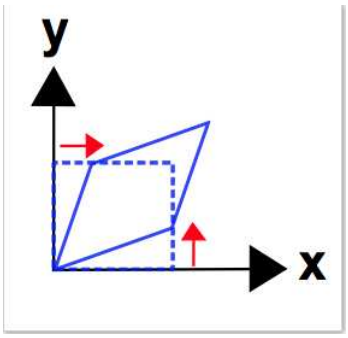

(C) Pure shear

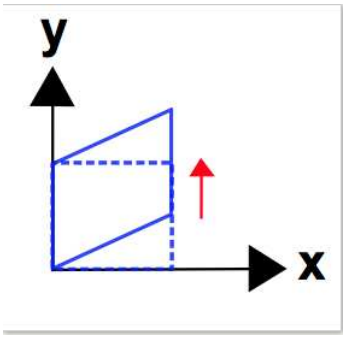

(D) Shear rotation

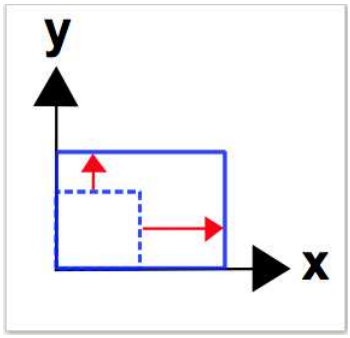

(E) Stretching

FIGURE 8.1: Deformations

For the the type of situations we will study, we will take into account all these options. This tensor will allow us to determine the expression of the Cauchy Green tensor and the deformation field.

Deformation Field

With **x** being the spatial position at time t of a material point with coordinate **X**. A material element **dX** at the initial configuration is changed into a material element **dx** at time t :

$$d\mathbf{x} = \mathbf{x}(\mathbf{X} + d\mathbf{X}, t) - \mathbf{x}(\mathbf{X}, t) = (\nabla \mathbf{x}) d\mathbf{X}$$

That can also be written :

$$d\mathbf{x} = \mathbf{F} d\mathbf{X},$$

where $\mathbf{F} = \nabla \mathbf{x}$ is the **deformation tensor**.

8.1.3 Left Cauchy Green deformation tensor

Using **F** and its transpose $\mathbf{F}^t$ we get a new tensor :

$$B = F.F^t, \tag{8.4}$$

B is called Left Cauchy Green tensor, another deformation tensor that will be helpful. The principal components of **B** are λ_i^2 where the λ_i are the principal stretches. Invariants of $B(I_i)$ will be calculated using the principal stretches and be used to find the strain energy density.

$$\text{Invariants of B} = \begin{cases} I_1 = tr\mathbf{B} = \lambda_1^2 + \lambda_2^2 + \lambda_3^2 : \\ I_2 = \frac{1}{2}[(tr\mathbf{B})^2 - tr(\mathbf{B})^2] = \lambda_1^2\lambda_2^2 + \lambda_2^2\lambda_3^2 + \lambda_3^2\lambda_1^2 \\ I_3 = det\mathbf{B} = \lambda_1^2\lambda_2^2\lambda_3^2 \end{cases} \tag{8.5}$$

For an isotropic material, consideration of the principle of material frame indifference leads to the conclusion that the strain energy density function depends only on the invariants of B.

Thus, the strain energy density function can be expressed uniquely in terms of the principal stretches i.e in terms of the invariants of the left Cauchy-Green deformation tensor.

8.1.4 Stress tensor or Cauchy stress tensor

On using the constitutive law for the Cauchy stresses **T** ([88]) we can write the stress tensor which is related to the three coordinates so that the components are :

$$\mathbf{T}.\mathbf{e}_i = \mathbf{T}_{mi}\mathbf{e}_m$$

Or :

$$\mathbf{T} = \begin{pmatrix} T_{11} & T_{12} & T_{13} \\ T_{21} & T_{22} & T_{23} \\ T_{31} & T_{32} & T_{33} \end{pmatrix}$$

T is symmetrical

$$T_{12} = T_{21} T_{13} = T_{31} T_{23} = T_{32}$$

Therefore, there are six independent components.
For each real symmetrical stress tensor, there are at least three perpendicular principal directions : these directions (vectors) are perpendicular to planes named principal planes.

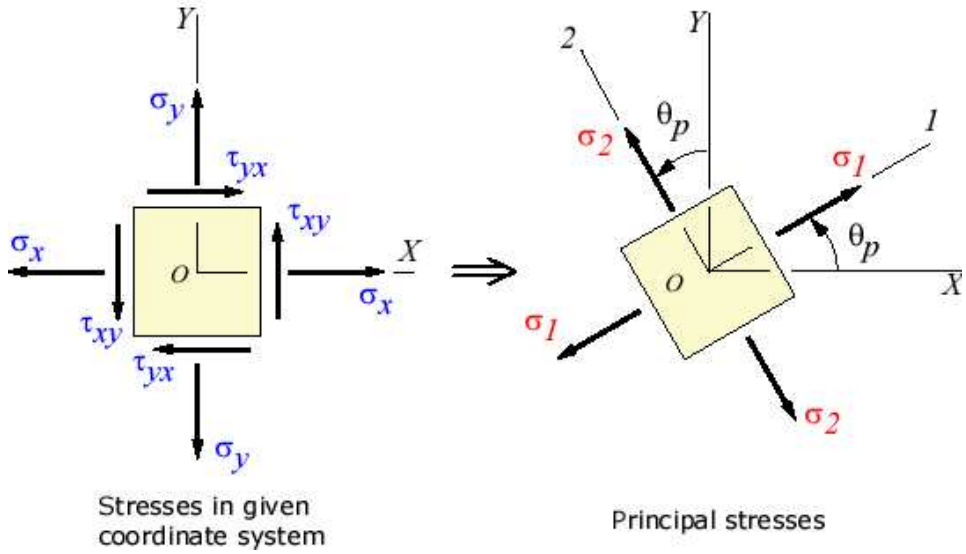

The stress vector of each principal plane is normal to the considered principal plane : they are named principal stresses.

8.2 Theory of a plane strain bending of a rectangular beam

In [89], one study the problem of plane strain bending of an incompressible rectangular beam into a curved circular conformation. In the following, we use the method of ref. [86]. We will study a finite undeformed rectangular beam of an incompressible isotropic hyperelastic material. Its coordinates (X, Y, Z) are defined by

$$-A < X < A, \quad -L < Y < L \quad \text{and} \quad 0 < Z < H \tag{8.6}$$

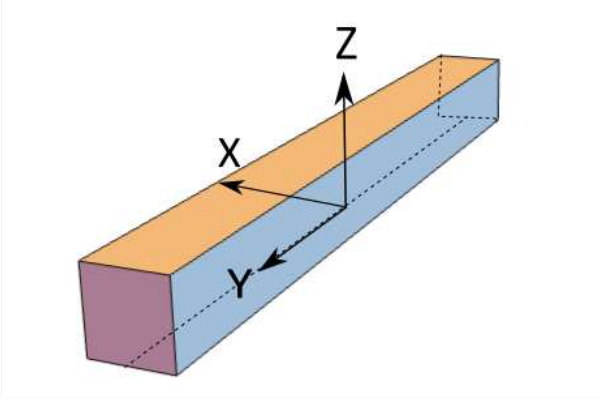

FIGURE 8.2: Axes and coordinates chosen for the bar

We assume that the rectangular beam is deformed in the plane (X, Y) into a curved beam with a circular sector best described with a cylindrical coordinates system (r, θ, z) such that the deformations read

$$r = f(X), \quad \theta = \frac{Y}{\rho}, \quad z = \lambda Z \tag{8.7}$$

where ρ is the radius of curvature of the beam and λ is a dimensionless variable which will be determined by energy minimization (see Fig. 8.2, 8.7 and 8.3). The **major innovation**, with respect to previous approaches [86][87], is the presence of **the additional parameter** λ. In the usual approach [86][87], $\lambda = 1$, but the corresponding bending energy is not minimal. As we will show, the elastic energy of the beam is actually minimal for a value $\lambda > 1$.

8.2.1 The left Cauchy–Green strain tensor

The deformation gradient Eq. (8.3) corresponding to the deformation Eq. (8.7) is explicitly

$$F = \begin{pmatrix} \frac{df}{dX} & 0 & 0 \\ O & \frac{f}{\rho} & 0 \\ 0 & 0 & \lambda \end{pmatrix} \tag{8.8}$$

A convenient equivalent writing is to use the tensor product:

$$F = \frac{df}{dX} e_r \otimes e_X + \frac{f}{\rho} e_\theta \otimes e_X + \lambda e_z \otimes e_Z.$$

The incompressibility condition is essential to solve the problem. It reads

$$\det F = 1$$

and is thus equivalent to the differential equation

$$\frac{f}{\rho/\lambda} \frac{df}{dX} = 1,$$

whose solution is

$$r = \sqrt{\beta + 2X\rho/\lambda} \tag{8.9}$$

where β is a constant of integration that will be determined from the equilibrium equations and boundary conditions. The condition Eq. (8.6) imposes the following ranges on the cylindrical coordinates in the bent state :

$$r_1 \leq r \leq r_2\,; \quad -L/\rho \leq \theta \leq L/\rho \quad \text{and} \quad 0 \leq z \leq \lambda H \tag{8.10}$$

where r_1 and r_2 are the inner and outer radii of the circular sector given by

$$r_1 = \sqrt{\beta - 2A\rho/\lambda} \ \text{ and } \ r_2 = \sqrt{\beta + 2A\rho/\lambda} \tag{8.11}$$

where β obviously satisfies the condition $\beta > 2A\rho/\lambda$.

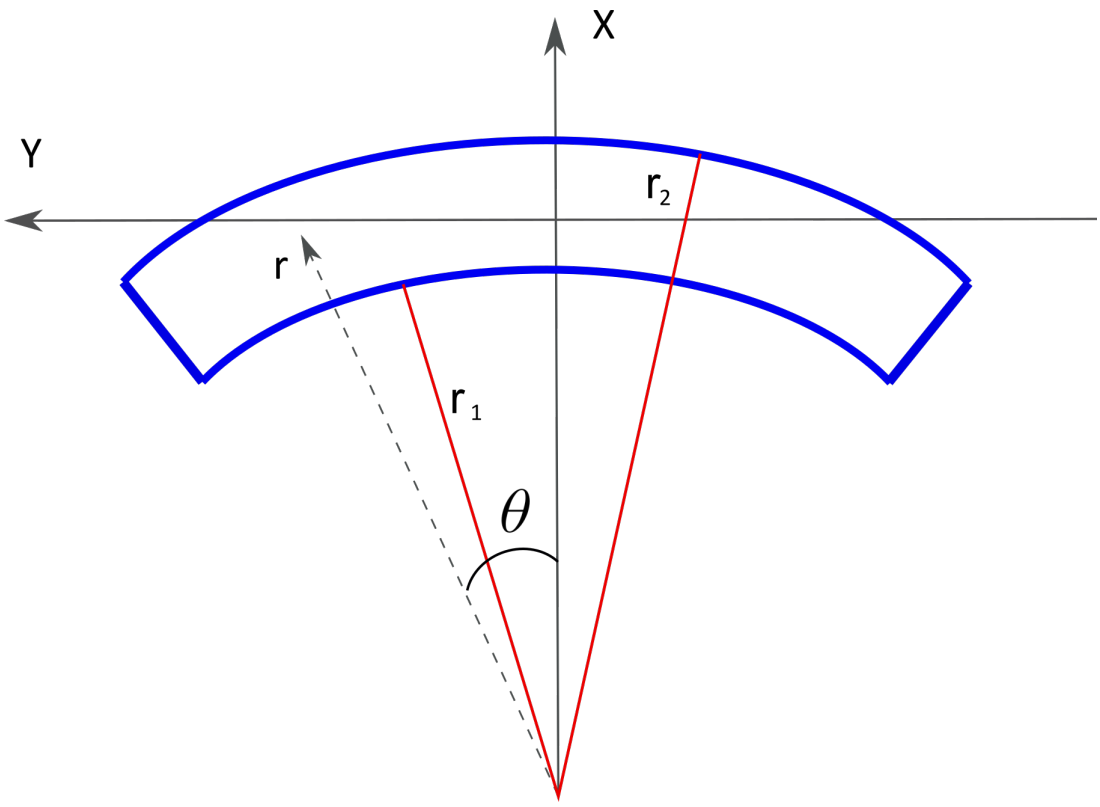

FIGURE 8.3: Large deformations after bending of the beam with a rectangular cross-section. Adapted from [86] and [90]

The left Cauchy–Green strain tensor $\mathbf{B} = FF^T$ is therefore expressed as :

$$\mathbf{B} = \frac{\rho^2}{r^2\lambda^2} e_r \otimes e_r + \frac{r^2}{\rho^2} e_\theta \otimes e_\theta + \lambda^2 e_z \otimes e_z \tag{8.12}$$

The associated principal scalar invariants Eq. (8.5) of $\mathbf{B}$ given by Eq. (8.12) are therefore

$$I_1 = \mathrm{tr}\mathbf{B} = \frac{\rho^2}{\lambda^2 r^2} + \frac{r^2}{\rho^2} + \lambda^2, \tag{8.13}$$

and

$$I_2 = \frac{1}{2}[(\mathrm{tr}\mathbf{B})^2 - \mathrm{tr}(\mathbf{B}^2)] = \frac{1}{\lambda^2} + \frac{\lambda^2 r^2}{\rho^2} + \frac{\rho^2}{r^2}. \tag{8.14}$$

The last one

$$I_3 = \det\mathbf{B} = 1, \tag{8.15}$$

is a consequence of the incompressibility of the material.

8.2.2 Constitutive law and neoHookean strain energy

The constitutive law for an incompressible isotropic elastic material expresses the Cauchy stress tensor $\mathbf{T}$ in terms of $\mathbf{B}$ is the following manner [86]:

$$\mathbf{T} = -p.\mathbf{I} + 2\frac{\partial W}{\partial I_1}\mathbf{B} - 2\frac{\partial W}{\partial I_2}B^{-1} \tag{8.16}$$

where $\mathbf{I}$ is the identity, p is the Lagrange multiplier to ensure incompressibility (hydrostatic pressure) and W is the strain-energy per unit undeformed volume. In the rest of the paper we will only consider the neoHookean strain energy density

$$W = \frac{\mu}{2}(I_1 - 3), \tag{8.17}$$

which becomes

$$W = \frac{\mu}{2}(\frac{\rho^2}{\lambda^2 r^2} + \frac{r^2}{\rho^2} + \lambda^2 - 3), \tag{8.18}$$

where we used Eq. (8.13) . Eq.(8.18) corresponds to the simplest incompressible hyperelastic material model. The constant μ is the shear modulus. In this case the constitutive law simplifies into

$$\mathbf{T} = -p.\mathbf{I} + \mu\mathbf{B}, \tag{8.19}$$

or in terms of the non-zero components

$$T_{rr} = -p + \mu\frac{\rho^2}{\lambda^2 r^2}; \quad T_{\theta\theta} = -p + \mu\frac{r^2}{\rho^2}, \quad T_{zz} = -p + \mu\lambda^2. \tag{8.20}$$

The equations of equilibrium are

$$\frac{\partial T_{rr}}{\partial r} + \frac{1}{r}(T_{rr} - T_{\theta\theta}) = 0, \quad \frac{\partial T_{\theta\theta}}{\partial \theta} = 0, \quad \frac{\partial T_{zz}}{\partial z} = 0.. \tag{8.21}$$

The last two equations of Eqs. (8.20) and (8.21) together imply that the hydrostatic pressure is a function of r only, $p = p(r)$ implying that the three components of $\mathbb{T}$ are function of r only. Observing that :

$$\frac{dW}{dr} = \mu\left(\frac{r}{\rho^2} - \frac{\rho^2}{r^3\lambda^2}\right) = \frac{1}{r}(T_{\theta\theta} - T_{rr}) = \frac{dT_{rr}}{dr} \tag{8.22}$$

we deduce the relation

$$T_{rr}(r) = W(r) - K, \tag{8.23}$$

with K a constant of integration satisfying the condition

$$K = W(r_1) = W(r_2), \tag{8.24}$$

as a result of the boundary conditions which are $T_{rr}(r_1) = T_{rr}(r_2) = 0$. From Eq. (8.24) we deduce $I_1(r_1) = I_1(r_2)$ which implies the relation

$$\rho^2/\lambda = r_1 r_2 = \sqrt{\beta^2 - 4A^2\rho^2/\lambda^2}, \tag{8.25}$$

where Eq. (8.11) was used. The solution of the later equation Eq. (8.25) gives the expression of β in Eq. (8.9) as a function of λ :

$$\beta(\lambda) = \frac{\rho}{\lambda} G, \tag{8.26}$$

where we introduce the notation

$$G = \rho\sqrt{1 + 4\frac{A^2}{\rho^2}}. \tag{8.27}$$

Replacing this result in Eq. (8.9) we obtain the radius of the bent beam in terms of λ :

$$r(\lambda) = \sqrt{\frac{\rho}{\lambda}(2X + G)}. \tag{8.28}$$

Then the energy density Eq. (8.18) becomes :

$$W(\lambda, \rho) = \frac{\mu}{2}\left(\lambda^2 + \frac{1}{\lambda}\left(\frac{\rho}{2X + G} + \frac{2X + G}{\rho}\right) - 3\right). \tag{8.29}$$

The total elastic energy of the beam for a given radius of curvature ρ and a given parameter λ is obtained as

$$E(\lambda, \rho) = \int_{-A}^{A} dX \int_{-L}^{L} dY \int_{0}^{H} dZ \left(W(\lambda, \rho)\right) \tag{8.30}$$

and the total volume of the beam being $V = 4ALH$, the total energy per unit volume $e(\lambda) = E/(4ALH)$ is consequently:

$$e(\lambda) = \frac{\mu}{2}\left(\lambda^2 - 3 + \frac{2}{\lambda}F\right) \tag{8.31}$$

with F given by

$$F = \frac{G}{2\rho} + \frac{\rho}{8A} \ln\left(\frac{G+2A}{G-2A}\right) \tag{8.32}$$

and G given by Eq. (8.27) . Eq. (8.31) **is the main result of this section**. It gives the energy density of the beam associated to the finite deformation given by Eq. (8.7) .

8.2.3 Energy minimization

Minimizing the energy density, i.e.;

$$\frac{d}{d\lambda} e = 0 = -\frac{\mu}{\lambda^2}\left(F - \lambda^3\right)$$

we obtain the surprisingly simple result

$$\lambda = F^{1/3}. \tag{8.33}$$

One can observe numerically that $F > 1$ for all values of ρ (See Fig. 8.4) so is $\lambda \geq 1$ From Eqs. (8.31) and (8.33) the minimal energy is expressed as

$$e_{\min} = \frac{3}{2}\mu\left(F^{2/3} - 1\right) \tag{8.34}$$

Comparing this energy with the standard energy

$$e_{\lambda=1} = \mu\left(F - 1\right) \tag{8.35}$$

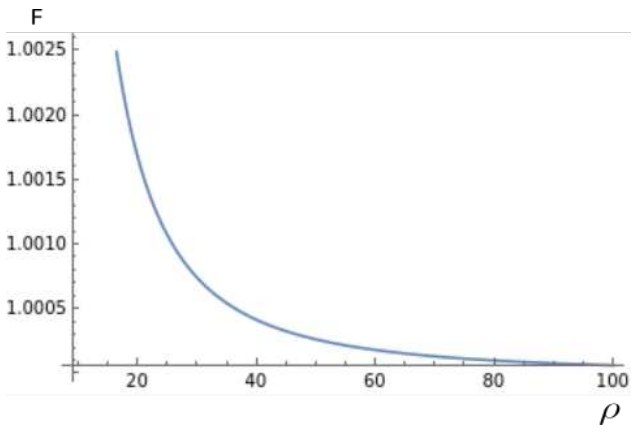

FIGURE 8.4: Evolution of F, quantity used to describe the energy, in terms of ρ the inverse of the geometric mean curvature

We see that $e_{\min}$ is always lower than the usual value $e_{\lambda=1}$ [86][87] for all values of F (and equal for $F = 1$) (See Fig 8.5 and 8.6). We conclude that the height of the beam increases during plain bending in a circular sector.

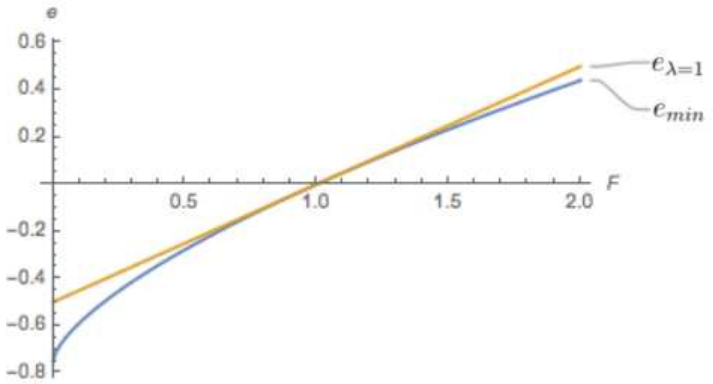

FIGURE 8.5: Comparison between $e_{\lambda=1}$ and the minimal energy e_{min}, for $0 < F < 2$

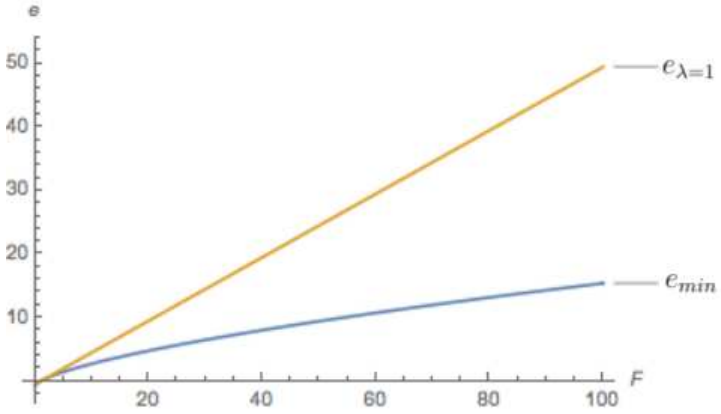

FIGURE 8.6: Comparison between $e_{\lambda=1}$ and the minimal energy e_{min}, for $0 < F < 100$

8.2.4 Stresses on the beam

It is important to highlight that the deformation field given by Eq.(8.7) is actually not the exact finite deformation of the beam submitted to large bending moments. It is actually an ansatz. that allows to solve the model analytically. The real shape has likely a deformed non rectangular cross section and get out of the plane. A planar deformation with $\lambda = 1$ can be obtained if a particular distribution of vertical forces f_z is imposed on the beam. Here we compute this force distribution for all values of λ.

The components of the stress tensor are given by Eq. (8.20):

$$T_{rr} = -p + \mu\frac{\rho^2}{\lambda^2 r^2}; \quad T_{\theta\theta} = -p + \mu\frac{r^2}{\rho^2}, \quad T_{zz} = -p + \mu\lambda^2 \tag{8.36}$$

Focusing on the $z-$component, T_{zz} can be written

$$T_{zz} = T_{rr} + \mu\left(\lambda^2 - \frac{\rho^2}{\lambda^2 r^2}\right). \tag{8.37}$$

From Eqs.(8.23) and (8.24) we have

$$T_{rr}(r) = W(r) - W(r_1) = \frac{\mu}{2}\left(\frac{\rho^2}{\lambda^2 r^2} + \frac{r^2}{\rho^2} - \frac{\rho^2}{\lambda^2 r_1^2} - \frac{r_1^2}{\rho^2}\right) \tag{8.38}$$

so that

$$T_{zz}(r) = \frac{\mu}{2}\left(-\frac{\rho^2}{\lambda^2 r^2} + \frac{r^2}{\rho^2} + 2\lambda^2 - \frac{\rho^2}{\lambda^2 r_1^2} - \frac{r_1^2}{\rho^2}\right) \tag{8.39}$$

The resulting out-of-plane resultant force is given by the expression

$$F_z = \int_{-L/\rho}^{L/\rho} d\theta \int_{r_1}^{r_2} T_{zz}(r) r dr = \frac{2L}{\rho}\int_{r_1}^{r_2} T_{zz}(r) r dr \tag{8.40}$$

which leads to

$$F_z = \frac{\mu L}{\rho}\left(-\frac{\rho^2}{\lambda^2}\ln\left(\frac{r_2}{r_1}\right) + \frac{1}{4\rho^2}\left(r_2^4 - r_1^4\right) + \left(\lambda^2 - \frac{\rho^2}{2\lambda^2 r_1^2} - \frac{r_1^2}{2\rho^2}\right)\left(r_2^2 - r_1^2\right)\right). \tag{8.41}$$

From the relations

$$r_2^4 - r_1^4 = 8A\frac{G}{\lambda^2}\rho^2 \quad \text{and} \quad r_2^2 - r_1^2 = 4\frac{A}{\lambda}\rho$$

the total force F_z can be written in the simple form

$$F_z = \mu 4AL\left(\lambda - \frac{1}{\lambda^2}F\right) \tag{8.42}$$

where F is given by Eq. (8.32). We see that the total force vanishes, i.e.; $F_z = 0$ when

$$\lambda = F^{1/3}$$

which is the same condition as the one obtained from energy minimization. For the

usual case $\lambda = 1$, the force necessary to maintain a state of plane strain $F_{z,\lambda=1}$ does not vanish [86]. Note that for $\lambda = F^{1/3}$, it is the total force that vanishes but a non zero force distribution or stress tensor $T_{zz}(r)$ is necessary to maintain the shape planar. Although we can not determine the real three dimensional shape we will nevertheless compute the change of surface ΔS for the deformation given Eq. (8.7). This will give us a good approximation for the ground state in the non linear regime and this will tell us if self-buckling induced by surface tension is possible.

8.2.5 Surface deformation

In order to infer the effect of a surface stress term, we compute the surface change after deformation. The original surface of the bar before deformation is

$$S_0 = 4L(2A + H) + 4AH$$

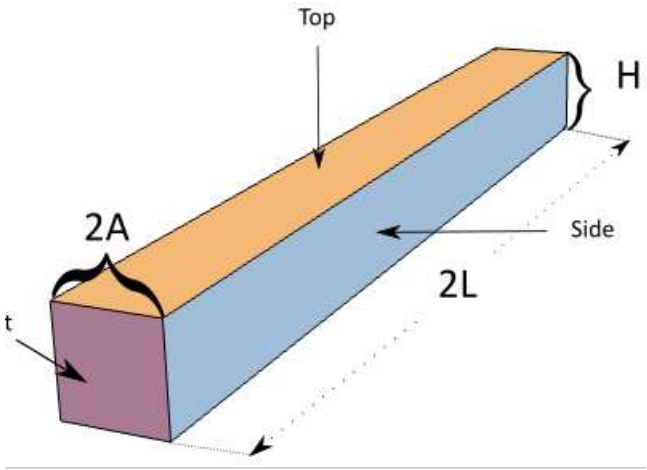

FIGURE 8.7: Surface areas to calculate

The deformed surface is given by

$$S = \theta(r_2^2 - r_1^2) + \lambda H\theta\,(r_2 + r_1) + \lambda 2H\,(r_2 - r_1)$$

with the internal and external radii are readily obtained from Eq. (8.28):

$$r_1 = \sqrt{\frac{\rho}{\lambda}\,(G - 2A)}$$
$$r_2 = \sqrt{\frac{\rho}{\lambda}\,(G + 2A)}$$

where we recall that (see Eq. (8.27))

$$G = \rho\sqrt{1+4\frac{A^2}{\rho^2}} \tag{8.43}$$

The total angle of deviation is

$$\theta = 2L/\rho \tag{8.44}$$

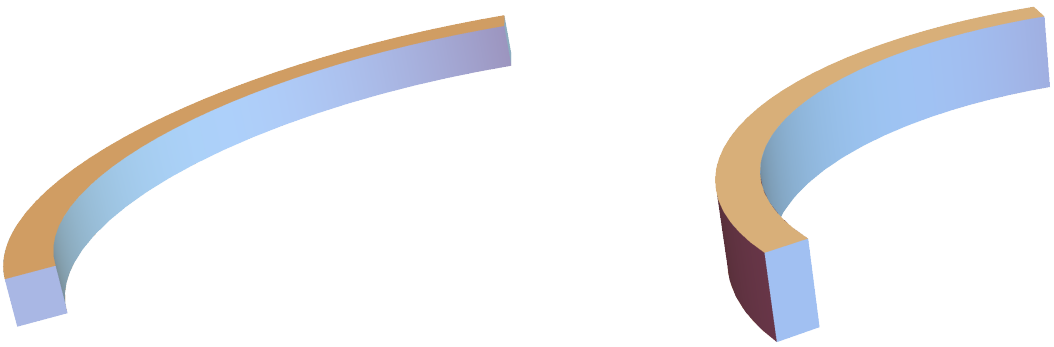

(A) Bent rod with same section, $\lambda = 1$

(B) Bent rod with new section, $\lambda \neq 1$

FIGURE 8.8: Rods after deformation

thus

$$\Delta S = 8AL\frac{(1-\lambda)}{\lambda} + 4HL\left(\lambda\left(\frac{r_2+r_1}{2\rho}\right)-1\right) + 4HA\left(\frac{\lambda}{A}\left(\frac{r_2-r_1}{2}\right)-1\right) \tag{8.45}$$

For verification purposes, let's consider the limiting case $\lambda = 1$ and $\rho \to \infty$ corresponding to the undeformed bar. Then we see that $r_2 + r_1 = 2\rho$ and $r_2 - r_1 = 2A$ so that $\Delta S = 0$ as expected. This complicated expression is not very appealing and we will consider limiting cases.

8.2.6 Bending stiffness renormalization, buckling instability and curved ground state

We now consider how does the surface tension renormalize the bending stiffness. The total energy of the beam is from Eq. (8.34) given by

$$E_{total} = \frac{3}{2}V\mu\left(F^{2/3}-1\right) + \gamma\Delta S \tag{8.46}$$

where $V = 4ALH$ is the volume of the beam and γ the surface tension. We consider first the limit of small deformations.

Limit of small deformations(linear regime)

For $\theta = 2L/\rho$ we have the following expansion with the curvature $\kappa = 1/\rho$ to the second order in κ :

$$F \approx 1 + \frac{2}{3}A^2\kappa^2, \tag{8.47}$$

leading to the following expansion for λ :

$$\lambda \approx 1 + \frac{2}{9}A^2\kappa^2. \tag{8.48}$$

The purely elastic energy thus expands as

$$E_{elastic} = \frac{3}{2}V\mu\left(\lambda^2 - 1\right) \approx \frac{8}{3}A^3HL\mu\kappa^2. \tag{8.49}$$

The bending stiffness in this model is thus define as

$$B = \frac{4}{3}A^3H\mu \tag{8.50}$$

In the same way we find :

$$(r_2 + r_1)\,\kappa \approx 2\left(1 + \frac{7}{18}A^2\kappa^2\right)$$

and

$$r_2 - r_1 \approx 2A\left(1 - \frac{11}{18}A^2\kappa^2\right).$$

With this expansion in hand we find for the surface change :

$$\Delta S \approx -\frac{2A^2}{9}\kappa^2\left(8AL + (7A - 11L)\,H\right). \tag{8.51}$$

Unfortunately this expression is not as simple as we would expect. We therefore consider in the rest of the chapter only the limit of large L with respect to the lengths A and H. In this limiting case we have

$$\Delta S \approx \frac{22A^3}{9}\kappa^2\left(\frac{H}{A} - \frac{8}{11}\right)L. \tag{8.52}$$

The sign of ΔS is not constant and depends on the ratio H/A. Introducing the constant Δ as

$$\Delta = \frac{22}{9}\left(\frac{H}{A} - \frac{8}{11}\right)$$

so that we can write

$$\Delta S \approx A^3 \Delta L \kappa^2. \tag{8.53}$$

From this analysis we therefore need to distinguish two cases

- **Case 1**: $H/A > 8/11$, and so is $\Delta S > 0$ which reads

$$\Delta S \approx A^3 \Delta L \kappa^2 \tag{8.54}$$

- **Case 2** : $H/A < 8/11$ and ΔS can be written as

$$\Delta S \approx -A^3 \left|\Delta\right| L \kappa^2$$

  which is negative, $\Delta S < 0$.

The total energy per unit length can be written in terms of an renormalized bending stiffness $\widehat{B}$ as

$$E/L \approx \frac{1}{2}\widehat{B}\kappa^2$$

with

$$\widehat{B} = 2A^3\left(\frac{2}{3}H\mu + \gamma\Delta\right)$$

It is clear that depending of the sign of Δ and the surface tension can either enhance or diminishe the bending modulus. In the regime $\Delta < 0$ when $H/A < 8/11$ the renormalized bending stiffness $\widehat{B}$ can cancel, leading to a buckling instability for a critical value

$$\gamma_c = \frac{2H\mu}{3\left|\Delta\right|} \tag{8.55}$$

Beyond this value for $\gamma > \gamma_c$ we have to consider the finite deformations or expand the energy and the surface change to higher order in κ. We will only consider the quartic order.

Non-linear regime (quartic order)

Keeping the quartic order in the expansion of all quantities we obtain

$$F \approx 1 + \frac{2A^2}{3}\kappa^2 - \frac{2A^4}{5}\kappa^4,$$

and for the elastic energy $E_{elastic}$

$$E_{elastic} \approx \frac{8\mu}{3} HLA^3(\kappa^2 - \frac{32}{45}A^2\kappa^4).$$

For the surface excess we have the following expansion in the large L limit

$$\Delta S = A^3\Delta\kappa^2 + A^5\Gamma\kappa^4$$

where we introduced another constant

$$\Gamma = \frac{1504}{810}\left(1 - \frac{2161}{1504}\frac{H}{A}\right) \approx 2.7\left(0.7 - \frac{H}{A}\right).$$

Therefore the total energy expansion can be written

$$E \approx \frac{1}{2}\widehat{B}\kappa^2 + \frac{C}{4}\kappa^4 \tag{8.56}$$

with the coupling constant

$$C \approx 8A^5\left(\gamma\Gamma - 1.9H\mu\right)$$

and the same renormalized bending modulus as before

$$\widehat{B} = 2A^3\left(\frac{2}{3}H\mu + \gamma\Delta\right)$$

In the regime of interest $\Delta < 0$, when $\gamma > \gamma_c$ we have $\widehat{B} < 0$ so the curved conformation is stable only if $C > 0$. This condition first requires that $\Gamma > 0$ leading to the condition $H/A < 0.7$ which is in agreement with the regime $\Delta < 0$. A short calculation shows also that the ratio

$$\frac{\gamma}{\gamma_c} \approx 2.6\frac{(0.72 - \frac{H}{A})}{(0.69 - \frac{H}{A})}$$

is indeed larger than unity. For a bar such that $H/A < 0.7$, the energy Eq. (8.56) has a non trivial minimum corresponding to the optimal curvature :

$$\kappa_{opt}^2 = -\frac{\widehat{B}}{C} \tag{8.57}$$

Therefore we see that the quartic term in the total energy Eq. (8.56) can stabilize a curved ground state.

Conclusion : By revisiting the famous problem of plane strain flexure of an incompressible rectangular beam into a curved circular sector we could determine the contributions of the surface tension to the bending modulus for all deformations and could go beyond the linear regime of small deformations. As already mentioned this model has some limitations when we want to apply it to self buckling of biofilaments. First, the section of the beam was rectangular and the symmetry breaking seems to happen in a regime where the section is very asymmetric ($H/A < 0.7$) which is not what we want for a single biofilaments. But this asymmetry might be also artificial since the real shape of the beam section is likely more deformed than the ansatz used. Additionally the force distribution that is necessary to maintain a planar beam is also not natural, although experiments with bioflaments confined onto a 2D plane are possible. But the tendency of the bent beam to get out of plane could be an indication that a torsion contribution is generated. This might be the clue for the understanding of helical conformations induced by a symmetry breaking mechanism. Despite all these drawbacks, this model shows that self-buckling induced by surface tension is a plausible mechanism that could explain the persistent experimental observations of strong curved biofilament's shapes.

Chapter 9

Conclusion and perspectives

This manuscript is all about the concepts of elastic instability and spontaneous symmetry breaking and how relevant they could be in the world of biofilaments. The origin of this idea comes from key experiments realized on the biological macromolecules of the cytoskeleton with a particular focus in this thesis on microtubules and intermediate filaments. Microtubules are fascinating macromolecules still full of mysteries. Due to their ubiquitous role in cells they have been in the center of biophysical research for several decades. Many experiments showed that the complex self-assembly nanotube structure was at the origin of the microtubules elastic and dynamic behavior.

Moreover, one has synthesized many structures with tubular and cylindrical lattices (made up of blocks from DNA or carbon). These structures tend to coil into a superhelix in order to minimize any existing prestress. This is very well illustrated in a recent experiment with neuronal microtubules growing in the presence of MAP6. It was discovered that, unexpectedly, MAP6 is an intraluminal protein that induces neuronal microtubules to coil into a superhelix (see chapter 4 and 5).

The thesis is somehow an attempt to answer the fundamental question: how can a microtubule, a rigid tubular structure, deform into a large-scale superhelix ? A first answer came from the recently introduced concept of confotronics that is presented in chapter 5 in a general setting and reviewed for microtubules. In that chapter we discussed the conditions for an elastic system to become conformationaly multistable, an essential ingredient of confotronics. It was found that a non-linear elastic subunit is necessary for multistability to emerge, a property that can induce an elastic instability and in turn a spontaneous symmetry breaking. Based on this mechanism the MAP6-microtubule curvature could be explained by a frustrated core-shell model built on switchable lattices.

Differently to the direct observation of the superhelical neuronal microtubule, an experiment on intermediate filaments (and actin filament not discussed in this thesis)

confined in a microchannel showed an anomalous behavior which could only be explained by assuming that an intermediate filament (and actin as well) is also a superhelix (chapter 5). Therefore a natural question arises, whether a more generic physical mechanism could explain the superhelical nature of all filaments. The general mechanism proposed in this thesis is a self-buckling, one where filaments exposed to surface stresses become elastically unstable. The study of this mechanism is at the core of chapters 6 to 8 and is my original contribution of this thesis.

In this spirit, chapter 6 introduces a simple model which is a two dimensional (planar) bundle of three cross-linked extensible filaments where the center filament has a longer free length than the two others at the bundle surface. It is known that a bundle of semi-flexible chains are usually not unstable and that the ground state is the straight shape (chapter 2 and 5). Nevertheless, we showed that relaxing the condition of fixed interdistance between the filaments is sufficient to induce an elastic instability of the straight state. In this model there is no need for non-linear elastic elements contrary to the confotronics model of microtubules. This is the simplest purely linear elastic model with a spontaneous symmetry breaking.

Chapter 7 presents a model that can be seen as continuous generalization of the bundle of three filaments which is not limited to planar deformations and is thus more realistic. This model consider an isotropic incompressible linear elastic rod where a surface stress is modeled by a surface tension term. We have shown that the surface tension can reduce the bending modulus of the rod making it more flexible. For a critical value of the surface tension the bending stiffness vanishes, leading to the elastic instability of the straight state of the rod. At the level of linear elasticity, the genuine curved ground state is not achievable and one has to consider the more complicated non-linear theory of elasticity developed for the study of large deformations. This work is presented in the last chapter 8 and complete the analysis of the self-buckling hypothesis.

This thesis shows that self-buckling of filaments exposed to surface stresses is a viable physical mechanism that could potentially explain the generic occurrence of curved conformations of biofilaments. Nevertheless, our analysis indicates that a surface stress can induce a broken symmetry to a circular arc but not to a helical shape. Therefore the precise molecular origin of the helical torsion at least for intermediate filaments remains currently unexplained and calls for further investigation.

This thesis shows also that biomacromolecules might be seen differently than just simple semiflexible polymers but merely as actuating fibers with fine tuning properties. It would be therefore interesting to realize experiments probing this property. One can think of extracting the tangent correlations of single filaments in microfluidics for different fluids. From the theoretical point of view, it would be interesting to consider the non-linear elastic regime of a rod with a circular cross-section which is more realistic. Even more important, one should consider the large deformations of a free rod with a more complex ansatz that the one considered here, or by a numerical modeling Another approach which does not rely on the surface tension concept and being more mechanistic in nature would be interesting. This could be done by defining a core and a small layer under the surface with two different elastic properties and not necessarily isotropic as with surface tension. Again numerical approaches might be useful.

Appendix A

Surface of revolution

Examples :

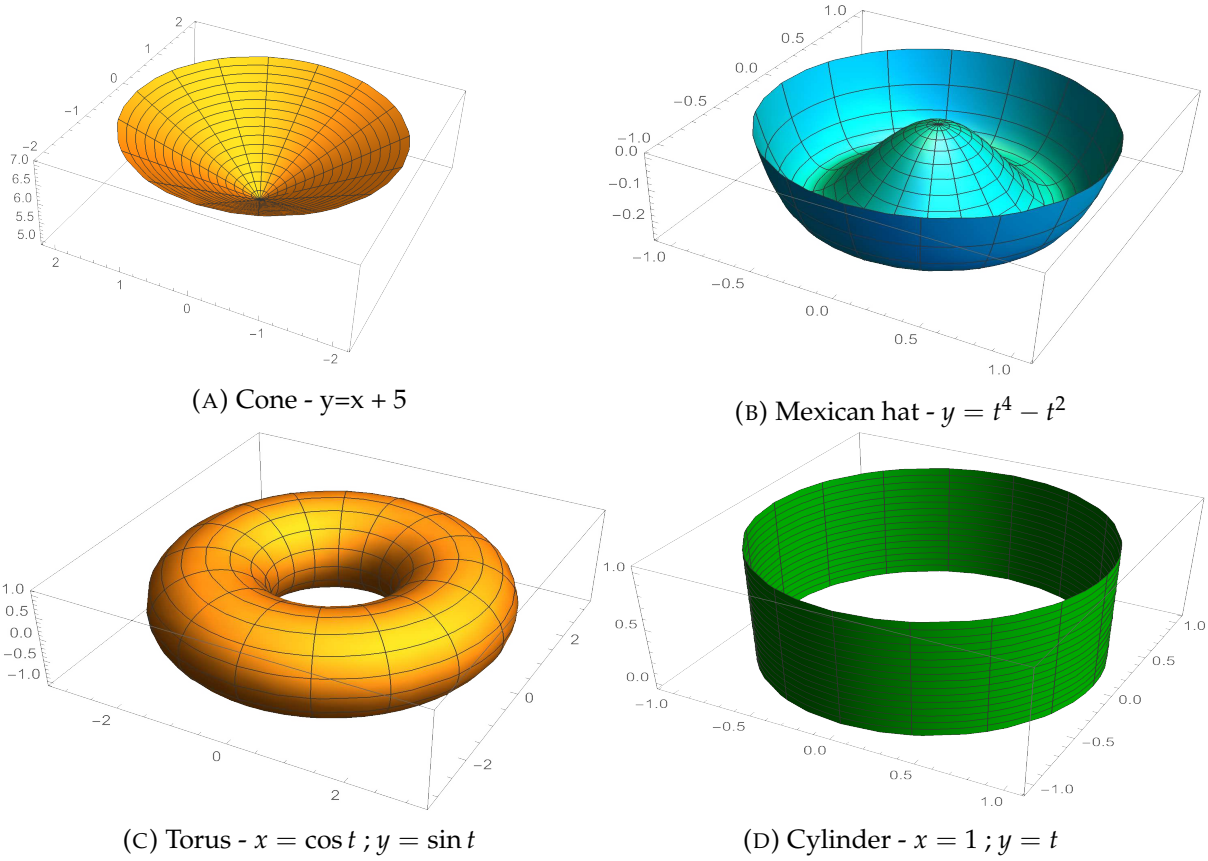

(A) Cone - y=x + 5

(B) Mexican hat - $y = t^4 - t^2$

(C) Torus - $x = \cos t$; $y = \sin t$

(D) Cylinder - $x = 1$; $y = t$

FIGURE A.1: Surfaces of revolution

A surface of revolution is the surface generated by the rotation of a curve (called generator) around a straight line (called axis of revolution). The resulting surface therefore always has azimuthal symmetry. Some of the previous examples (See Fig. A.1) of surfaces of revolution are **generated by a straight line** : the surfaces are cylindrical and conical surfaces depending on whether or not the line is parallel to the axis of revolution.

Using a **circle**, we can get different volumes depending on the choice of the axis of

revolution : if it is rotated around a diameter, we get a **sphere**; if the circle is rotated around an axis that does not intersect the inside of the circle, it generates a **torus** which does not intersect itself. For example, using an ellipse we get a ring torus, (See Fig.A.1c).

A.1 Lateral surface of a cone

The most simple surface of revolution we can obtain is the one given by a line segment rotating around an axis. We will note the coordinates of its ends by (x_1, z_1) and (x_2, z_2). The surface of revolution obtained by rotating this segment around the z-axis is a cone. This solid is a truncated cone with circular bases of respective radii z_1 and z_2.

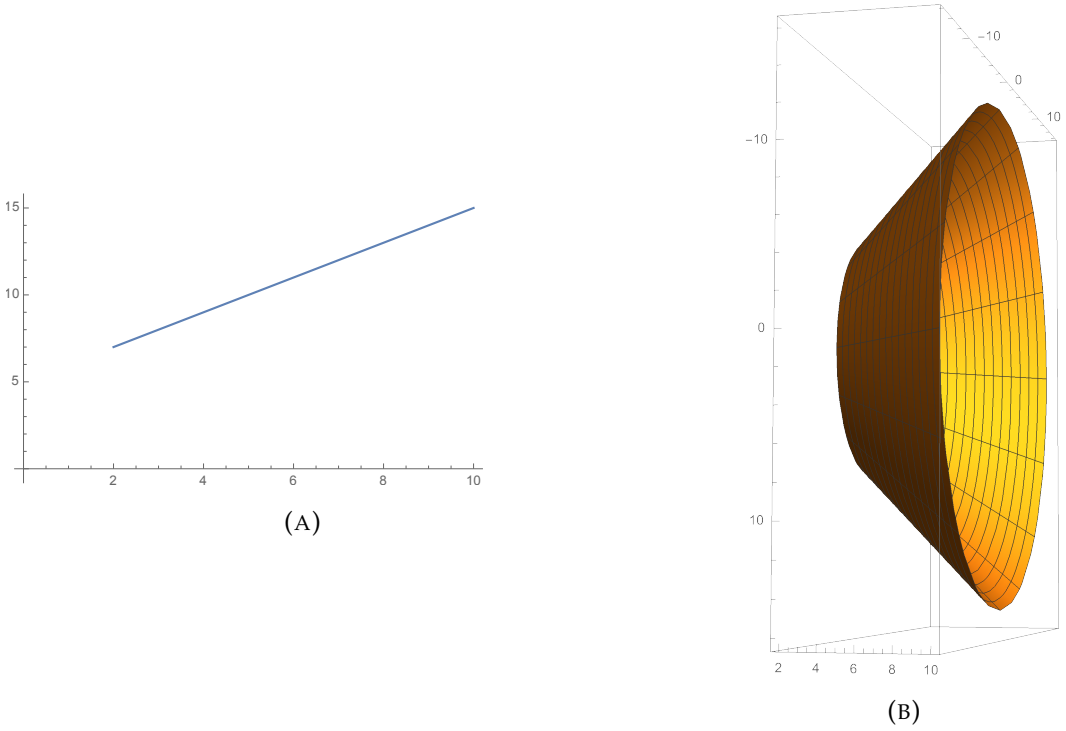

(A) (B)

FIGURE A.2: Line and cone

How do we calculate the surface?

At first, we could calculate it intuitively by saying that the surface can be split into a limited number of trapezia having bases of lengthes a and b and height h. Then, the surface area would approximately be :

$$A \approx n \times \frac{a+b}{2} \times h$$

Obviously, we can get a more precise value by assuming that n (number of trapezia) will tend to infinity :

- the lengthes, $n \times a$ and $n \times b$ will tend to be the circumferences of both circles, $2\pi z_1$and $2\pi z_2$
- h will tend to be equal to length l which reads $l = \sqrt{(x_2 - x_1)^2 + (z_2 - z_1)^2}$

Then, the surface area becomes :

$$A = \pi(z_1 + z_2)l$$

A.2 Surface obtained with any generator

$y = f(x)$ or $x = g(y)$?

Let's take in account the graph : $y = f(x)$ so that $a \leqslant x \leqslant b$. First, we choose to make the curve rotate around x-axis. Just like we did to calculate the length of a curve, we can split the interval $[a; b]$ in n intervals having the same dimension :

$$\Delta x = \frac{(b-a)}{n}$$

This is like considering the curve as an assembly of consecutive segments $x_{i-1}x_i$. The surface area will be the sum of areas equal to the one found in the first section, with limits equal to x_{i-1} and x_i instead of a and b :

$$A \approx \Sigma_{i=1}^{n} \pi(f(x_{i-1}) + f(x_i)).l_i$$

Knowing that :

$$\Delta y_i = f(x_i) - f(x_{i-1})$$

and,

$$l_i = \sqrt{(\Delta x)^2 + (\Delta y_i)^2} = \sqrt{1 + (\frac{\Delta y_i}{\Delta x})^2}.\Delta x$$

The surface area, with n tending to the infinity, reads :

$$A = \int_a^b 2\pi f(x)\sqrt{1 + f'(x)^2}dx$$

If we had to change $y = f(x)$ into $x = g(y)$, the area would read :

$$A = \int_{a'}^{b'} 2\pi g(y)\sqrt{1 + g'(y)^2}dy$$

Axis of revolution

Let's assume the function is : $f(x) = \sin 2x$, the surface isn't the same depending on the chosen axis of revolution. Then it is important to knwo which axis will be used in order to get the right surface.

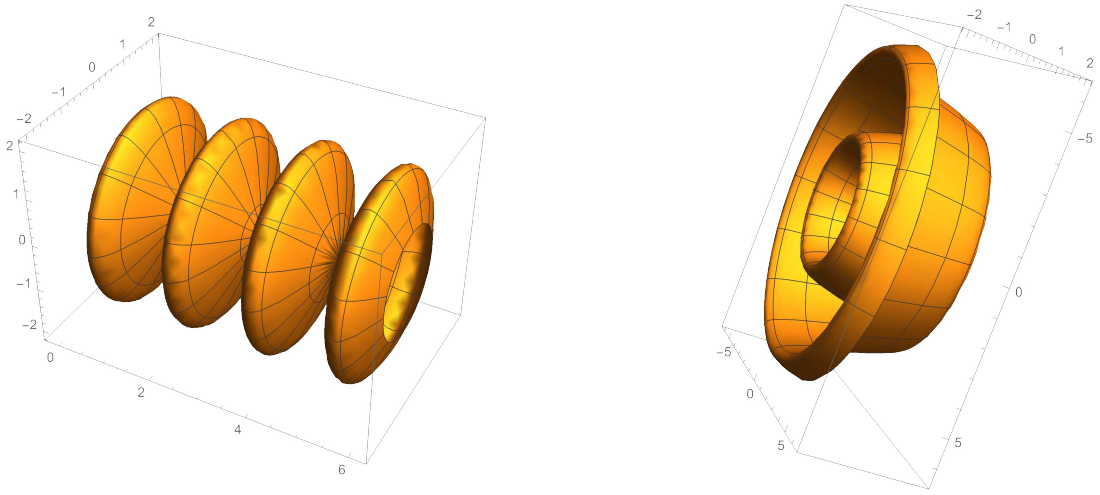

(A) Around X-axis

(B) Around Z-axis

FIGURE A.3: Same generator ($2\sin 2x$), different axis

Appendix B

Self buckling - Maximal length

Based on [91]. Let's suppose a uniform column fixed in a vertical direction at the bottom. We study how this column can buckle due to its own weight we're looking for the limit height, l_{max}, in which the vertical position becomes unstable. When the column is curved (due to its own weight), the curve $w(x)$ describes the deflection in the vertical direction (y) at position x. The first step to find l_{max} is to write the moment equilibrium :

$$M = -\int_0^x q(y-w)dx$$

which is the moment of the weight of the beam, only force taken into account. Note that the body force per unit length, q, is $q = \rho g A$ (acceleration due to gravity, mass density, cross sectional area).
The moment can also be written, after Euler-Bernoulli beam theory

$$M = -YI\frac{d^2w}{d^2x}$$

with Y, Young modulus and I, moment of inertia. The differential equation reads :

$$-YI\frac{d^2w}{d^2x} = -\int_0^x q(y-w)dx$$

If we differentiate with respect to x, and simplify :

$$YI\frac{d^3w}{d^3x} = q\int_0^x -\frac{dw}{dx}dx$$

That also reads :

$$YI\frac{d^3w}{d^3x} = -qx\frac{dw}{dx}$$

In order to solve the problem, we must :

- use new variables n, z, k and r :

$$k^2 = \frac{4q}{9YI}; r^2 = x^3; \sqrt{x}z = \frac{dw}{dx}; n^2 = \frac{1}{3^2}$$

- transform the equation into Bessel equation;

$$r^2\frac{d^2z}{dr^2} + r\frac{dz}{dr} + (k^2r^2 - n^2)z = 0$$

Then, the solution is :

$$z = AJ_{\frac{1}{3}}(kr) + BJ_{-\frac{1}{3}}(kr)$$

Finally, the solution of the initial equation reads :

$$\frac{dw}{dx} = \sqrt{x}(AJ_{\frac{1}{3}}(kx^{\frac{3}{2}}) + BJ_{-\frac{1}{3}}(kx^{\frac{3}{2}}))$$

The boundary conditions will completely define the solution :

- $x = 0 : M = 0$ because the column is fixed, then $\frac{d^2w}{dx^2} = 0$ meaning that $A = 0$
- $x = l : w(l) = 0$ then $J_{-\frac{1}{3}}(kl^{\frac{3}{2}}) = 0$

The second boundary conditions also gives the value of the critical length :

$$J_{-\frac{1}{3}}(kl^{\frac{3}{2}}) = 0$$

Then

$$l_{max} = (\frac{J_{\frac{1}{3},1}}{k})^{\frac{2}{3}} = (\frac{J_{\frac{1}{3},1}9YI}{4q})^{\frac{2}{3}} \tag{B.1}$$

Knowing that $J_{\frac{1}{3},1} \approx 1.86635$
Finally,

$$l_{max} \approx (7.8373\frac{YI}{\rho g A})^{\frac{1}{3}} \tag{B.2}$$

Appendix C

Gauss theorem and bending

A sheet of paper can bend under the effect of its own mass ([92]), rolled into a cylinder can it undergo buckling under the effect of a load, an external force or an energy input? Through the study of sheets of paper, the goal is to show the important stability of cylinders, a form that we use as a model for bio-filaments. We will then be able to present the energetic criteria allowing to obtain the instability (thus the buckling) and the first consequences on the cylinder of this instability which will give us tracks to follow for the models that we wish to use to study biological filaments.

C.1 Gauss's Theorema Egregium

The goal of this theorem is to get tools to predict the shape of a surface, that is both thin and elastic. In particular, we will present the conditions under which a sheet of paper will or will not bend ([93]).

C.1.1 Isometric surfaces

A sheet of paper is a surface just like a sphere is, but the properties of both surfaces are different, we will come back to this later. But a piece of fishing line is not a surface: if were small enough, we could only walk from one end to the other, so it is of dimension 1. A class C^3 surface, which is the type of surface concerned by the theorem, is a surface that can be considered as being smooth.

- A brand new sheet of paper, never used but possibly slightly curved, is a smooth surface.
- If we bend or curve the same sheet in order to change its shape (boat, airplane, etc) then it is no longer smooth at the folds.

FIGURE C.1: Plane and string - Adapted from [93]

C.1.2 Isometry between surfaces

Two isometric surfaces are somehow surfaces "of the same nature": one is said to be obtained by applying to the other an isometric transformation, i.e. a transformation that preserves the distances between the two surfaces. The initial sheet is "the same nature" as the curved sheet: they are isometric. However, if you want to cover the surface of a sphere with a sheet of paper, you will have to either stretch the sheet (if it can be stretched) or tear or crumple it in some places. It is therefore impossible to cover a sphere with paper without going too rough: **a sphere and a plane are not isometric**.

If the deformation is soft (no tearing or stretching) the two surfaces before and after deformation are of the same nature, i.e. isometric. This is the case, for example, of a sheet of paper that is rolled up on itself to form a cylinder: **a flat surface** (sheet of paper at the beginning) and **a cylinder** (rolled up sheet of paper) are **isometric surfaces**. This result will be used later in section C.2.

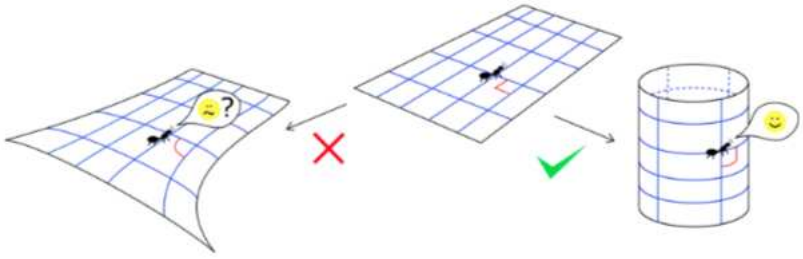

FIGURE C.2: Isometric or not

C.1.3 Curvature at a point

A curve is a dimension 1 object, like a string (assuming it's thin enough). This object can be straight or curved, if it is curved we tell how curved it is using the **curvature**. The more curved is the curve around a point, the larger is the curvature : the curvature describes how curved is a curve. But, how do we calculate the curvature?

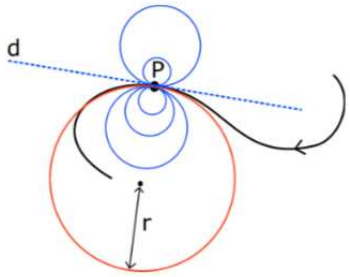

FIGURE C.3: Osculating circle

There are an infinite number of circles tangent to a curve at one point (See figure C.3) P , i.e. circles that have only P in common with the tangent **d** to the curve in this point. Among all these circles, the one that **fits the best** with the curve is the **osculating circle** (in red). Its radius is noted **r** and the curvature of the curve in P is then by definition equal to

$$\rho = \frac{1}{r}$$

with a sign "+" if the circle is to the left of the curve relative to the direction of travel, and a sign "−" if it is on the right.
In figure C.3, the curvature of the P-curve is therefore $+\frac{1}{r}$, whereas if the curve had been oriented in the opposite direction, it would have been equal to $\frac{-1}{r}$.

- If the considered curve is a **straight line**, at any point P, the tangent circles are of radius r as large as you want, they all fit very well the curve, and thus **the curvature at any point is zero** :

$$\frac{1}{r} \to 0 \qquad \text{if} \qquad r \to \infty$$

- If the curve is a **circle of radius R**, at any point P , the ideal tangent circle is the curve itself. **The curvature at any point is equal to $\frac{1}{R}$** . Consequence : the smaller the circle, the smaller R, the greater the curvature at each of its points, and vice versa.

C.1.4 Curvature for a plane surface

Given a surface and a point P on this surface, an infinite number of curves can be defined at this point as follows. There are an infinite number of planes that intersect perpendicularly the surface in P, that is, perpendicular to the plane tangent to the surface in P. The intersection of each of these planes with the starting surface is a curve: if we orientate it, we can define its curvature at point P. Among all these curvatures

thus defined, there is a maximum and a minimum, these two curvatures can be of identical or opposite signs. They are called **main curvatures**. For example, here are the curves associated with the main curves on our saddle-shaped surface.

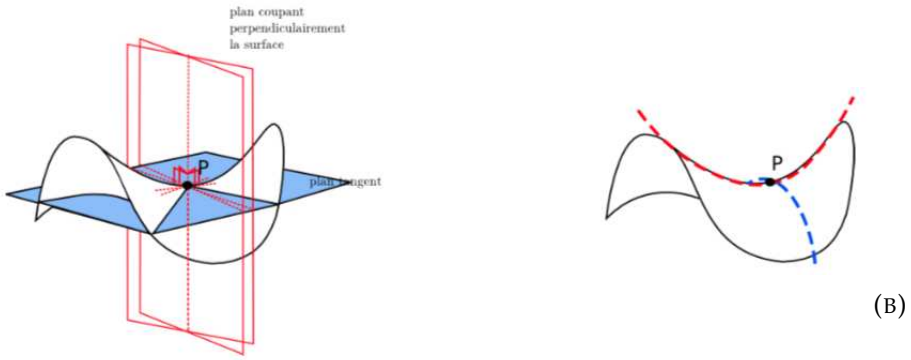

(A) (B)

FIGURE C.4: Isometry between surfaces

Let's give two concrete examples right away. Let's start by calculating the main curvatures at any point P in a plane, which is positioned flat and perpendicular to a vertical axis. In this configuration, all the perpendicular planes define sections that are straight lines, therefore with zero curvature in P.

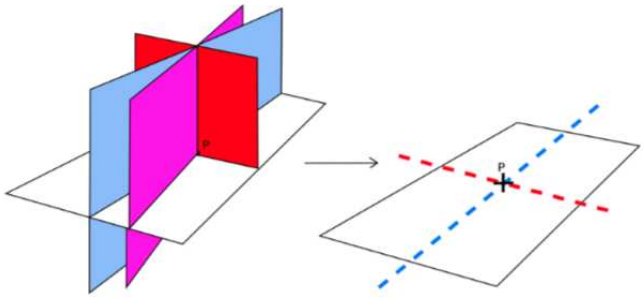

FIGURE C.5: Plane surface

Then, **the main curvatures are zero for the plane sheet**.
Second example: let's calculate the main curvatures at a point P of a cylinder of radius R. If we position the cylinder vertically, the planes intersecting the cylinder perpendicularly in P are all the planes carried by a straight line radial to the cylinder.

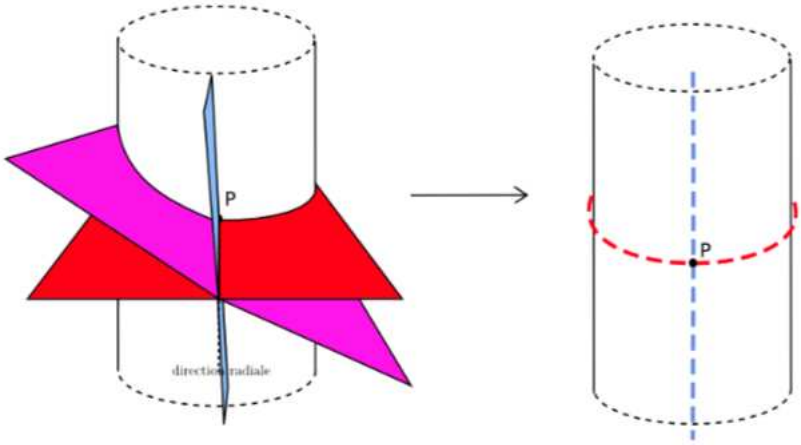

FIGURE C.6: Cylinder

- The plane defining a **maximum curvature** cut is the horizontal plane : the cut is a circle , of radius R, therefore of curvature $\frac{1}{R}$ ("Â±" depending on the chosen orientation).
- The plane defining a **minimum curvature** cut is the vertical plane perpendicular to the cylinder : the cut is a straight line, therefore of **zero curvature**.

The main curvatures of a cylinder of radius R at any point are therefore $\frac{1}{R}$ and 0.
This concept of principal curvatures will be implemented in the theorem that we will present in the next section.

C.1.5 Theorem

Two locally isometric C^3 surfaces have the same Gauss curvature at any point. The Gauss curvature of a surface at a point is the product of the main curvatures at that point.

Example : A cylinder of radius R and a plane have the same Gaussian curvature at each of their points, which is exactly what the Gaussian theorem states since a plane sheet can be bent into the shape of a cylinder isometrically. Indeed, the Gaussian curvature of a plane in one point is zero because both curvatures are zero

$$0 \times 0 = 0$$

This is the same for the curvature of a cylinder with radius R

$$0 \times \frac{1}{R} = 0$$

C.1.6 A first application in physics: how to hold a slice of pizza?

A problem we have all encountered when eating a slice of pizza: what is the best way to hold the slice so that the topping doesn't fall off? As physicists, or simple consumers, we know that there are several options for holding that slice of pizza with different consequences for each case: A pizza slice is more than a part of a plane: it's very easy to find the Gauss curvature at one of its points, we will find 0, the calculation being the same as for the plane.

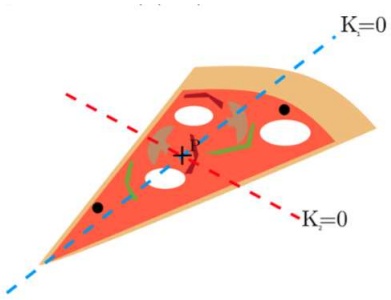

FIGURE C.7: On the table

If we want hold the pizza without any caution, it would bend and the topping would fall down. Indeed, in this configuration the crust remains straight, i.e. defines a zero curvature curve $K_1 = 0$. The weight at the end of the pizza slice makes it bend and fall, but this bending remains isometric : Gauss Theorem is always respected, since even if the dough is curved in the radial direction, defining a curve of curvature $K_2 > 0$, the product $K_1 - - - K_2 = 0 \times K_2$ remains zero.

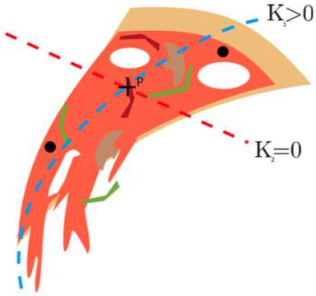

FIGURE C.8: In your hand

We want the curvature on the radial direction to be equal to zero ($K_1 = 0$), this implies that the second main curvature can be non-zero : when we hold the slice of pizza in our hands and bend the crust between our fingers. We make it undergo a transformation that remains reversible and gentle, i.e. isometric and according to the theorem, the Gauss curvature must remain zero at all points. In this configuration, the

shape given by the fingers to the slice of pizza imposes a strictly negative K_2 direction of curvature (direction parallel to the crust). Then, $K_1 - - - K_2 = 0 \times K_2 = 0$.

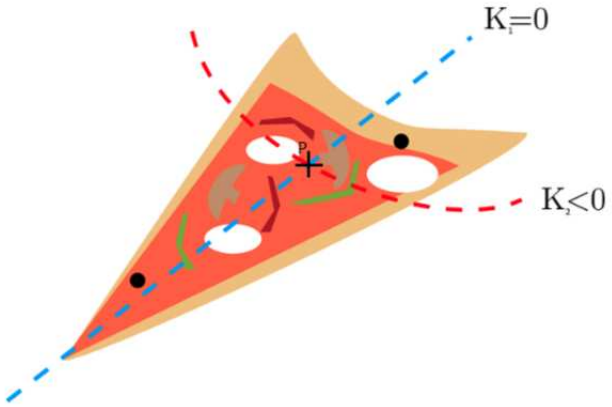

FIGURE C.9: Option 2 - Bent in your hand, you win!

We have just seen that a curved plane always has the same properties with respect to Gauss' theorem. It seems logical that in a certain limit (mass of the topping too important) the part will end up curving. In the next part, we will define to what extent and under what conditions we can reach a state of instability for a cylinder which has the same properties as the sheet from which it is generated.

C.2 Cylinders

We just observed A sheet of paper can also be rolled to get a cylinder. As explained in section C.1.5 the Gauss curvature will be equal to zero. With the slice of pizza we observed that, under it's own weight, the slice will stay straight.

Usually, bio filaments are organized in order to form tubes, i.e circular bars, that can be bent under conditions. What would happen for the sheet, cylinder shaped, under an external stress? The second question could be : how large can be stress before deforming the sheet?

We want to see if cylinders can easily change their shape for buckling or if buckling can happen for any load on the cylinder(s).

As I read many books for my studies, I have several masses to put on tubes. In order to get something steady, I used two tubes (paper cylinders) to hold the books.

I used pieces of tapes : 2 for the first cylinder, 3 for the second one. Low number of tape-pieces means they have no influence over the stability of the cylinders.

(A) Paper taped

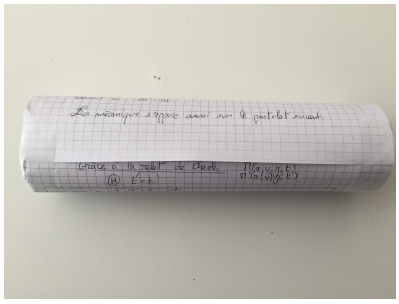

(B) Paper taped

FIGURE C.10: Paper taped

I used three books, having different masses.

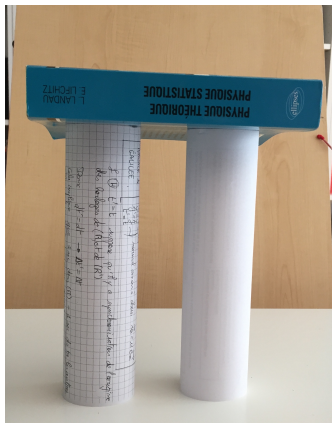

(A) Cylinders - book 1 - $m_1 = 0.62kg$

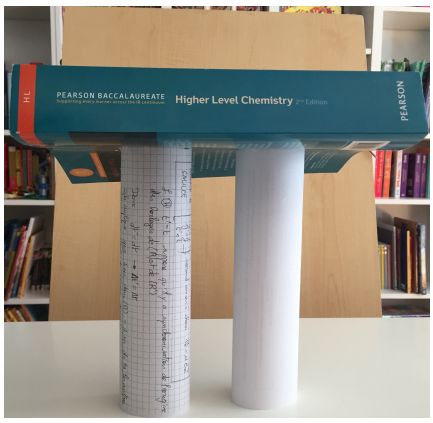

(B) Cylinders - book 2 - $m_2 = 2.4kg$

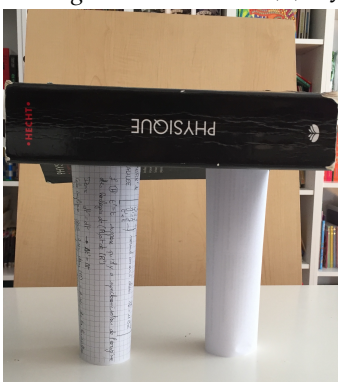

(C) Cylinders - book 3 - $m_3 = 3.0kg$

FIGURE C.11: Cylinders holding book with increasing masses

As showed on the pictures, the cylinders kept being steady whatever the mass was. Gauss Theorem was still respected.

By significantly increasing the mass, I notice that the tubes start to buckle but also that this buckling implies a change of shape of the surface. I conclude:

- that the external action (force, surface tension, etc.) must be of significant intensity to cause buckling
- the buckling, and therefore the state of instability, involves a change in the shape of the tube section.

It seems important to me now to check under which conditions on the energy of the tube we can observe this instability.

Bibliography

[1] L. D. Landau and E. M. Lifshitz, *Theory of Elasticity, Course of theoretical physics*. 1986, vol. 7.

[2] L. Bouzar, M. M. Müller, P. Gosselin, I. M. Kulic, and H. M. Mohrbach, "Squeezed helical elastica," *Europhys. Lett*, vol. 39, p. 114, 2016.

[3] N. Chouaieb, A. Goriely, and J. H. Maddocks, "Helices," *Proc. Natl. Acad. Sci. U.S.A.*, vol. 103, p. 9398, 2006.

[4] T. Odijk, "Macromolecules," *Biophys. J.*, vol. 28, p. 7016, 1995.

[5] B. Alberts, A. Johnson, J. Lewis, M. Raff, K. Roberts, and P. Walter, *Molecular Biology of the Cell*. 2005.

[6] T. Strick and al., *Rep. Prog. Phys.* 1. 2003, p. 66.

[7] R. Rief and al., *Science*, vol. 1109, p. 276, 1997.

[8] S. B. Smith, L. Finzi, and C. Bustamante, "Science," vol. 1122, p. 258, 1992.

[9] T. R. Strick, J. F. Allemand, D. Bensimon, A. Bensimon, and V. Croquette, *Science*, vol. 271, p. 1835, 1996.

[10] S. B. Smith, Y. Cui, and C. Bustamante, *Science*, vol. 271, p. 795, 1996.

[11] M. D. Wang, *Biophys. J.*, vol. 72, p. 1335, 1997.

[12] T. T. Perkins and al., "Science," vol. 268, p. 83, 1995.

[13] C. Bustamante, Z. Bryant, and S. B. Smith., *Nature*, vol. 421, p. 423, 2003.

[14] O. Kratky and G. Porod, *Recl. Trav. Chim.*, vol. 68, p. 1106, 1949.

[15] C. Bustamante, J. F. Marko, E. D. Siggia, and S. Smith, *Science*, vol. 265, p. 1599, 1994.

[16] I. M.Kulic, H. Mohrbach, R. Thaokar, and H. Schiessel, "Equation of state of looped dna," *Phys Rev E.*, vol. 75, p. 011 913, 2007.

[17] R. Everaers, S. Bundschuh, and K. Kremer, "Fluctuations and stiffness of double-stranded polymers: Railway-track model," *Europhys. Lett.*, vol. 29, pp. 263 –268, 1995.

[18] F. Pampaloni and al., "Thermal fluuctuations of grafted microtubules provide evidence of a length-dependent persistence length," *Proc. Natl. Acad. Sci. U. S. A.*, vol. 103, p. 10 248, 2006.

[19] H. Mohrbach and I. Kulic, "Motor driven microtubule shape fluctuations: Force from within the lattice," *Phys Rev Lett.*, vol. 218102, p. 99, 2007.

[20] N. Taberlet, J. Ferrand, E. Camus, L. Lachaud, and N. Plihon, "How tall can gelatin towers be? an introduction to elasticity and buckling," *American Journal of Physics, American Association of Physics Teachers*, vol. 85, pp. 908–914. 2017.

[21] M. Emanuel, H. Mohrbach, M. Sayar, H. Schiessel, and I. Kulic, *Phys. Rev. E*, vol. 061907, p. 76, 2007.

[22] R. Phillips, J. Kondev, J. Theriot, H. G. Garcia, and N. Orme, *Physical Biology of the Cell*. 1998.

[23] N. Mücke, L. Kreplak, R. Kirmse, T. Wedig, H. Herrmann, U. Aebi, and J. Langowski, "Assessing the flexibility of intermediate filaments by atomic force microscopy," *J Mol. Biol*, vol. 335, p. 1241, 2004.

[24] L. Kreplak, H. Bär, J. F. Leterrier, H. Hermann, and U. Aebi, "Exploring the mechanical behavior of single intermediate filaments," *J. Mol. Biol.*, vol. 354, p. 569, 2005.

[25] L. Kreplak, H. Hermann, and U. Aebi, "Tensile properties of single desmin intermediate filaments," *Biophys. J.*, vol. 94, p. 2790, 2008.

[26] J. Block, H. Witt, A. Candelli, E. J. G. Peterman, G. J. L. Wuite, A. Janshoff, and S. Köster, "Nonlinear loading-rate- dependent force response of individual vimentin intermediate filaments to applied strain," *Phys. Rev. Lett.*, vol. 118, p. 048 101, 2017.

[27] S.Winheim, A. R. Hieb, M. Silbermann, E.-M. Surmann, T. Wedig, H. Herrmann, J. Langowski, N. Mücke, and L. Kreplak, "Deconstructing the late phase of vimentin assembly by total internal reflection fluorescence microscopy(tirfm)," *PLoS One*, vol. 6, e19202, 2011.

[28] M. Schopferer, H. Bär, B. Hochstein, S. Sharma, N. Mücke, H. Herrmann, and N. Willenbacher, "Desmin and vimentinintermediate filament networks: Their viscoelastic properties investigated by mechanical rheometry," *J Mol. Biol*, vol. 388, p. 133, 2009.

[29] G.-M. Nam, N.-K. Lee, H. Mohrbach, A. Johner, and I. M. Kulic, "Helices at interfaces," *Europhys. Lett.*, vol. 100, p. 28 001, 2012.

[30] L. Bouzar, M. M. Müller, R. Messina, B. Nöding, S. Köster, H. Mohrbach, and I. M. Kulic, *Phys. Rev. Lett.*, vol. 122, p. 098 101, 2019.

[31] B. Nöding and S. Köster, "Intermediate filaments in small configuration spaces," *Phys. Rev. Lett.*, vol. 108, p. 088 101, 2012.

[32] E. Nogales and al., "High resolution model of the microtubule," *Cell*, vol. 96, pp. 79 –88, 1999.

[33] J. Huilin, D. J. D. Rosier, W. V. Nicholson, E. Nogales, and K. H. Downing, "Microtubule structure at 8 a resolution," *Structure*, vol. 10, p. 1317, 2002.

[34] D. Chretien, H. Flyvbjerg, and S. D. Fuller, "Limited flexibility of the inter-protofilament bonds in microtubules assembled from pure tubulin," *Eur Biophys J*, vol. 27, p. 490, 1998.

[35] R. Wade, D. Chrétien, and D. job., "Characterization of microtubule protofilament numbers. how does the surface lattice accommodate?" *J. Mol. Bio*, vol. 212, pp. 775–786, 1990.

[36] H.Mohrbach and I. Kulic, "Solvable model for polymorphic dynamics of biofilaments," *Phys Rev E.*, vol. 85, p. 031 903, 2012.

[37] E. Nogales, S. G. Wolf, and K. H. Downing., "Structure of the alpha-beta tubulin dimer by électron crystallography.," *Nature*, vol. 391, pp. 199 –203, 1998.

[38] J. Lowel, H. Li, K. H. Downing, and E. Nogales, "Refined structure of tubulin at 3.5 a resolution," *J. Mol. Biol.*, vol. 313, p. 10 457, 2001.

[39] C. Cuveillier, J. Delaroche, M. Seggio, S. Gory-Fauré, C. Bosc, E. Denarier, M. Bacia, G. Schoehn, H. Mohrbach, I. M. Kulic, A. Andrieux, I. Arnal, and C. Delphin, "Map6 is an intraluminal protein that induces neuronal microtubules to coil," *Sci. Adv*, vol. 6, eaaz4344, 2020.

[40] H. Mohrbach, A. Johner, and I. M. Kulic, "Cooperative lattice dynamics and anomalous fluctuations of microtubules," *Eur. Biophys. J*, vol. 217, p. 41, 2012.

[41] E. Ising, "Beitrag zur theorie des ferromagnetismus," *Z. Phys.*, vol. 31, p. 253, 1925.

[42] L. Onsager, "Crystal statistics. i. a two-dimensional model with an order-disorder transition," *Physical Review, Series II*, vol. 65, p. 117, 1944.

[43] N. Mermin and H. Wagner, "Absence of ferromagnetism or antiferromagnetism in one- or two-dimensional isotropic heisenberg model," *Phys. Rev Lett.*, vol. 17, p. 1133, 1966.

[44] C. Lu, M. Reedy, and H. Erickson, *J. Bacteriol.*, vol. 182, p. 164, 2000.

[45] M. Osawa, D. Anderson, and H. Erickson, *Science*, vol. 320, p. 792, 2008.

[46] F. VandenEnt, L. Amos, and J. Lowe, *Nature*, vol. 413, p. 39, 2001.

[47] R. Kamiya and S. Asakura, *J. Mol. Biol.*, vol. 106, p. 167, 1976.

[48] E. Hasegawa, R. Kamiya, and S. Asakura, *J. Mol. Biol.*, vol. 160, p. 609, 1982.

[49] J. Tang, J. Kas, J. Shah, and P. Janmey, *Eur. Biophys. J.*, vol. 30, p. 477, 2001.

[50] T. Sanchez, I. M. Kulic, and Z. Dogic, *Phys. Rev. Lett.*, vol. 104, p. 098 103, 2010.

[51] H. Mohrbach, A. Johner, and I. M. Kulic, "Cooperative lattice dynamics and anomalous fluctuations of microtubules," *Eur. Biophys. J.*, vol. 41, p. 217, 2012.

[52] J. Fierling, M. M. Müller, H. Mohrbach, A. Johner, and I. Kulic, *EPL*, vol. 107, p. 68 002, 2014.

[53] M. Arroyo, L. Heltai, D. Millan, and A. DeSimone, *Proc. Natl. Acad. Sci. USA*, vol. 109, p. 17 874, 2012.

[54] S. Asakura, *Adv. Biophys.*, vol. 1, p. 99, 1970.

[55] O. Kahraman, H. Mohrbach, M. Muller, and I. M. Kulic, "Soft matter," vol. 10, p. 2836, 2014.

[56] C. R. Calladine, *Nature (London)*, vol. 255, p. 121, 1975.

[57] S. V. Srigiriraju and T. R. Powers, *Phys. Rev. Lett.*, vol. 94, p. 248 101, 2005.

[58] H. Wada and R. R. Netz, *EPL*, vol. 82, p. 28 001, 2008.

[59] J. Baschnagel, H. Meyer, J. Wittmer, I. Kulic, H. Mohrbach, F. Ziebert, G-M., N. N.-K. Lee, and A. Johner, "Semiflexible chains at surfaces: Worm-like chains and beyond," *Polymers*, vol. 8, p. 286, 2016.

[60] C. Heussinger, M. Bathe, and E. Frey, "Statistical mechanics of semiflexible bundles of wormlike polymer chains," *Phys Rev Lett.*, vol. 048101, p. 99, 2007.

[61] F. Gittes, J. Nettleton, and J. Howard, *J. Cell Bio*, vol. 120, p. 923, 1993.

[62] H. Feigner, R. Frank, and M. Schliwa, *J. Cell Sci*, vol. 109, p. 509, 1996.

[63] P. Venier, A. C. Maggs, M. F. Carlier, and D. Pantaloni, "Analysis of microtubule rigidity using hydrodynamic flow and thermal fluctuations," *J Biol. Chem.*, vol. 269, p. 13 353, 1994.

[64] K. M. Taute, F. Pampaloni, E. Frey, and E.-L. Florin, "Microtubule dynamics depart from the from the wormlike chain model," *Phys. Rev. Lett.*, vol. 02810, p. 100, 2008.

[65] S. Kasas, B. Babic, A. Kulik, W. Benoit, G. Briggs, C. Schonenberger, S. Catsicas, and L. Forro, "Nanomechanics of microtubules," *Phys Rev Lett.*, vol. 248101, p. 89, 2002.

[66] H. Mohrbach, A. Johner, and I. M. Kuli, "Tubulin bistability and polymorphic dynamics of microtubules," *Phys. Rev. Lett.*, vol. 268102, p. 105, 2010.

[67] C. E. Caille and al., "Straight gdp–tubulin protofillaments form in the presence of taxol," *Curr. Biol.*, vol. 17, p. 1765, 2007.

[68] F. Ziebert, H. Mohrbach, and I. M. Kulic, "Why microtubules run in circles: Mechanical hysteresis of the tubulin lattice," *Phys. Rev. Let.*, vol. 114, p. 148 101, 2015.

[69] R. D. Vale, B. Schnapp, T. S. Reese, and M. P. Sheetz, *Cell*, vol. 40, p. 559, 1985.

[70] L. A. Amos and W. B. Amos, "The bending of sliding microtubules imaged by confocal light microscopy and negative stain electron microscopy, j.," *Cell. Sci. Suppl.*, vol. 14, p. 95, 1991.

[71] R. Vale, C. Coppin, F. Malik, F. Kull, and R. A. Milligan, *J. Biol. Chem.*, vol. 269, p. 23 769, 1994.

[72] L. Landau and E. Lifshitz, *Statistical Physics*, P. I. Library, Ed. Robert Maxwell and M.C.

[73] J. Bico, E. Reyssat, and B. Roman, "Elastocapillarity: When surface tension deforms elastic solids," *Annual Review of Fluid Mechanics*, vol. 50, pp. 629–659, 2018.

[74] B. Andreoti and J. Snoeijer, "Soft wetting and the shuttleworth effect, at the crossroads between thermodynamics and mechanics," *Europhys. Lett*, vol. 66001, p. 113,

[75] M. Nicolson, "Surface tension in ionic crystals," *Proc. R. Soc.*, vol. 228, pp. 490 –510,

[76] C. Hui, A. Jagota, Y. Lin, and E. Kramer, "Constraints on microcontact printing imposed by stamp deformation," *Langmuir*, vol. 18, pp. 1394–407, 2002.

[77] S. Mora, C. Maurini, T. Phou, J. Fromental, B. Audoly, and Y. Pomeau, "Solid drops: Large capillary defor- mations of immersed elastic rods.," *Phys Rev Lett.*, vol. 111, p. 114 301, 2013.

[78] P. Poncharal, Z. L. Wang, D. Ugarte, and W. A. de Heer, *P. Poncharal, Z. L. Wang, D. Ugarte, and W. A. de Heer*, vol. 283, p. 1513, 1999.

[79] S. Cuenot, C. Fretigny, S. Demoustier-Champagne, and B. Nysten, "Surface tension effect on the mechanical properties of nanomaterials measured by atomic force microscopy," *Phys. Rev. B*, vol. 69, p. 165 410, 2004.

[80] X. Li, H. Zhang, and K. Y. Lee, "Dependence of young's modulus of nanowires on surface effect," *International Journal of Mechanical Sciences*, vol. 81, p. 120, 2014.

[81] B. Nöding and S. Köster, "Intermediate filaments in small configuration spaces," *Phys. Rev. Lett.*, vol. 108, p. 088 101, 2012.

[82] S. Köster, J. Kierfeld, and T. Pfohl, "Characterization of single semiflexible filaments under geometric constraints," *Eur. Phys. J.*, vol. E 25, p. 439, 2008.

[83] S. A. Mora, C. Maurini, T. Phou, J.-M. Fromental, B. Audoly, and Y. Pomeau, "Solid drops: Large capillary deformations of immersed elastic rods," *Phys. Rev. Lett.*, vol. 111, p. 11 430, 2013.

[84] M. Lai, E. Krempl, and D.Ruben, *Introduction to continuum mechanics*. 2010, vol. Fourth edition.

[85] A. Baumann, A. Sánchez-Ferrer, L. Jacomine, P. Martinoty, V. L. Houerou, F. Ziebert, and I. M. Kulic, "Motorizing fibres with geometric zero-energy modes," *Nat. Mater.*, vol. 17, p. 523, 2018.

[86] L. M. Kanner and C. O. Horg, "Plane strain bending of strain-stiffening rubber-like rectangular beams," *International Journal of Solids and Structures*, vol. 45, p. 1713, 2008.

[87] W. M. Lai, D. Rubin, and E. Krempl, *Introduction to Continuum Mechanics*. Elsevier, 2010.

[88] J. Schouten, *Tensor Analysis for Physicists*. Dover, Mineola, 1989.

[89] R. S. Rivlin, "Large elastic deformations of isotropic materials, part v, the problem of flexure," *Proc. R. Soc. Lond. A*, vol. 195, p. 463, 1949.

[90] P. Dadras, "Plane strain elastic–plastic bending of a strain-hardening curved beam," *Int. J. of Mech. Sciences*, 2001.

[91] 2021. [Online]. Available: https://en.wikipedia.org/wiki/Self-buckling.

[92] S. Venkataramani, "Buckling sheets open a door to understanding self-organization in soft matter," *National Academy of Sciences*, 2019.

[93] N. Rocher, "Un théorème et une part de pizza," [Online]. Available: http://images.math.cnrs.fr/Un-theoreme-et-une-part-de-pizza.html#partager.